

**Design of a new fluorogenic molecular
probe of lipases that will be specific for
monoacylglycerol lipase**

Judith Chikwadoro Ajaezu

MRes

June 2023

**Design of a new fluorogenic molecular probe of lipases that will be specific for
monoacylglycerol lipase**

Judith Chikwadoro Ajaezu

Thesis submitted in partial fulfilment of the requirements of Edinburgh Napier
University for the degree of Master of Science by research (MRes)

June 2023

ABSTRACT

Homeostatic imbalances in enzyme activities have been linked to an array of human pathological conditions. Evidence exists for the role of monoacylglycerol lipase (MAGL) in the development and progression of malignant forms of cancers, including breast, prostate, melanoma and ovarian, as well as tuberculosis, Alzheimer's, and other forms of neurological disorders. There is great need to develop improved sensing methods for the determination of activity of lipases, including MAGL, to probe mechanisms of disease development and progression.

This research successfully developed two rhodamine B-based FRET (Fluorescence Resonance Energy Transfer) molecular probes (JA4 and JA7) targeted at lipases. The probes were achieved by a convergent synthesis in which a novel piperazine-linked rhodamine fluorophore (as donor) and an aminoanthraquinone 'black-hole' acceptor (as quencher) were coupled via a key ester bond destined to be the site of cleavage (activation) by lipase hydrolytic action.

All new target compounds and intermediates were characterized by high resolution electrospray (+) mass spectrometry. The structures of the target compounds JA1 (fluorophore), JA4 (probe 1) and JA7 (probe 2) were confirmed by NMR spectroscopy.

Novel substrate FRET probes, JA4 and JA7 were demonstrated to be smart probes in which rhodamine fluorescence was completely quenched until activated by lipase(s) as demonstrated by the efficient restoration of rhodamine fluorescence emission upon incubation with probes JA4 and JA7 by UV fluorescence spectroscopy experiments. The identities of the PPL-induced cleavage products of JA4, i.e., JA1 and JA3, were determined by HPLC using UV/Visible detection; this was possible because standards of JA1 and JA3 were already available by synthesis (and their structures determined, originally by mass spectrometry and latterly by NMR spectroscopy). Efficient restoration of intense rhodamine fluorescence upon incubation of the probes with porcine pancreatic lipase (PPL) enzyme, as a model for human lipases, served as a proof of concept that the probes could be activated by lipase action. The probes have potential to determine over-expressed lipase activity in human tissues *ex vivo*, without any interference from molecules of the biological matrix, to aid diagnosis, and monitor stage and progression of disease.

Declaration

It is hereby declared that this thesis and the research work upon which it is based were conducted by the author.

Judith Chikwadoro Ajaezu

Acknowledgement

I give praise to God Almighty for His benefits which has taken me this far in my career.

My special thanks go to my supervisors: Dr Agnes Turnbull, Dr Janis McCallum, and Dr David Mincher for their unalloyed support during this research, without which this programme would not have been achievable.

I thank Amy Dilon and Giacomo Russo for the HPLC analysis of my work.

My warm appreciation to Dr Lesley Ingram Sills, for overseeing the progress of this study.

Finally, my immense gratitude to my family for their great love and support, which has made this MRes programme a dream come true.

Contents

ABBREVIATIONS	i
Chapter 1: Introduction	1
1.0 Aims.....	1
1.1 Literature review.....	1
1.1.1 MAGL chemistry.....	1
1.1.2 MAGL structure.....	2
1.1.3 Binding mechanism and selectivity of MAGL.....	5
1.1.4 MAGL in diseases	8
1.1.5 Enzyme targeted small molecule fluorogenic substrate probes.	10
1.1.6 FRET.....	12
1.1.7 Rhodamine B derivatives in FRET probe design.....	14
1.1.8 Previous work on MAGL substrate probes.	15
1.1.9 Previous work on anthraquinone quenched rhodamine-based FRET (substrate) probes. .	16
Chapter 2: Results and Discussion	18
2.0 Design strategy for the novel MAGL probes.....	18
2.1 Synthesis and characterisation of compounds	19
2.1.1 Synthesis of JA1 the rhodamine-B derived fluorophore 1 bearing the alcohol group of probes 1 and 2	19
2.1.2 Synthesis of tert-butyl 3-[(4-hydroxy-9,10-dioxo-9,10-dihydroanthracen-1-yl) amino] propanoate (JA2).....	24
2.1.3 Synthesis of 3- [(4-hydroxy-9,10-dioxo-9,10-dihydroanthracen-1- yl) amino] propanoic acid (JA3, Quencher 1).....	26
2.1.4 Synthesis of JA4 the rhodamine-B derived aminoanthraquinone (Probe 1).....	29
2.1.5 Synthesis of tert-butyl 3-[(4-hydroxy-9,10-dioxo-9,10-dihydroanthracen-1-yl) amino] propanoate (JA5).....	34
2.1.6 Synthesis of 4-[(4-hydroxy-9,10-dioxo-9,10-dihydroanthracen-1-yl)amino] butanoic acid, JA6 (Quencher 2).....	35
2.1.7 Synthesis of rhodamine-B derived aminoanthraquinone, JA7 (probe 2)	38
2.2 UV-Vis Absorption Assay for JA1.....	41
2.3 FRET studies	42
2.3. 1 Demonstration of spectral overlap between the donor chromophore, JA1 and the acceptor chromophores, JA3 and JA6.....	42
2.3.2 Fluorescence Spectroscopy Assay.....	45
2.4 Determination of relative Quantum yield of probe 1.....	46
2.5 Fluorescence studies: pH Dependence of fluorescence of rhodamine b derived fluorophore JA1	51

2.6 Activation of probes JA4 and JA7 by porcine pancreatic lipase (PPL) in vitro	53
2.7 TLC analysis of PPL incubation products	57
2.8 Distribution coefficient assay.....	58
2.9 HPLC STUDIES.....	61
2.9.1 Development of an HPLC method for separation of probe JA4 and its in vitro metabolites	61
2.9.2 HPLC determination of JA4 PPL-mediated cleavage into JA1 and JA3	63
Chapter 3: Experimental	67
3.0 Experimental (synthesis) procedure	67
3.1 General.....	67
3.2 Column sizes used for column chromatography	67
3.3 Solvents used for column chromatography.....	67
3.4 Solvents for TLC.....	68
3.5 solvents for HPLC	68
3.6 HPLC column size and condition	69
3.7 Synthetic procedures	69
3.7.1 Synthesis of rhodamine B derived fluorophore (JA1)	69
3.7.2 Synthesis of 3-(9, 10-Dihydro-anthracen-9-ylamino)-propionic acid tert-butyl ester (JA2) 70	
3.7.3 Deprotection of 3-(9, 10-Dihydro-anthracen-9-ylamino)-propionic acid tert-butyl ester (JA2) to form 3-[(4-hydroxy-9,10-dioxo-9,10-dihydroanthracen-1-yl) amino] propanoic acid (JA3)	71
3.7.4 Synthesis of rho-B derived aminoanthraquinone (JA4, probe 1)	72
3.7.5 Synthesis of 4- (9, 10-Dihydro-anthracene-9-ylamino)-butyric acid tert-butyl ester (JA5) . 73	
3.7.6 Deprotection of 4- (9, 10-Dihydro-anthracene-9-ylamino)-butyric acid tert-butyl ester (JA5) to form 4-[(4-hydroxy-9,10-dioxo-9,10-dihydroanthracen-1-yl) amino] butanoic acid (JA6)	74
3.7.7 Synthesis of rhodamine-B derived aminoanthraquinone, JA7 (probe 2)	75
3.8 UV-Vis Absorption Assay for JA1.....	76
3.9 FRET studies	76
3.9.1 Demonstration of spectral overlap between the emission spectrum of the donor chromophore, JA1 and the absorption spectra of the acceptor chromophores, JA3 and JA6.	76
3.9.2 Fluorescence Spectroscopy Assay.....	77
3.10 Determination of relative Quantum yield of JA1	77
3.11 Fluorescence studies: pH Dependence of fluorescence of rhodamine b derived fluorophore JA1	78
3.12 Activation of probes JA4 and JA7 by porcine pancreatic lipase (PPL) in vitro	79
3.13 TLC analysis of PPL incubation products	79

3.14 Distribution coefficient assay.....	80
3.15 HPLC STUDIES.....	81
3.15.1 HPLC method development	81
3.15.2 HPLC Analysis of JA4 (FRET probe) incubation with PPL (pancreatic porcine lipase)	81
STRUCTURE LIBRARY AND CHARACTERIZATION AND EVALUATION SUMMARY	83
REFERENCE	

ABBREVIATIONS

Act – Acetic acid

2-AG – 2-arachidonoyl glycerol

But - Butanol

DCC- Dicyclohexylcarbodiimide

DCM- Dichloromethane

DCU-Dicyclohexylurea

DIC - N,N'diisopropylcarbodiimide

DIPEA- N,N-Diisopropylethylamine

DMAP -4-Dimethylaminopyridine

DMF- Dimethylformamide

DMSO – Dimethyl sulfoxide

Eq- equivalent

ESI – Electrospray ionisation

ETOH - Ethanol

FAAH – Fatty acid amide hydrolase

FFA – free fatty acid

FRET- Förster/Fluorescence resonance energy transfer

Glu – glutamate/glutamic acid

hr(s)- hour(s)

HATU- Hexafluorophosphate Azabenzotriazole Tetramethyl Uronium

HCl – Hydrochloric acid

His – histidine

H₂O - water

HOAt -1-hydroxy-7-azabenzotriazole

HPLC – High Performance Liquid Chromatography

LPA - lysophosphatidic acid

MAGL- Monoacylglycerol lipase

Mass – spec – mass spectrometer

MeOH- Methanol

Min- minute(s)

Mix - mixture

m/z- mass/charge

nm- nanometer

NMR – Nuclear Magnetic Resonance

PPL – porcine pancreatic lipase

PGE2 - prostaglandin E2

qPCR – quantitative polymerase chain reaction

Rf - Retardation Factor

Rho-B - Rhodamine B

RT- Room temperature

Ser- serine

STR - stirring

TFA -trifluoroacetic acid

TFA⁻ - trifluoroacetic acid anion

TLC- Thin layer chromatography

UV-Vis – ultraviolet – visible

Chapter 1: Introduction

1.0 Aims

To design, synthesise and evaluate an efficient, novel, FRET based fluorogenic molecular probe that will be specifically cleaved by monoacylglycerol lipase (MAGL) to generate fluorescence and serve as a measure of lipase activity.

1.1 Literature review

1.1.1 MAGL chemistry

Monoacylglycerol lipase is a membrane bound enzyme, and a soluble cytosolic protein found in most tissues of the body; however, displaying tissue specific physiological roles (Bertrand et al., 2010; Chen, Tian, et al., 2014; Karlsson et al., 1997; Schalk-Hihi et al., 2011). Evidence from its structure and tissue distribution show that it is amphipathic, being able to attach to lipid membranes and at the same time able to solubilize in aqueous cytosol. It is one of the α/β hydrolase group of enzymes based on a serine nucleophile (Labar et al., 2010a). Its major function was found to be the catalysis of the last step in the lipolytic cascade that releases fatty acids from lipid stores (Karlsson et al., 1997). It shows a selectivity towards monoglycerides (Bertrand et al., 2010). In adipocytes, it breaks down 1 and 2-monoglycerides into free fatty acids and glycerol, while in neurons (the central nervous system) it is the major enzyme involved in the hydrolysis of 2-arachidonoyl glycerol (2-AG) (Figure 1) to arachidonic acid and glycerol (Blankman, Simon and Cravatt, 2007; Bowman and Makriyannis, 2009; Schlosburg et al., 2010; Schalk-Hihi et al., 2011).

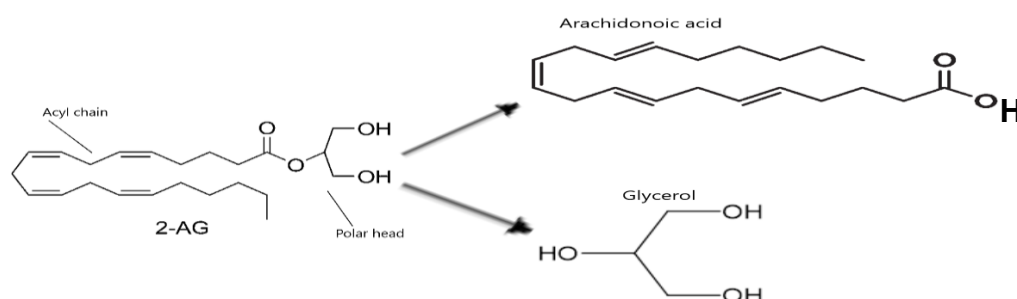


Figure 1: Structure of 2-arachidonoyl glycerol (2-AG), showing the long acyl/aliphatic chain and the polar head, as well as the breakdown products. Adapted from (Bertrand et al., 2010)

In cancer cells, MAGL controls a fatty acid network that supplies signalling molecules involved in cancer growth and metastasis (Liu et al., 2013; Nomura et al., 2010). Based on its known physiological functions, MAGL has been proposed to be a putative target for development of biomarkers, probes, pro-drugs, and drugs for several diseases of humans (Baba et al., 2017; Deng & Li, 2020; Scalvini et al., 2016).

1.1.2 MAGL structure

Homology models based on the α/β hydrolase superfamily have been employed in attempts to describe the three-dimensional structure of monoacylglycerol lipase (Karlsson et al., 1997). It was found that, MAGL showed no widespread similarity to known human proteins (Karlsson et al., 1997) but, a rather remote link to microbial haloperoxidases, esterases, lysophospholipases, lipid hydrolases, peptide hydrolases, dehalogenases, and C-C carbon breaking enzymes, all of which share a common β core surrounded by α helices, a highly conserved catalytic site and an extremely variable cap domain (Bowman & Makriyannis, 2009; King et al., 2009a; Saario et al., 2005; Scalvini et al., 2016). Evidence from x-ray diffraction as well as mass spectrometry studies confirmed MAGL to be a dimeric protein (Bertrand et al., 2010; Chen, Tian, et al., 2014; Scalvini et al., 2016).

In line with the other members of the superfamily, the whole MAGL protein is comprised of eight β sheets made up of seven parallel and one antiparallel strand and a total of eight α helices (six in majority of the homologues), arranged on both sides of the strands together with loops that join the various strands and helices (Bertrand et al., 2010; Labar et al., 2010b; Scalvini et al., 2016; Schalk-Hihi et al., 2011).

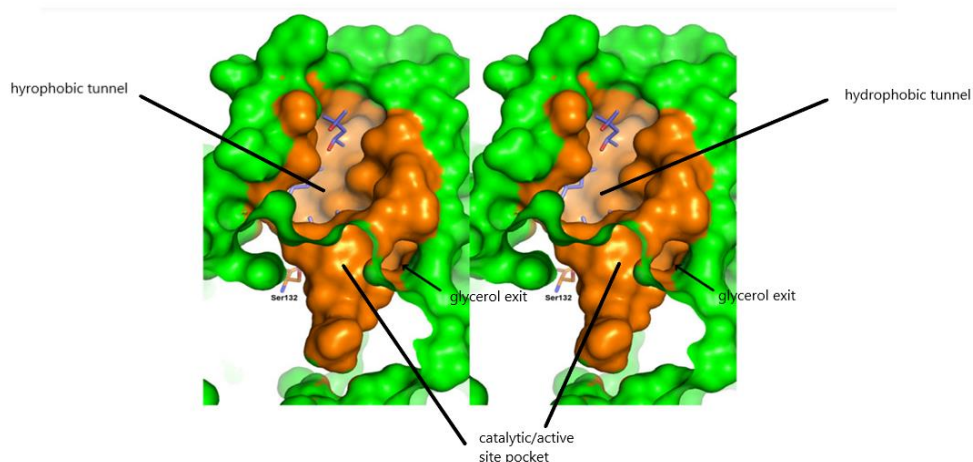


Figure 2: Surface representation of apo (unbound) MAGL (in green). The tunnel is depicted in orange. The possible exit of glycerol is indicated by a black arrow. Adapted from (Bertrand et al., 2010).

Information from molecular modelling studies show that the general architecture of the enzyme comprises of an unusually large and long hydrophobic tunnel with the cap domain at its top (entry) and the active site domain buried at its end (Figure 2) (Bertrand et al., 2010). This lower end of the tunnel (catalytic region) is found to be more hydrophilic and closed-up (avoiding contact with the solvent region), while the top part (cap region) is very lipophilic and has a broad exit to the solvent region (Bertrand et al., 2010). Lining the walls of the cavity/tunnel and leading into the hydrophilic alcohol binding pocket (the active site centre) are hydrophobic residues Leu148, Ala164, Leu176, Ile179, Leu205, Val207, Ile211, Leu213, Leu214, Val217 and Leu241 that shape the wall of this cavity, believed to contain the lipophilic chain of the endogenous ligand, 2-AG during catalysis.

Also, the consensus is that the arachidonic acid moiety (the long acyl chain) of 2-AG (Figure 1) diffuses outward through the flexible lid/cap after 2-AG hydrolysis. One other interesting structural feature of the enzyme, revealed from x-ray studies and supported by data from in silico studies is the presence of a thin opening of diameter about 5 Angstroms (Figure 2) delineated by residues Pro178 to Ser181, Leu184, Tyr194, Asn195, Arg202 and Ala203 and, found near the end of the tunnel (the active site region) that links the catalytic site to the solvent region (Bertrand et al., 2010; Scalvini et al., 2016). This opening is presumed to be the glycerol exit door through which the glycerol moiety of 2-AG leaves the enzyme after cleavage at the active site (Labar et

al., 2010b). The three-dimensional structure of the enzyme depicts an excellent pharmacophore and an attractive model for rational drugs and probes design and discovery (Bertrand et al., 2010; Labar et al., 2010b).

The active site region of the protein made up of the catalytic triad comprising residues Ser122, Asp239 and His269 has been confirmed by site directed mutagenesis (Karlsson et al., 1997; Bertrand et al., 2010). The catalytic Ser122 is located at a tight bend between the α 3 helix and β 5 strand, comprising an interconnection of hydrogen bond donors and known as the 'nucleophilic elbow'. This structurally preserved system of hydrogen bond donors together with the backbone NH of Ala51 and Met123, and residues Gly50 and Gly124 form the oxyanion hole that stabilizes the anionic transition state during catalysis (Labar et al., 2010a; Schalk-Hihi et al., 2011). The basic residue His269 is found within the loop connecting helix α 8 and strand β 8 while the catalytic acid Asp239 is housed within the turn after strand β 7. Alongside the oxyanion hole formed by backbone nitrogen atoms of Ala51 and Met123, the Tyr58 hydroxyl group, the imidazole nitrogen of His121 and His272, the guanidinium group of Arg57, the carboxylate of Glu53 and the backbone of Ala 51 define a polar crevice which makes up the enzyme's catalytic centre (Scalvini et al., 2016). Labar and co-workers found glycerol moieties used in purification protocol for the crystal structure, 3HJU (Labar et al., 2010), to be contained within this cavity, which is in proximity of the assumed exit route for glycerol and, with its hydroxyl groups making hydrogen bonds with the Ala51 carbonyl, Glu53 carboxylate and the hydroxyl group of Tyr94. Labar and colleagues hypothesized that this region would bind the polar head of 2-AG within the active site (Labar et al., 2010a; Scalvini et al., 2016). The flexible and hydrophobic cap domain (residues 151 – 225) of MAGL that shields the substrate-binding pocket from surrounding solvent is believed to control substrate entry into the catalytic centre (Nasr et al., 2013) through a reversible interaction with the cell membrane thereby leading to the open (active) and closed (in-active) conformations of the enzyme. It is made up of three α helices (α 4, α 5 and α 6) as well as the loops joining the helices (Labar et al., 2010a). The cap regions of MAGL which comprised of highly non-polar residues were found to be well positioned to interact with the phospholipid membrane (Labar et al., 2010a; Scalvini et al., 2016) to extract its lipophilic substrate from the associated

membrane (Labar et al., 2010a) as well as to enhance adhesion to hydrophobic cell membrane (Nasr et al., 2013)

Scalvini and co-workers also confirmed the presence of polar residues Asn152, Glu154 and Lys160 on the cap's helix α_4 that is believed to enhance polar interaction with the polar head (glycerol end) of its endogenous substrate 2-AG, while the positive charge on Lys160 is purported to promote association with phosphate groups of membrane phospholipids (Scalvini et al., 2016).

1.1.3 Binding mechanism and selectivity of MAGL

The crystal structures of the apo and ligand bound forms of MAGL have been studied by researchers to provide improved insight into the active site properties and binding mode of MAGL (King et al., 2009a; Liu et al., 2013; Saario et al., 2005; Tyukhtenko et al., 2020). It is believed that hydrophobic interactions between the enzyme's cap domain and its ligand facilitates the opening of the cap, allowing the ligand to plunge (with its polar head leading) into the hydrophobic tunnel of the enzyme (Nasr et al., 2013; Tyukhtenko et al., 2020). The aliphatic moiety of the ligand is stabilized by aromatic bonds along the length of the tunnel while hydrogen bond interactions position the polar head within the active site for hydrolysis (Nasr et al., 2013; Tyukhtenko et al., 2020). This primary binding is rapidly followed by the attack of the catalytic serine onto the reactive ester (Bertrand et al., 2010).

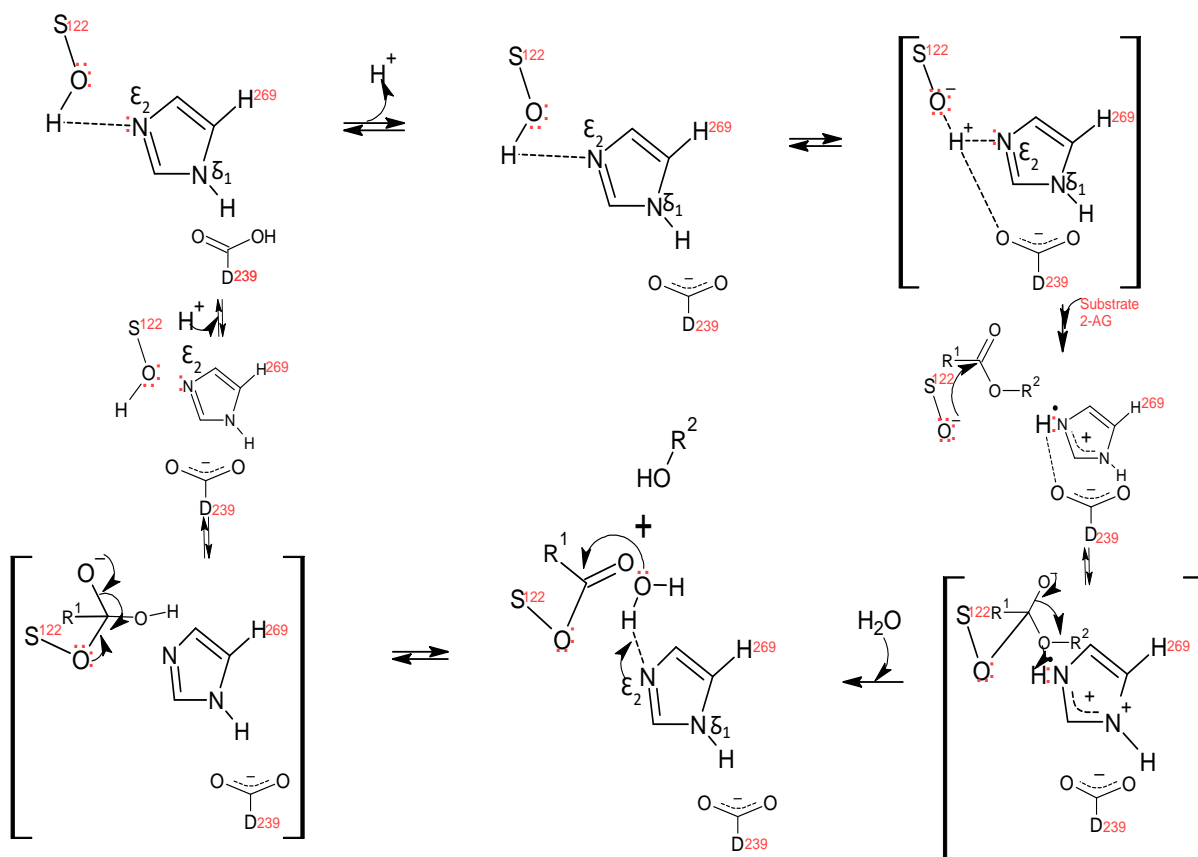


Figure 3: Enzyme catalysis of human MAGL (hMAGL). Adapted from (Kokkinou, Theodorou and Papamichael, 2012).

During ester hydrolysis, the active site (catalytic triad) aspartic acid forms a hydrogen bond with histidine, increasing the pKa of the histidine imidazole nitrogen (Figure 3) (Kokkinou, Theodorou and Papamichael, 2012). This activates the histidine to act as a powerful general base and deprotonate the active site serine (Figure 3). The deprotonated serine ensues a nucleophilic attack on the ester carbonyl carbon of the lipid substrate. Upon attacking the lipid, a negatively charged tetrahedral intermediate is formed (Figure 3). This is stabilized in the oxyanion hole of the lipase active site by the two residues: phenylalanine and leucine (Figure 3) (Kokkinou, Theodorou and Papamichael, 2012). The carbonyl reforms with the glycerol backbone segment acting as the leaving group. A water molecule then donates a proton to the histidine, creating a reactive hydroxyl anion (Figure 3). The hydroxyl anion can then attack the carbonyl carbon of the lipid, forming another negatively charged tetrahedral intermediate, which is stabilized in the oxyanion hole. Upon reformation of the carbonyl, the catalytic serine is released, and the metabolites diffuse away. Tyukhtenko and colleagues showed that a system of hydrogen bonds (H-bonds) involving a H-bond bond between Oδ2 of

Asp-239 and H δ 1 of His-269 and a H-bond respectively between the backbone amide protons of Leu-241 and Cys-242 and O δ 1 of Asp-239, as well as π - π aromatic interactions (involving His-121, His-269 and Tyr-268, as well as His-272, Tyr58 and Arg-57) within the alcohol binding pocket is required for the correct aligning of all catalytically relevant residues (Tyukhtenko et al., 2020). By utilising the techniques of site directed mutagenesis and HDX-MS techniques they concluded that the aspartic acid H-bond was critical to allosteric regulation within the active site of MAGL (Tyukhtenko et al., 2020). Aromatic interactions between His-272 and Tyr-58 as well as His-121 and a His-272 cation- π interaction with the cationic $-\text{NH}_2^+$ group of Arg-57 were found to stabilize the enzyme in its open/active conformation. Data from the docking pose for 2-AG into the crystal structures of the apo form of human MAGI and RsbQ from *Bacillus subtilis* (PDB ID: 1WOW), also supported the presence of stabilising interactions of the enzyme with the ligand (Bertrand et al., 2010; Bowman & Makriyannis, 2009). The head group was found to occupy the hydrophilic region of the binding pocket and was stabilised by hydrogen bonds formed from H ζ 1 and H ζ 2 of Asn195 and the carbonyl backbone oxygen of Ala51 to the oxygens of the hydroxyl groups of the substrate (Bowman & Makriyannis, 2009). The aliphatic tail of 2-AG was found coiled up in the hydrophobic region of the binding pocket (Bertrand et al., 2010; Bowman & Makriyannis, 2009). Furthermore, these techniques have been utilised to highlight the differences in the cap domain architecture, size, and organisation of the alcohol binding pocket as well as the hydrophobic tunnel of MAGL when compared to other closely related lipases such as fatty acid amide hydrolase (FAAH), esterases and haloperoxidases, which points to the putative selectivity of MAGL to potential specific ligands (Bowman & Makriyannis, 2009). In the esterases and haloperoxidases, the cap or gate was found to be two superimposed V-shaped structures permitting access to smaller sized molecules while that of MAGL was found to be a U-shaped structure that accommodates bulkier ligands. In addition, when compared to the closely related arylesterases (ligands are small esters) and chloroperoxidases (ligands are organic acids), the cap region and hydrophobic tunnel (in MAGL) were found to be more hydrophilic in these enzymes. This is seen to be in line with these enzymes metabolising more hydrophilic substrates that are present in the cytosol. On the contrary MAGL ligands are very hydrophobic and membrane bound or solubilised in micelles. In addition, the hydrophobic tunnel of MAGL is seen to be wider at top and narrowing down towards the catalytic site, while that of FAAH

is found to be narrower with a tiny exit at the top. According to Labar et al. (2010a), hydrophobic residues Leu148, Ala164, Leu176, Ile179, Leu205, Val207, Ile211, Leu213, Leu214, Val217 and Leu241 lining the MAGL tunnel interact with the arachidonoyl moiety of 2-AG and enhance MAGL substrate specificity for lipid substrates. The wider tunnel in MAGL also encourage selectivity towards ligands with bulkier hydrophobic rear that fits properly within the tunnel, making efficient hydrophobic contacts with the non-polar residues of the enzyme's tunnel (Chen, Sun, et al., 2014a; Labar et al., 2010a). the wider exit in MAGL also allows the bulky hydrophobic moiety of its ligand to diffuse out after cleavage. In the case of FAAH, ligands with smaller rear moiety would be preferred to avoid steric hindrance (Bowman & Makriyannis, 2009; Chen, Sun, et al., 2014a; Labar et al., 2010a; Morera et al., 2012).

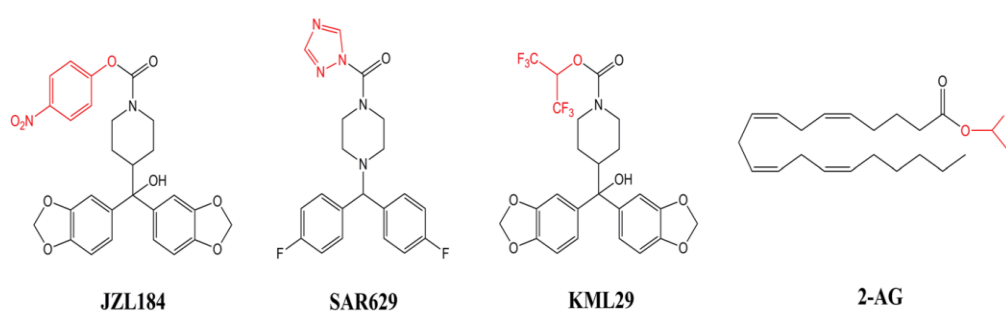


Figure 4: Chemical structures of JZL184, SAR629, KML29, and 2-AG. The reactive moieties of these compounds are highlighted in red. Adapted from (Chen, Sun, et al., 2014a)

Chen and co-workers had compared the docking poses of three MAGL inhibitors JZL184, SAR629, KML29 (Figure 4), to relate their structures to their selectivity for the enzyme and concluded that JZL184 and KML29 displays high affinity and selectivity for MAGL compared to FAAH, which showed greater affinity for SAR629. A bulky branched rear moiety is the preference for MAGL selectivity (Chen, Sun, et al., 2014a).

1.1.4 MAGL in diseases

There has been profound evidence for increased MAGL activity in certain physiological and disease states, including pain, metabolic disorders, inflammation, Alzheimer's disease, Parkinson's disease, and cancer (Chen, Sun, et al., 2014b; Jha et al., 2021a;

Mulvihill & Nomura, 2013; Rempel et al., 2017). The significant role of MAGL in these health conditions is believed to be associated with its function in lipogenesis (generation of fatty acids). A major physiological role of MAGL is known to be the biocatalysis of the hydrolysis of monoacylglycerol lipids (Baba et al., 2017; Bertrand et al., 2010; Hernández-Torres et al., 2014; Pascual et al., 2017, 2018) and the concomitant release of free fatty acids (FFAs), which are the precursors of prostaglandins and other inflammatory/signaling molecules (Pascual et al., 2018). In metabolic disorders such as obesity, higher levels of plasma free fatty acids, inflammatory cytokines, and lipid intermediates has been observed in patients (Heymsfield & Wadden, 2017), while decreased serum lipid levels and leanness were found to correlate with MAGL gene knockout in obese mice (Deng & Li, 2020). Extensive studies of the role of MAGL in inflammatory and neurodegenerative disorders such as Alzheimer's disease, multiple sclerosis, Parkinson's disease, and stroke, suggest it to be a putative biomarker and drug target in these diseases (Hernández-Torres et al., 2014). Its increased activity has been evidenced in these diseases (Hernández-Torres et al., 2014), while its inhibition or genetic knockout resulted to reduction in inflammatory eicosanoids (arachidonic acid and prostaglandins) levels in tissues and to observed neuroprotective effects in animal models of the diseases (Deng & Li, 2020). In cancer cells, free fatty acids were found to be necessary for the biogenesis of pro-tumourigenic signalling molecules such as lysophosphatidic acid (LPA) and prostaglandin E2 (PGE2) (Gupta et al., 2007; Mills & Moolenaar, 2003; Nomura et al., 2010). Nomura et al. (2010), Pascual et al. (2017) and Pascual, Domínguez and Benitah (2018), postulated that MAGL elevation could be one of the earliest indicators of metastasis in cancer cells. According to Pascual, Domínguez and Benitah (2018), pro-metastatic events occur early in cancer development and are the limiting steps in the metastatic transformation of cancer cells. Pascual et al., (2017), Makohon-Moore et al. (2017) and Pascual, Domínguez and Benitah (2018), also hypothesized that the driver mutations required for tumour initiation and metastasis are inherent in potential cancer cells. However, not all cells of this population eventually become cancerous (Pascual et al., 2018). A metabolic preconditioning of the microenvironment has been purported to be required to turn on the epigenetic mechanism necessary for tumour initiation and metastasis (Kaplan et al., 2005; Kinnaird et al., 2016; Peinado et al., 2012). This is to prepare the abnormal niche within which cancer cells can survive (Pascual et al., 2018). According to

Nomura et al. (2010) Pascual et al. (2017) Pascual, Domínguez and Benitah (2018) and Hu et al. (2020), successful early cancer detection is dependent upon the discovery, elucidation, and specific targeting of such markers of pro-tumourigenic metabolic conditioning such as MAGL. In addition, MAGL and other mycobacterium lipases have been found to be critical to the dormant but infectious stage of *Mycobacterium tuberculosis*, the causative organism of tuberculosis (TB), an infectious and contagious disease that has ravaged the world for decades (Daniel et al., 2011; Delorme et al., 2012; Grininger et al., 2021; Henry Boom et al., 2021). Although currently on the decrease in its spread, TB is still considered an infectious disease of significance to the world health organisation (WHO) (Grininger et al., 2021), a situation made worst by the prevalence of the multidrug resistant strains of its infectious agent. The MAGL variant of *Mycobacterium tuberculosis*, Rv0183 has been found to be upregulated during the inactive stage and is utilized in the breakdown of monoacylglycerols to glycerol and fatty acids (Grininger et al., 2021; Tallman et al., 2016). The fatty acids are then utilized by the pathogen to maintain its energy balance and cell membrane integrity (Grininger et al., 2021). Overexpression of some lipases was found to lead to increased bacterial virulence. MAGL targeted pro-drugs and probes is a promising strategy in drug development and treatment adaptation (Grininger et al., 2021).

1.1.5 Enzyme targeted small molecule fluorogenic substrate probes.

Small molecule fluorogenic probes (Figure 5) have gained tremendous research interest in chemical biology, medical and drug design fields (Kobayashi et al., 2010; Linder et al., 2011b). Some enzyme targeted small molecule fluorogenic probes (Figure 5) rely on the application of click chemistry to release the fluorescence of a pro-fluorophore targeted to a specific enzyme (Meimetis et al., 2014).

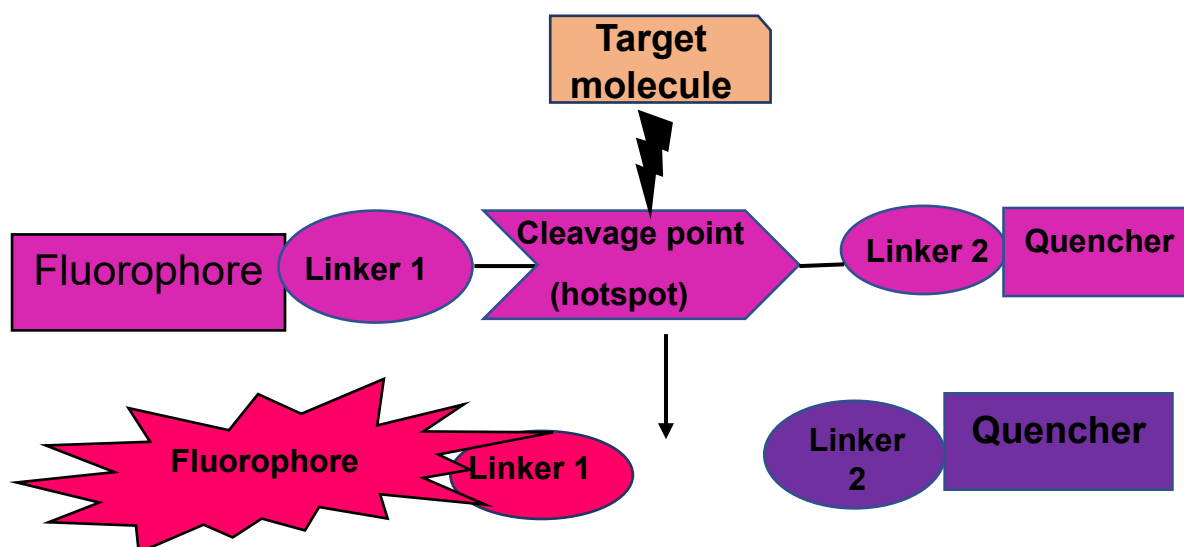


Figure 5: Basic structure and mode of activation of a small molecule fluorogenic probe comprised of two linkers, a fluorescent molecule (fluorophore), a fluorescence dampening molecule (quencher) and a point of action (cleavage 'hotspot') for an activator (e.g., an enzyme, an ion etc).

Such probes have been termed smart or activatable since, they remain inert until triggered by exposure to specific stimuli such as bond cleavage by an enzyme (Wu et al., 2020; Zhao et al., 2017a). They find a wide application in medicine, molecular biology, and environmental science. Small molecule, fluorogenic, imaging probes are designed as smart optical sensors within which a cleavable bond (the cleavage hot spot) for the enzyme of interest has been incorporated (Chyan & Raines, 2018; Jun et al., 2018a, 2018b; Mathur et al., 2020; Zhao et al., 2017b). This ensures that such probes provide information only on the target biomolecule (Lee et al., 2010; Rempel et al., 2017; Wu et al., 2020; Zhao et al., 2017a). The probes respond to enzymatic catalysis to illuminate the complex dynamics of biological processes, at a level and detail unmatched by any other techniques (Chyan and Raines, 2018). Fluorescent probes have been used to provide an understanding of the physiological roles of target molecules as they give information on the real time activities of specific biomolecules within cells (Soh, 2006).

First observed in 1950 as a visible emission from aqueous quinine solution, innovations in small molecule probe technology have enabled the development of

imaging equipment (Jun et al., 2018b; Zhao et al., 2017a), such as fluorimeters, super resolution fluorescence microscopy, flow cytometry, qPCR, UV-vis spectrophotometers, and techniques such as genome sequencing, throughput screening, and activity-based protein profiling (Jun et al., 2018b, 2018a). These probes offered the benefits of small size, ease of use and flexibility in molecular design and application (Jun et al., 2018b, 2018a). A major challenge in the use of imaging techniques became the lack of selectivity and specificity of the dyes which hampered their specific use in experiments. The discovery of specific enzyme probes has been the highlight of recent literature (Grimm et al., 2015; Rempel et al., 2017). The use of fluorescent proteins and peptides (large molecules such as genetically encoded green fluorescent proteins, GFP), favour the specific labelling of samples but, have reduced brightness and photostability (Grimm et al., 2015). The emergence of targeted studies/experiments has enabled the favourable photophysical qualities of small molecule probes to be built into fluorogenic ligands targeted at specific enzymes of interest (Grimm et al., 2015; Rempel et al., 2017). Cell based studies have shown that the expression levels of some protein enzymes differ in normal and abnormal health states (Glen et al., 2010; Nomura et al., 2010; Xu et al., 2015; Esteves and Cardoso, 2020). This finding in addition to the unique active site structures of enzymes has been explored in drug design, medicine, and bioresearch for the development of novel selective and specific small molecule probes as well as biomarkers, drugs, and diagnostic molecules, based on the cleavage hot spot (unique amino acid sequence required for catalysis), By exploring the techniques of virtual screening, and guided by the active site structure of MAGL, Tuccinardi et al. (2014), Poli et al. (2019) and Jha et al. (2021a) designed and optimised hit molecules for the development of selective MAGL inhibitors.

1.1.6 FRET

Fluorescence Resonance Energy Transfer, FRET, occurs when the emission spectrum of a donor fluorophore overlaps the absorption spectrum of an acceptor/quencher (Figure 6 A1 and Figure 6B) and the donor and acceptor are within a sufficiently close distance known as the Forster distance (Kozma & Kele, 2019a; Linder et al., 2011a).

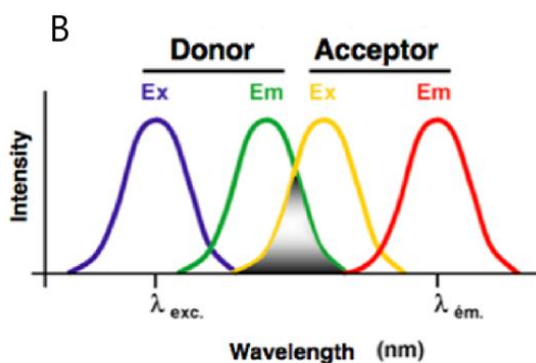
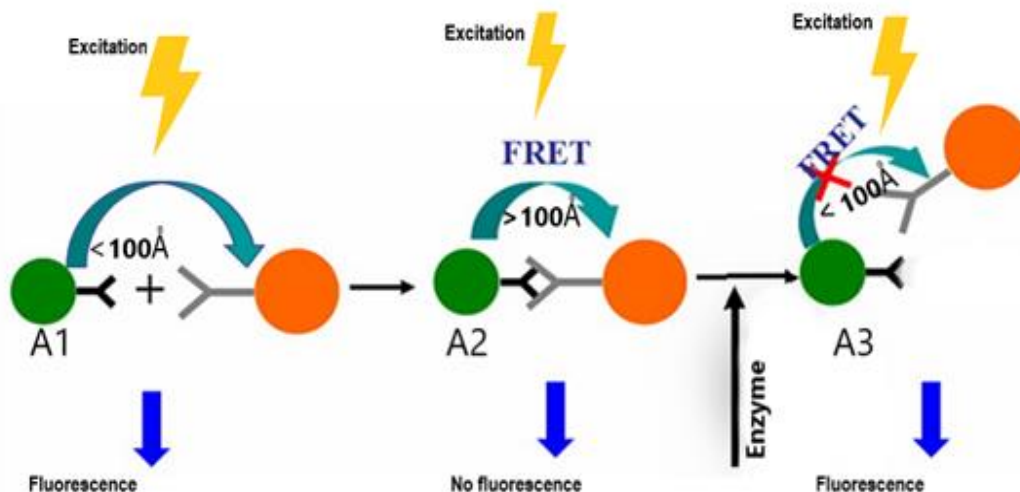


Figure 6: (A1 – A3) The principle of fluorescence energy transfer using a darkhole quencher. (B) Spectral overlap required for FRET to occur.

The energy absorbed by an acceptor/quencher can subsequently be released, through a variety of mechanisms depending upon the chemical nature of the acceptor/quencher (Patent, 2010). The captured energy is either released through fluorescence or through non-fluorescent means, including charge transfer and collision mechanisms, or a combination of such approaches. When a quencher release captured energy through non-fluorescent mechanisms, FRET is simply observed as a reduction in the fluorescence emission of the donor fluorophore (Patent, 2010). The efficiency of resonance energy transfer depends primarily on the Forster distance. Usually, this distance is about 10 to 100 \AA (Chen et al, 2013).

Linking a donor fluorophore to an acceptor through a spacer via covalent bonds achieves this distance in small molecule fluorogenic probes [Figure 6 (A2)] (Kozma & Kele, 2019a). In-situ separation of the fluorogenic dyad by the bond cleaving action of

an enzyme restores the fluorescence of the fluorophore (Kozma & Kele, 2019a) by increasing the distance between the donor and quencher [Figure 6 (A3)]. Dark hole quenchers which emit energy through non-fluorescent routes have the advantage of no background signal and high sensitivity of assays that utilize them (Linder et al., 2011a).

1.1.7 Rhodamine B derivatives in FRET probe design

Rhodamine-B is a widely used fluorophore in biological assays due to its favourable fluorescent qualities, relatively low cost, and ease of modification (Birtalan et al 2011). However, its major drawback is its limited fluorescence at high pH, as it undergoes a conformational change to its non-fluorescent spirolactam form under basic pH conditions ((Adamczyk & Grote, 2003) (Figure 7). Rhodamines having a carboxylic group at their 2' position tautomerises between the open and closed ring form (Figure 7 (A) and (B) respectively), based on the pH of their microenvironment (Kozma & Kele, 2019a).

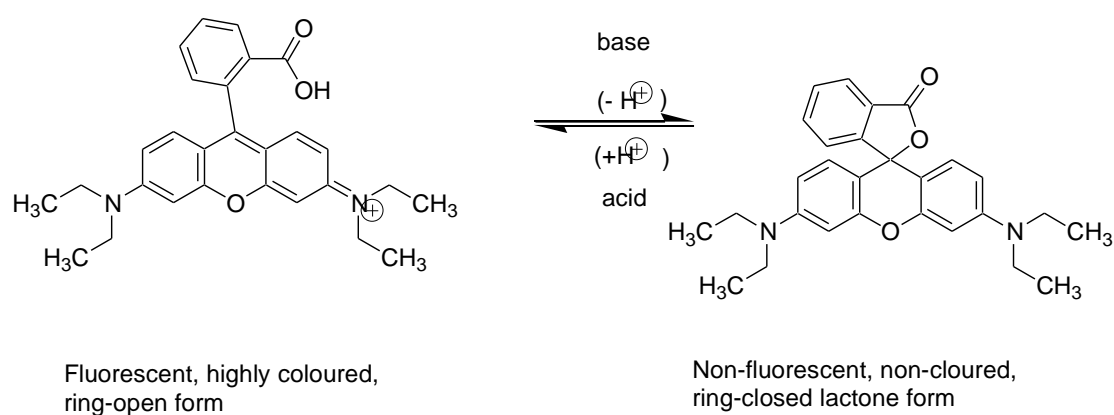


Figure 7: Polarity dependent fluorescent (A) and non-fluorescent (B) (spirolactam) forms of Rhodamine B. adapted from Nguyen and Francis (2003).

Interestingly, commercially available rhodamines could be conveniently modified by covalently linking a secondary amine to the carboxylic acid group (Nguyen & Francis, 2003a). This locks up the lactone into a ring- opened form by tertiary amide formation, thereby preventing cyclisation to non-fluorescent lactam forms (Mathur et al., 2019), allowing the creation of inexpensive functionalised Rho-B derivatives for bio and other imaging applications. Birtalan et al. (2011), observed an improved fluorescence at pH

(7.5 – 8.5), in peptoids labelled with a rhodamine B having tertiary amide linkage when compared to that attached to primary amines.

1.1.8 Previous work on MAGL substrate probes.

The critical roles which MAGL play in an array of health conditions: regulation of 2-AG levels in neurons through which it impacts on neurological conditions, increased activity in cancer malignancy as well as implication in obesity and other illnesses has necessitated the study and the discovery of potent MAGL probes and screening assays (Holtfrerich et al., 2010; Lauria et al., 2015; Miceli et al., 2019). This is to help understand its contributions to diseases and its potential as a drug target. Assay methods for the evaluation of MAGL activity include radiolabeling of substrates and the use of high-performance liquid chromatography (HPLC) coupled with UV or mass detection of catalysis products (Holtfrerich et al., 2010; King et al., 2009b; Lauria et al., 2015; Miceli et al., 2019; Minkkilä et al., 2009). Several research attempts have focused on developing reliable, straightforward, cost effective and sensitive as well as high throughput assays for investigating the MAGL pharmacological potentials in health disorders. Consequently, small molecule substrate probes of MAGL based on coumarin and resorufin fluorescent cores have been synthesised and evaluated.



Figure 8: A = hydroxy resorufin core, coumarin ester core. Adapted from (Lauria et al., 2015; Miceli et al., 2019)

Notably, Lauria, Casati and Ciuffreda (2015) successfully synthesised a long wavelength fluorogenic substrate probe containing a resorufin fluorophore (Figure 8a), having an appreciable sensitivity for MAGL, which could be applied to MAGL screening assays and in the identification of potential MAGL inhibitors. Miceli et al. (2019) have synthesised and characterized a substrate probe of MAGL with a red fluorescent coumarin core (Figure 8b) that is suitable for high throughput screening (HTS) of MAGL assays.

1.1.9 Previous work on anthraquinone quenched rhodamine-based FRET (substrate) probes.

In an earlier study in this lab, Mathur et al (2019), successfully synthesised a novel peptide substrate probe of the enzyme legumain, a putative protein biomarker of prostate and other forms of cancer. The project had focused on the development of selective legumain targeted substrates by utilizing the tertiary amide of proline to create a bio-active theranostic molecule comprising of rhodamine (as donor fluorophore) and an aminohydroxyanthraquinone (as darkhole quencher) FRET pair, having a high quantum yield and stability over a wide pH range. In this previous work by Mathur et al. (2019), rhodamine-B was linked to the tertiary amine of proline to lock it into its ring-opened form by tertiary amide formation, thereby preventing cyclisation to non-fluorescent lactam forms, analogous to the properties of piperazine derivatives of Rho-B (Beija et al., 2009). This gave rise to the highly fluorescent tripeptide reporter fluorophore, 4b (Rho-Pro-Ala-Asn-OH) (Figure 9a), which was then linked to the aminoanthraquinone derivative, 3 (quencher) (Figure 9b) to yield a novel aminoanthraquinone quenched FRET based substrate probe, 5 [Rho-Pro-Ala-Asn-PEG-AQ(4-OH)] (Figure 9c) of legumain, having a log D of +1.78 (Mathur et al., 2020). The novel molecule, 5 was shown to have been efficiently absorbed through the cell membrane and was activated by legumain to regenerate the rho-B fluorescence as the reporter fluorophore tripeptide (Rho-Pro-Ala-Asn-OH), as evidenced by the accumulation of fluorescence in the lysosomes of live PC3 cancer cells (Mathur et al., 2020). The substrate probe was also found to have sufficiently crossed the cell membrane to exert morphological changes consistent with apoptosis in prostate cancer cell lines (Mathur et al., 2020). Aminoanthraquinones are known to be non-fluorescent black hole quenchers (May et al., 2005), which have been found to function on fluorophores that emit in the visible region (Jernigan & Lawrence, 2013; Mathur et al., 2020) and also having the advantage of ease of syntheses.

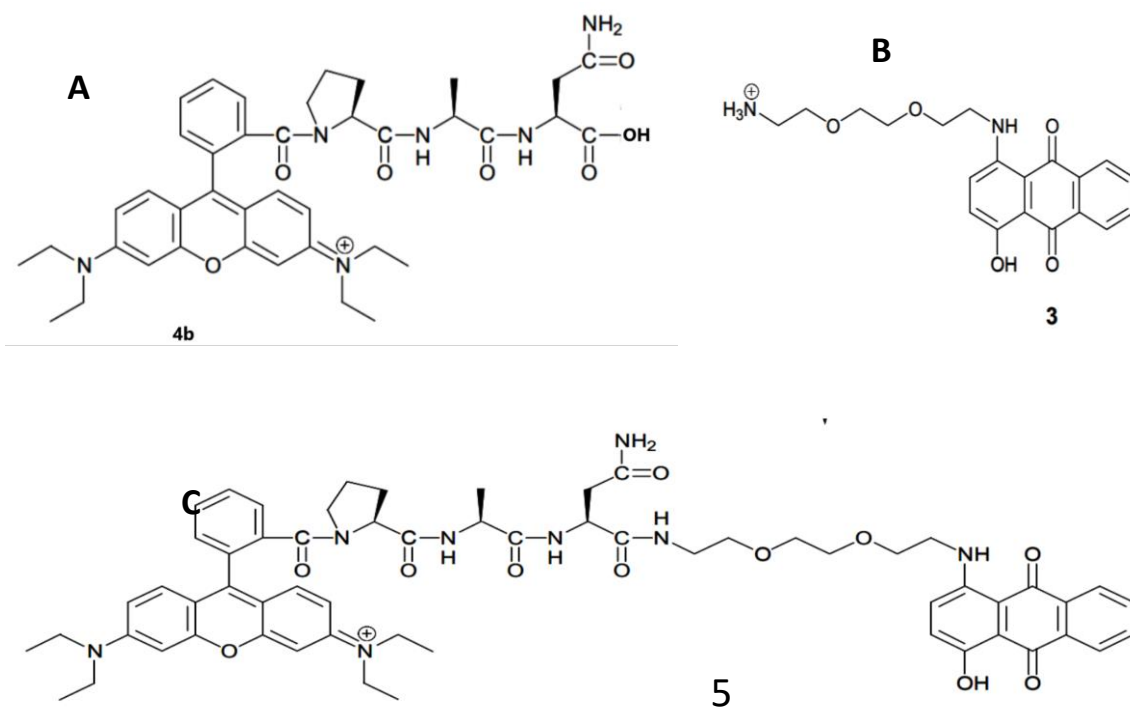


Figure 9: **A** = Rho-Pro-Ala-Asn-OH, a rho-B derived fluorophore (compound 4b) **B** = aminoanthraquinone derived dark hole quencher (compound 3) and **C** = [Rho-Pro-Ala-Asn-PEG-AQ(4-OH)], the legumain probe consisting of rho-B and anthraquinone FRET pair (compound 5).

Based on this previous work, a rhodamine-B based, aminohydroxyanthraquinone- quenched, FRET pair containing an ester bond (the MAGL cleavage hotspot) has been synthesised in the current research to yield an efficient MAGL probe that could be of relevance in pathology and bioresearch. The novel probe has the FRET probe advantage for minimised background fluorescence essential to biological assays.

Chapter 2: Results and Discussion

2.0 Design strategy for the novel MAGL probes

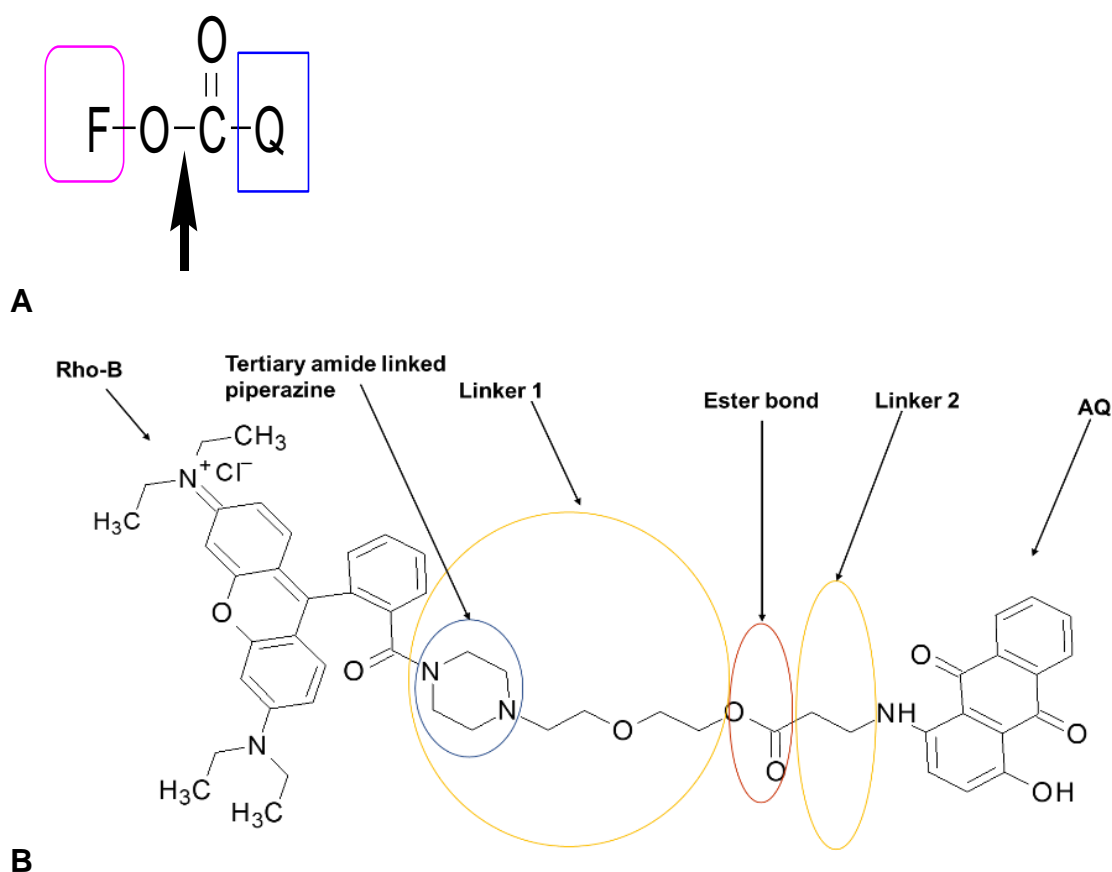


Figure 10 A: Simplified structures of the proposed MAGL probe (F = a fluorophore-labelled hydrophobic group; Q = a 'black hole' quencher-labelled group). **B:** Structure of the proposed MAGL probe with the component moieties in place.

Figure 10 A is an outline of the general structure of the target probes which have been synthesised in this research. These probes are designed and synthesised as FRET-based fluorogenic molecular probes consisting of a fluorescent donor molecule (the fluorophore), a fluorescence acceptor molecule (the dark quencher), and a targeting moiety (Kobayashi et al., 2010; Kozma & Kele, 2019b; Suzuki & Yokoyama, 2015). Both the fluorophore and the quencher must have overlapping fluorescence properties whereby, the emission wavelength of the fluorophore is within the absorption wavelength of the quencher. This ensures that most of the non-radiative energy loss from the donor is captured by the dark hole quencher. In the outline for this research,

the fluorophore (F in Figure 10 A) bears the alcohol group of the target ester bond while the quencher (Q in Figure 10 A) bears the carboxyl group of the ester bond. Figure 10 B is the structure of the proposed MAGL probe with the component moieties in place. Rho-B and AQ (aminoanthraquinone derivative) form the FRET pair. Based on previous work in this laboratory, (during which a rho-B and AQ FRET pair was successfully designed as substrate probe for the putative cancer biomarker, legumain) (Mathur et al., 2019), it was hypothesized that the incorporation of an ester bond cleavage hotspot for MAGL would yield a similar substrate probe for lipase enzyme. The piperazine moiety (linker 1) provides the tertiary amide for locking up the carboxylic acid of rho-B in a ring open form. This ensures the rho-B is not closed in high pH as demonstrated in previous studies (Mathur et al., 2019), thereby maintaining its fluorescence over a wider pH range. The linkers 1 and 2 positions the fluorophore and quencher at acceptable distance (usually 1 to 10 nm) for FRET to occur.

2.1 Synthesis and characterisation of compounds

The synthesis of the target probes preceded through the convergent method. The fluorophore component was first synthesised from its constituent compounds rhodamine B and 1-(2-hydroxyethyl) piperazine. The quencher components were synthesised via series of intermediates before being coupled to the fluorophore component using appropriate coupling agents. The convergent method was adopted to ensure the efficient synthesis of the desired probes.

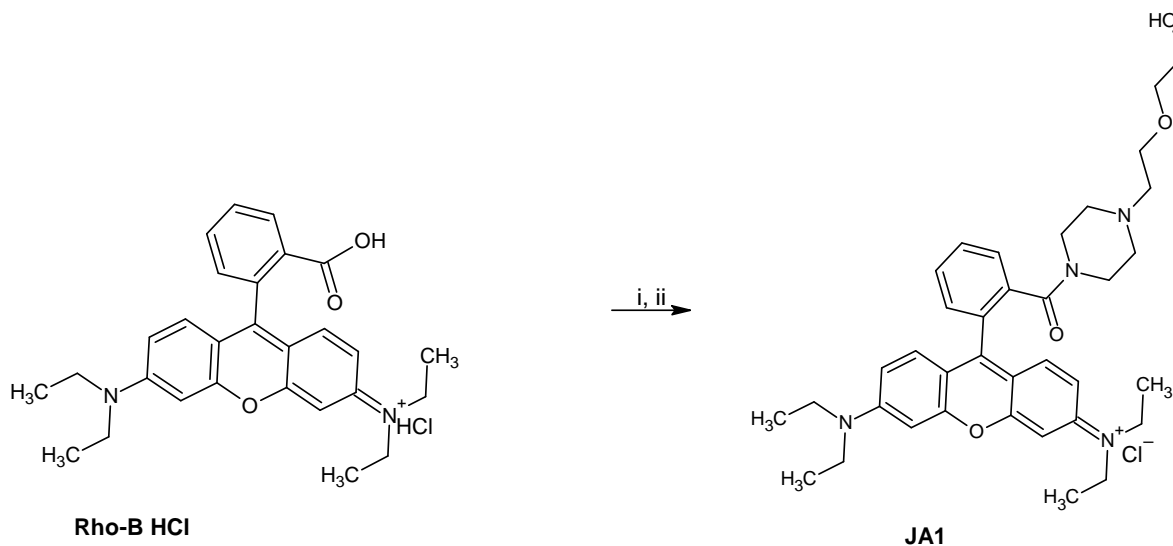
2.1.1 Synthesis of JA1 the rhodamine-B derived fluorophore 1 bearing the alcohol group of probes 1 and 2

Rhodamine B has been used as a parent chromophore in the design of probes for a wide range of applications. It is useful in biological assays as an efficient fluorophore due to its robustness, tunability through covalent linkage to other molecules, high quantum yield, and favourable spectral characteristics with regards to absorption and emission wavelengths, as well as cost effectiveness (Birtalan et al., 2011b; Mathur et al., 2020). In addition, modifications at its 2'-carboxylic acid group have been found to improve its usefulness for imaging across a wide pH range (Beija et al., 2009; Mathur

et al., 2020; Nguyen & Francis, 2003b). In earlier research in this laboratory, modifications at the 2' position were found to favour improved photostability in both the basic and acidic pH ranges, high relative fluorescence quantum yield, longer emission wavelength, and ease of synthesis (Mathur et al., 2020).

In this research, the synthetic procedures used to prepare the 2'-carboxylic acid modified rhodamine-B derivative, JA1, possessing a tertiary amide linkage and a free alcohol group, is as outlined in scheme -1. The synthetic procedures used were as adapted from literature (Bossi et al., 2006). 1-(2-Hydroxyethyl) piperazine was linked to the 2'-carboxylic acid of rhodamine B using the coupling agent HATU (Scheme 1). The joining of the tertiary amide of piperazine was intended to lock the rhodamine B in its ring opened form, preventing the formation of the non-fluorescent spiro lactam form in basic pH (Beija et al., 2009; Mathur et al., 2020; Nguyen & Francis, 2003b). The linked piperazine also furnished the alcohol group of the target ester bond, in probes 1 and 2.

Scheme 1- Reaction of 1-(2-hydroxyethyl) piperazine with rhodamine-B (HCl)



Reagents and conditions: (i) DIPEA, HATU, DMF, RT, 15 min (ii) 1-(2-hydroxyethyl) piperazine, DMF, RT, STR, 2h

Rhodamine B (1 eq) and HATU (1.5 eq) were combined in a small volume of DMF and the tertiary amine N,N-Diisopropylethylamine (DIPEA) (3.6 eq) was added. The solution was left standing for 15 minutes at room temperature to allow the coupling

agent to create an active ester in-situ, before 1-(2-hydroxyethyl) piperazine (1.1 eq) was added and the solution stirred at room temperature for 2 hours. The secondary amine of the piperazine performs a nucleophilic attack on the carbonyl carbon of the ester bond to complete the coupling (Figure 11).

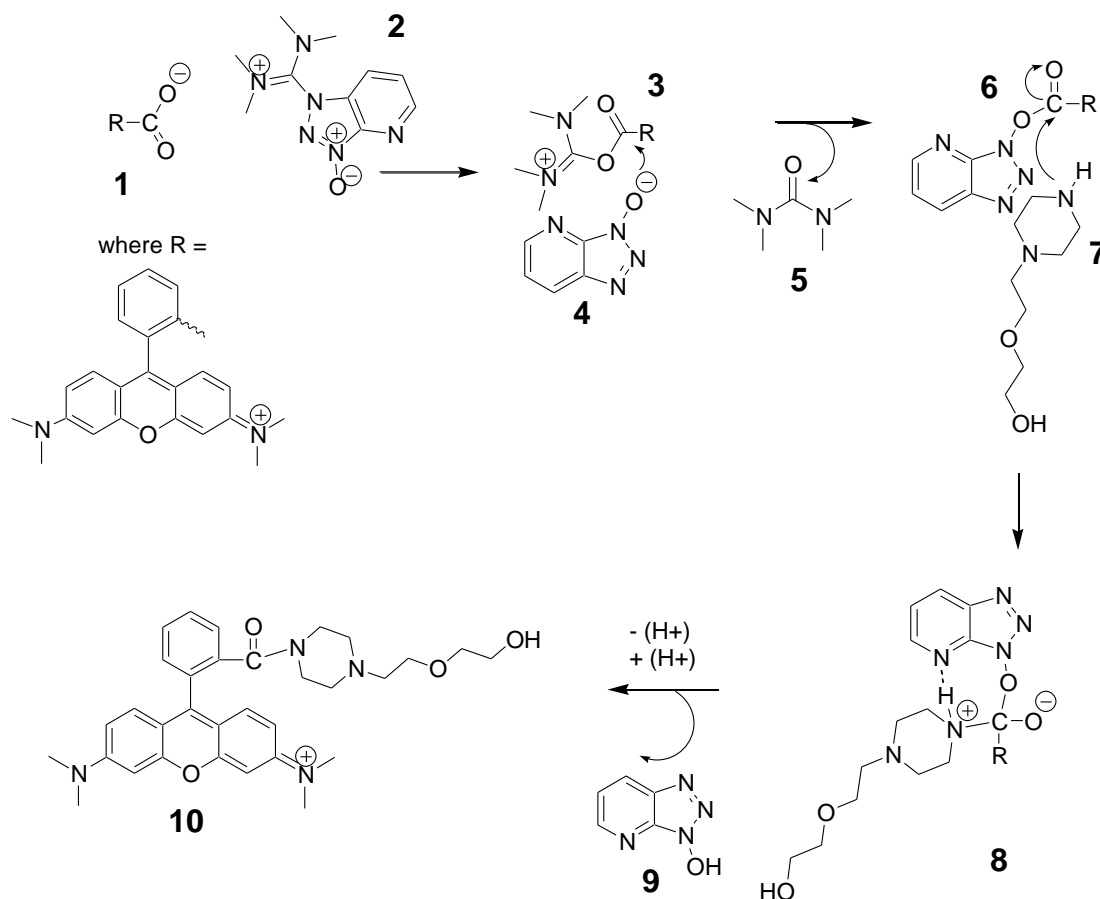


Figure 11: Mechanism of coupling reaction with HATU

The iminium salt HATU used as the coupling agent in this reaction functions in 4 steps to successfully couple a tertiary amine to carboxylic acid (Figure 11) (Joullié & Lassen, 2010). First, the carboxylate anion **1** reacts with HATU **2** to produce the O-acyl(tetra methyl)isouronium salt **3**. The OAt anion **4** then attacks the salt to create an active ester **6**. Nucleophilic attack from an amine **7** then results in the formation of the amide bond of the hydrogen-bonded 7-membered cyclic transition state intermediate **8** which rearranges to give the acylated product **10** (Carpino et al., 2000; Joullié & Lassen, 2010; Vrettos et al., 2017).

A small portion of the reaction mixture was partitioned between water and dichloromethane, with JA1 in the organic layer. This was to remove any by products and excess DMF, prior to monitoring the reaction progression using TLC. The spots on the TLC revealed the presence of a new major pink product, indicating that the reaction had gone to completion. A full-scale solvent extraction was performed on the rest of the product before being air dried at room temperature. A silica gel column (11.5 cm X 4.5 cm) was prepared using chloroform. The mobile phase was gradually increased in polarity and the product of interest, JA1 was eluted using chloroform: methanol; 95: 5. The resulting solution of the product was then dried under reduced pressure to obtain the title compound, JA1 as a deep pink solid, after solid precipitation in diethyl ether at 4°C. The product was vacuum dried to give a purplish pink crystalline solid of JA1.

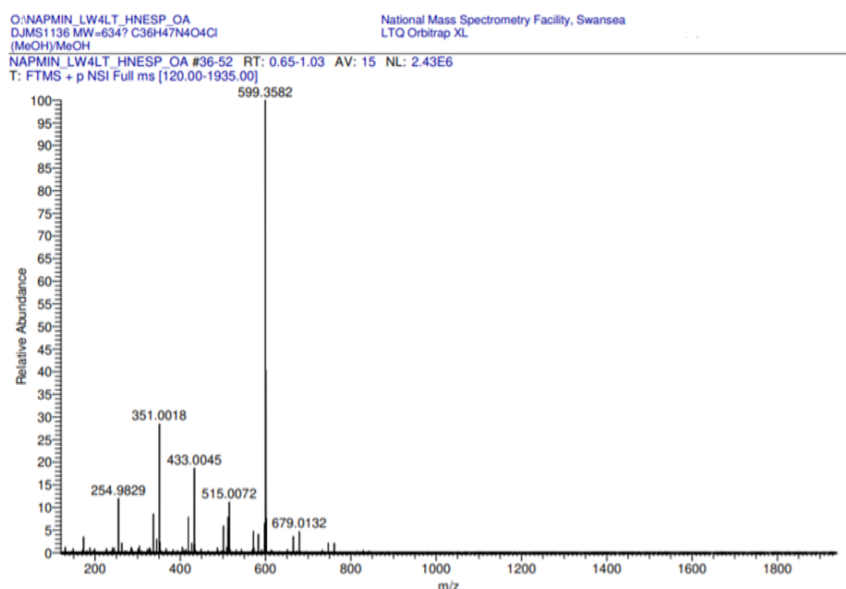


Figure 12: Results from the high-resolution electrospray (+) mass spectroscopy of JA1.

The structure of the compound was confirmed by electrospray (+) mass spectrometry (Figures 12 and 13). The synthesised compound JA1 is a salt with a relative molecular mass and structural formula of 634.3286 Daltons and C₃₆H₄₇N₄O₄Cl, respectively. The base peak in the electrospray (+) mass spectrum at m/z 599.3582 for the ion (M-Cl)⁺, as shown in the full spectrum (Figure 12) confirmed the expected molecular mass of 599.3592, for the cation component, C₃₆H₄₇N₄O₄⁺ (C₃₆H₄₇N₄O₄Cl minus Cl⁻).

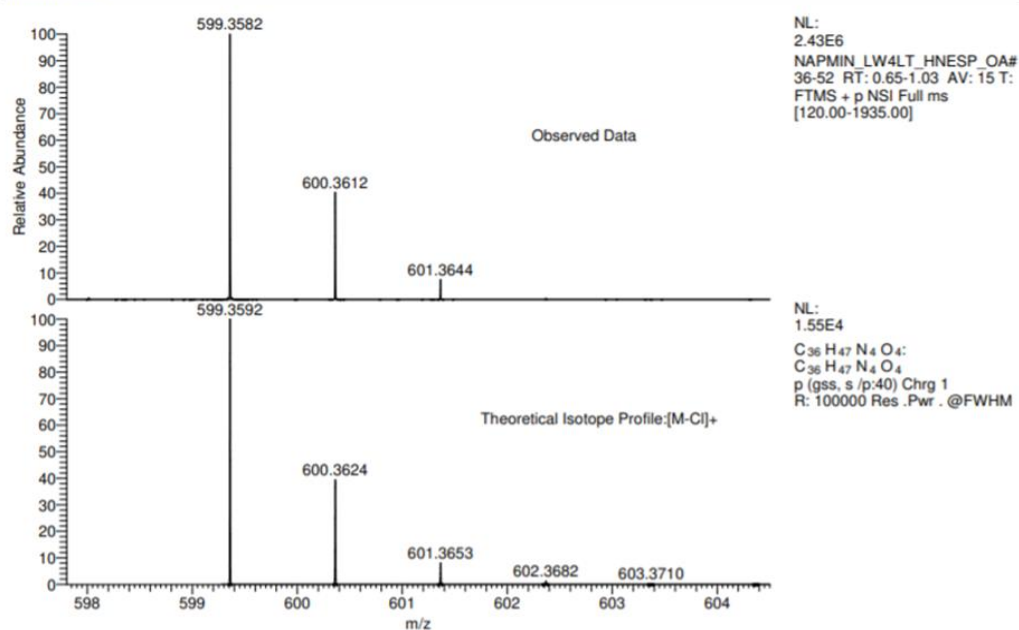


Figure 13: Mass spectroscopy results of PA compared to the theoretical isotope model.

A comparison between the experimentally observed data for $C_{36}H_{47}N_4O_4^+$ ($C_{36}H_{47}N_4O_4Cl$ minus Cl^-) and the theoretical isotope pattern, shows an excellent agreement between the experimentally observed data ($m/z = 599.3582$) and the expected value ($m/z = 599.3592$) (Figure 13).

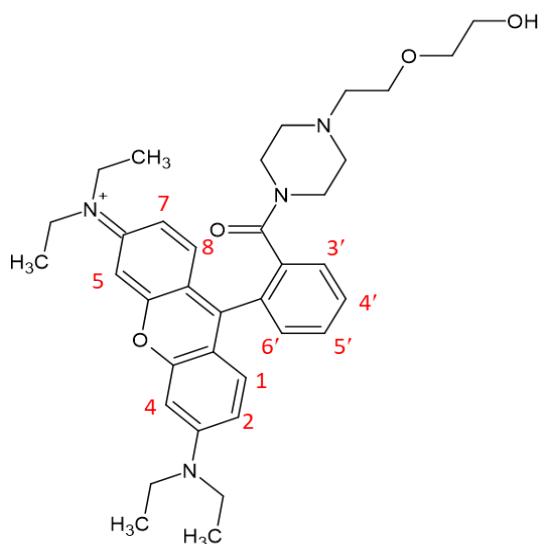


Figure 14: Structure of JA1 and numbering system for the rhodamine chromophore.

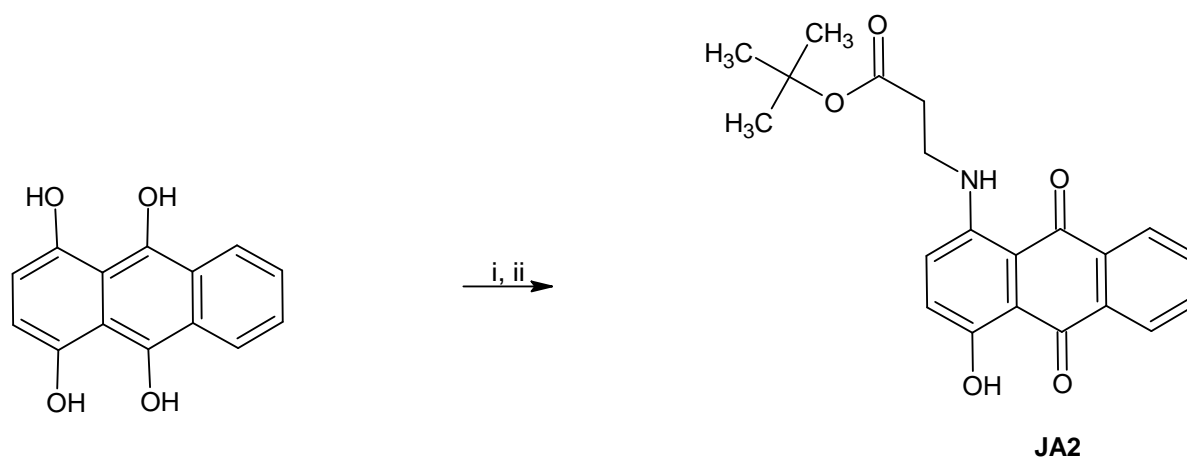
JA1 (Figure 14) was also characterized by its ^1H NMR spectrum (in $\text{DMSO-}d_6$), which showed a twelve-proton triplet for the four methyl groups of rhodamine at 1.23 ppm. Signals for the sixteen methylene groups of the piperiziny spacer and rhodamine were found between 2.21 and 3.65 ppm. In the aromatic region of the spectrum, H-4 and H-5 protons were assigned to a signal at 6.95 ppm and H-1, H-2, H-7, H-8 protons to a four proton multiplet at 7.13 ppm. Signals for the remaining four aromatic protons were found between 7.53 and 7.74 ppm.

The proton-decoupled, ^{13}C NMR spectrum showed signals for all carbon environments. A DEPT experiment differentiated the methylene CH_2 carbons from the methine CH carbons, with a signal at 12.93 ppm for the four rhodamine methyl carbons. Signals for the quaternary carbons were present in the proton-decoupled, ^{13}C NMR spectrum, but absent in the DEPT one. Signals between 41.59 ppm and 72.63 ppm were assigned to the methylene carbons. Signals for the aromatic methines and quaternary carbons were between 96.35 and 166.63 ppm.

2.1.2 Synthesis of tert-butyl 3-[(4-hydroxy-9,10-dioxo-9,10-dihydroanthracen-1-yl) amino] propanoate (JA2)

The synthesis of the quencher 1, the aminoanthraquinone component and bearer of the carboxylic acid group of the target probe 1 proceeded through a tert-Butyl protected intermediate, JA2. The hydroxyanthraquinone moiety of leucoquinizarin was linked to the amino ester, β -Alanine tert-Butyl Ester to obtain the hydroxy acid-derived aminoanthraquinone - JA2. (Y axis = RFI, X axis = nm)

Scheme 2: Reactions of β -Alanine Tert-Butyl Ester hydrochloride with anthracene - 1,4,9,10-tetrol (leucoquinizarine)



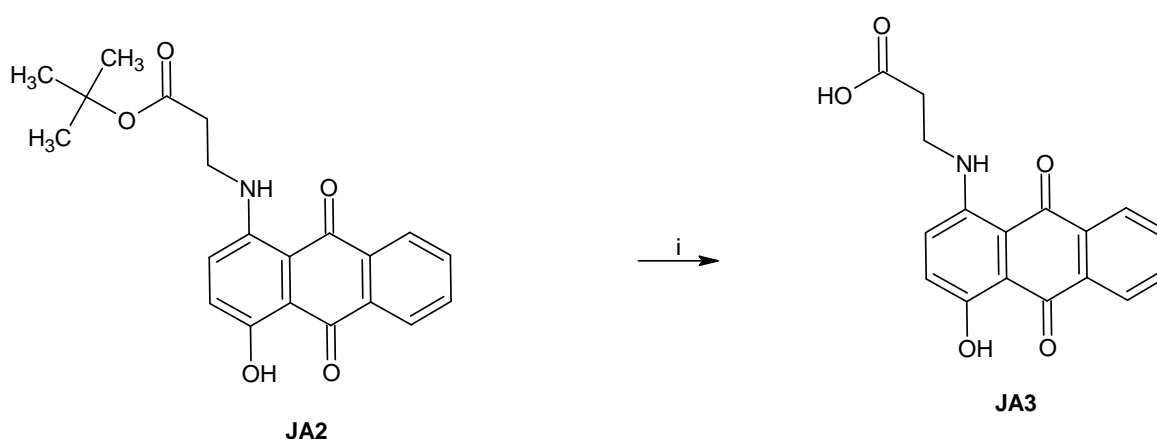
Reagents and conditions: (i) β -Alanine tert-Butyl Ester hydrochloride, K_2CO_3 , $95^\circ C$, RT (ii) aeration/oxidation

Anthracene-1,4,9,10-tetrol (leucoquinizarin) (1.0 eq), β -alanine tert butyl ester hydrochloride (3.5 eq) and anhydrous potassium carbonate (5.0 eq) were heated in DMF over a steam bath at $95^\circ C$ for 1 h. The resulting deep brown solution containing the 4,9,10-hydroxy substituted form of the product was aerated at room temperature with close monitoring by TLC which indicated that a major purple product has been formed. The anhydrous potassium carbonate served to remove the HCl conjugated to β -alanine tert butyl ester hydrochloride. The whole solution was partitioned between dichloromethane and water to obtain the organic layer, which was washed in a large excess of water (100%) and air dried at room temperature to give a deep purple solid of JA2. The crude extract was re-dissolved in dichloromethane and subjected to a silica gel chromatography (column size: 10 cm X 4.5 cm), using first 100% dichloromethane to remove the high running impurities from unreacted starting material, before gradually increasing the polarity of the solvent system. The major fractions were eluted using dichloromethane: ethyl acetate (19:1) and the solution was air dried overnight. The resultant solid was further subjected to column chromatography using dichloromethane (100%), and the pure fractions were eluted using dichloromethane: ethyl acetate (19:1). The solution was air dried to give a purple solid which was re-dissolved in dichloromethane before being evaporated at reduced pressure to give the title compound, JA2 as a purple solid.

2.1.3 Synthesis of 3- [(4-hydroxy-9,10-dioxo-9,10-dihydroanthracen-1- yl) amino] propanoic acid (JA3, Quencher 1)

The tert-Butyl group of JA2 was removed to generate the free carboxylic acid group of the anthraquinone-beta-alanine conjugate, JA3 which will be used in the subsequent esterification reaction during the synthesis of probe 1. The anthraquinone-beta-alanine conjugate will provide the carboxylic acid component of the ester bond that will be cleaved by lipase enzyme as well as part of the hydrophobic linker for easy access to the enzyme active site. Removal of tert-Butyl group was achieved by the addition of TFA as shown in Scheme 3.

Scheme 3: Reaction of trifluoroacetic acid (TFA) with tert-butyl 3-[(4-hydroxy-9,10-dioxo-9,10-dihydroanthracen-1-yl) amino] propanoate (JA2) to give JA3.



Reagents and conditions: (i) TFA, RT, 3h

TFA was added dropwise into PB until completely dissolved and the solution was left standing at room temperature for 3 hours, with close monitoring by TLC, which showed that a major purple product had formed, with no trace of the starting material remaining. Addition of TFA protonates the oxygen in the carbamate group to give a tert-butyl cation and a deprotonated form of TFA, while regenerating the acid group (in this case JA3). The resulting solution was evaporated at 40°C, under reduced pressure. The residue was solid precipitated in diethyl ether at 4°C overnight and vacuum dried to give the title compound JA3 as a purple amorphous solid.

Depending on the species present and the reaction conditions, the charged groups ($C_4H_9^+$ and TFA^-) may remain in solution or combine with any reactive group present in the reaction medium. This has the potential to give rise to undesired side reactions and by products, which may complicate purification of the desired product. This can be prevented using trapping agents, which mops up the ions generated during the reaction (Dias et al., 2005). However, in the present work, no trace of any other tangible compound was detected by the TLC, and all traces of impurities were removed in diethyl ether during solid precipitation.

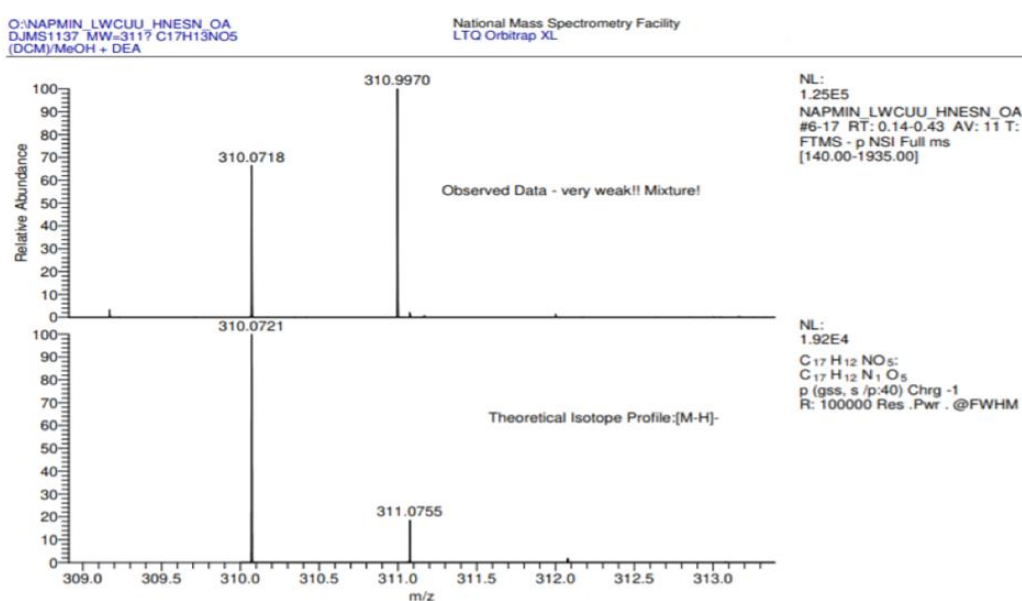


Figure 15: Mass spectroscopy results of JA3 compared to the theoretical isotope model.

The structure of the compound was confirmed by electrospray mass spectrometry in the negative mode. The signal for the expected species $(M-H)^-$ was at m/z 310.0718, this showed excellent agreement with the theoretical calculated at m/z 310.0721 (Figure 15), confirming a molecular mass (M) of 311.0794 Daltons for the whole compound.

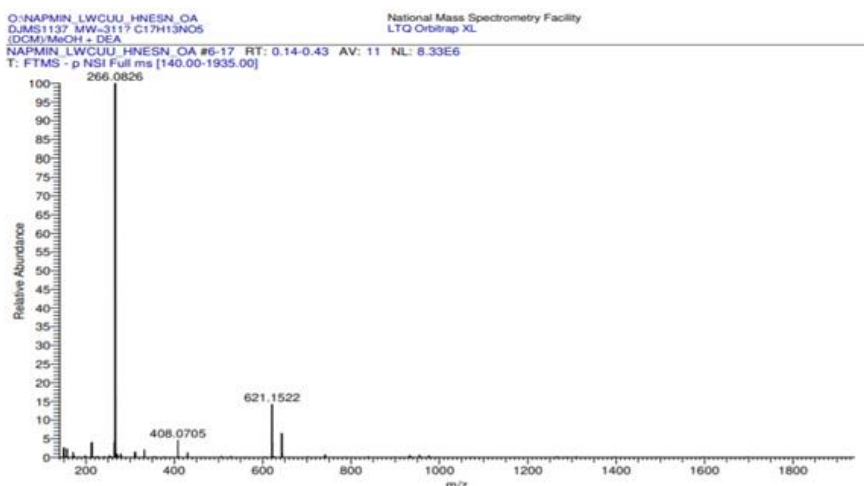


Figure 16: Results from the high-resolution electrospray (-) mass spectroscopy of JA3

The base peak was found to be at m/z 266.0826 (Figure 16), which corresponds to the species $(M - \text{COOH})^-$, while a second significant signal was found at m/z 621.1522 (Figure 16), equivalent to the species $(2M-H)^-$ and $(2M+\text{Na}-2H)^-$. The synthesised compound of mass M was ionised to the expected $(M-H)^-$ species but only in tiny amounts; it prefers to fragment into $(M - \text{COOH})^-$ and to dimerise into $(2M-H)^-$, and a small amount of $(2M+\text{Na}-2H)^-$ species.

JA3 was further characterized by its ^1H NMR spectrum (in $\text{DMSO-}d_6$). A two-proton triplet at 2.37 ppm and a two-proton quartet at 3.51 ppm were assigned to the methylene groups of beta alanine. The aromatic protons were all successfully assigned; H-2 and H-3 gave one proton doublets at 7.19 and 7.38 ppm, respectively. The H-6 and H-7 protons were present at 7.75 ppm and the H-5 and H-8 protons at 8.07 ppm. The anthraquinone amino group gave a triplet at 10.14 ppm. Two singlets at 12.31 and 13.46 ppm were assigned to the carboxylic acid and aryl hydroxy protons, respectively.

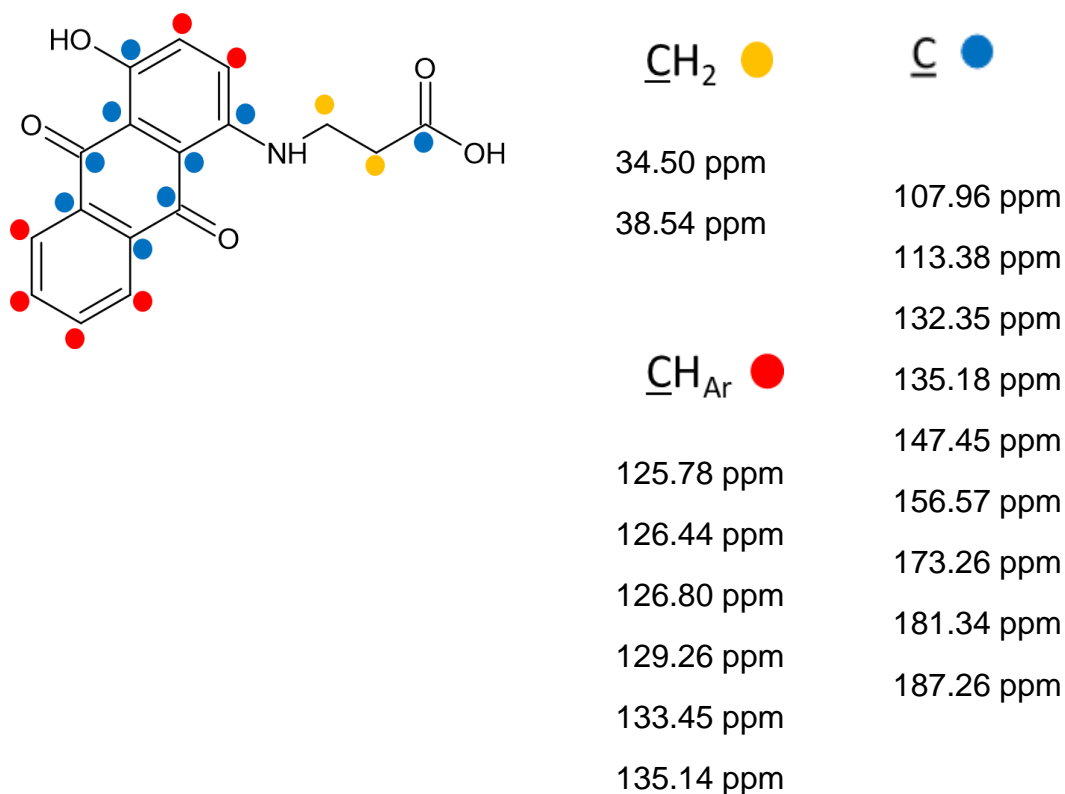


Figure 17: structure of JA3 and colour coding for the various kinds of protons and their chemical shifts (ppm)

Additionally, the proton-decoupled, ¹³C NMR spectrum showed signals for all carbon environments (Figure 17). A DEPT experiment clearly differentiated the six methine CH carbons, two methylene CH₂ carbons, with the remaining nine quaternary carbons being accounted for by difference.

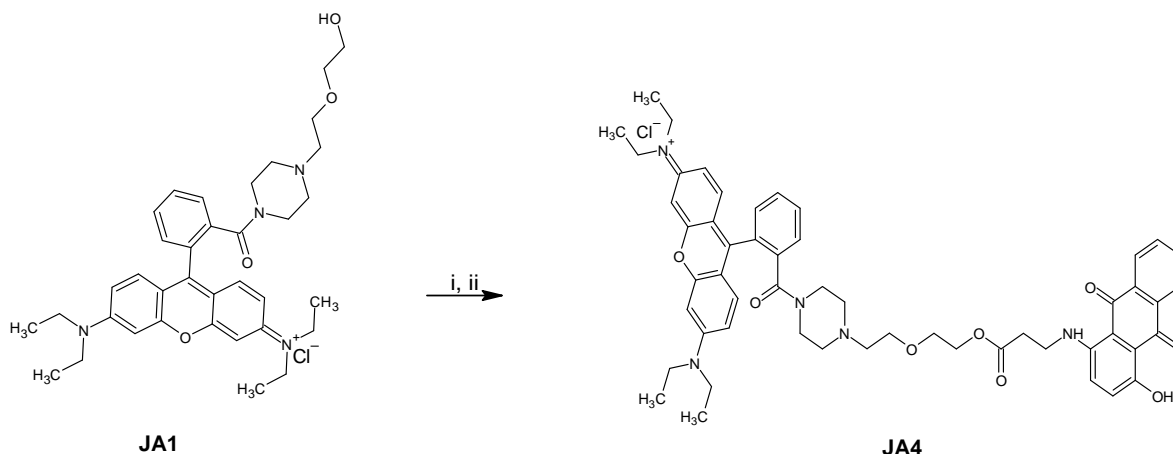
2.1.4 Synthesis of JA4 the rhodamine-B derived aminoanthraquinone (Probe 1)

2.1.4.1 Synthetic strategy

The novel lipase-activatable FRET probe 1, JA4 (scheme 4) was synthesised by the convergent method. The alcohol fragment, JA1 (fluorophore 1) was synthesised in several steps from rhodamine B before being joined to the carboxylic acid fragment, JA3 (quencher 1) synthesised from leucoquinizarin via a tert-Butyl protected intermediate, JA2.

The target rho-B derived fluorogenic probe of lipase, JA4 (Scheme 4) was finally synthesised by coupling the rhodamine-B derivative JA1 to the aminoanthraquinone JA3 using the coupling agent *N,N*-dicyclohexylcarbodiimine (DCC).

Scheme 4- Reactions of rhodamine_B derivative, JA1 (fluorophore 1) and 3-[(4-hydroxy-9,10-dioxo-9,10-dihydroxy-9,10-dioxo-9,10-dihydroanthracen-1-yl) amino] propanoic acid JA3 (quencher 1) to yield JA4.



Reagents and conditions: (i) JA3, DCC, DMAP, DCM, RT, 10 min (ii) DCM, RT, 1h.

3-[(4-Hydroxy-9,10-dioxo-9,10-dihydroanthracen-1-yl) amino] propanoic acid, JA3 (1.1 eq), *N,N*-dicyclohexylcarbodiimide, DCC (1.5 eq) and DMAP were dissolved in a small amount of DCM and the solution was left standing at room temperature for 10 minutes to activate the carbonyl carbon of JA3 (Scheme 4), allowing the coupling agent to generate the more active *O*-acylurea ester in-situ. The resulting solution was transferred into a solution of JA1 (1 eq) in a small amount of DCM and left standing at room temperature for 1 hour with close monitoring by TLC which showed that a major non-fluorescent (UV 254 nm), purple product had formed but, in small amount with a large excess of the starting material JA1 (the fluorophore component) remaining. An additional amount (0.2 eq) of JA3 (the anthraquinone component) was used to top up the reaction, which was then left standing at room temperature overnight to give an oily purple paste. A TLC check of the reaction showed that more of the target purple product was formed with little or no starting material remaining.

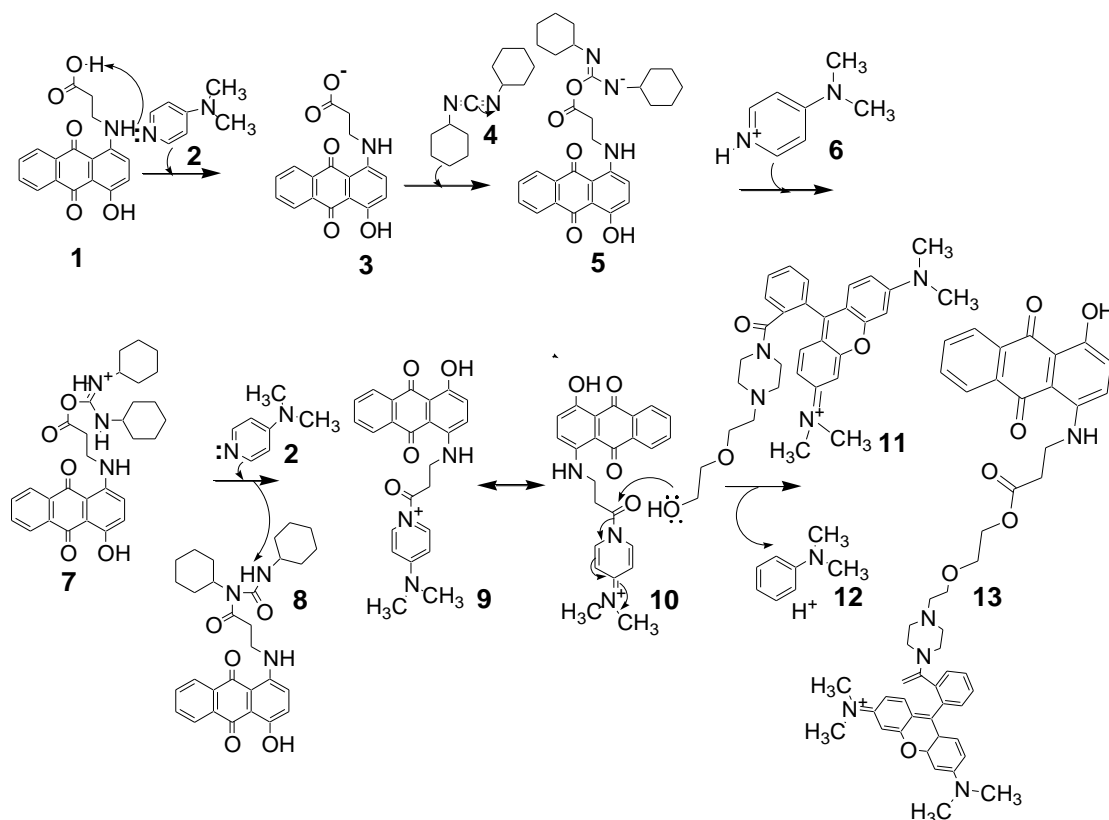


Figure 18: Mechanism of DCC/DMAP ester coupling

The carbodiimide *N,N*-dicyclohexylcarbodiimide (DCC) which was used as the coupling agent in this reaction functions in a 5-step reaction to effectively couple an alcohol group to carboxylic acid (Figure 18), while *N,N*-dimethylpyridine-4-amine (DMAP) serves as catalyst. Firstly, DMAP **2** protonates the carboxylic acid **1** to form the carboxylate anion **3**, which attacks DCC **4** to form the O-acyl anion **5**. The O-acyl anion abstracts a proton from 4-(dimethylamino) pyridin-1-ium **6** to form the O-acyl urea intermediate **7** (active ester). A cross coupling reaction between DMAP and the O-acylisourea forms the acyl pyridinium species 4-(dimethylamino)-1-propanoylpyridin-1-ium **9** and *N,N*-dimethyl-1-propanoylpyridin-4(1*H*)-iminium **10**. The *N,N*-dimethyl-1-propanoylpyridin-4(1*H*)-iminium form of the acyl pyridinium then reacts with the alcohol **11** to form the target ester **13**.

The reaction mixture was solubilized in DCM and filtered using sintered funnel before vacuum evaporation to remove residual DCU formed during the reaction from DCC. The filtrate was washed twice in a large excess of water (100%) and the organic layer air dried at room temperature to give a purplish pink solid of JA4. A silica gel column (was prepared using chloroform. The mobile phase was gradually increased in polarity

as follows: chloroform: methanol; 24: 1 + 0.1 acetic acid → chloroform: methanol; 19: 1 + 0.1 acetic acid. The product of interest, JA4 was eluted using chloroform: methanol; 9: 1. The resulting solution of the product was dried under reduced pressure to obtain the title compound, JA4 as a purplish pink solid, after solid precipitation in diethyl ether at 4°C. The product was vacuum dried to give a purplish pink amorphous solid of JA4.

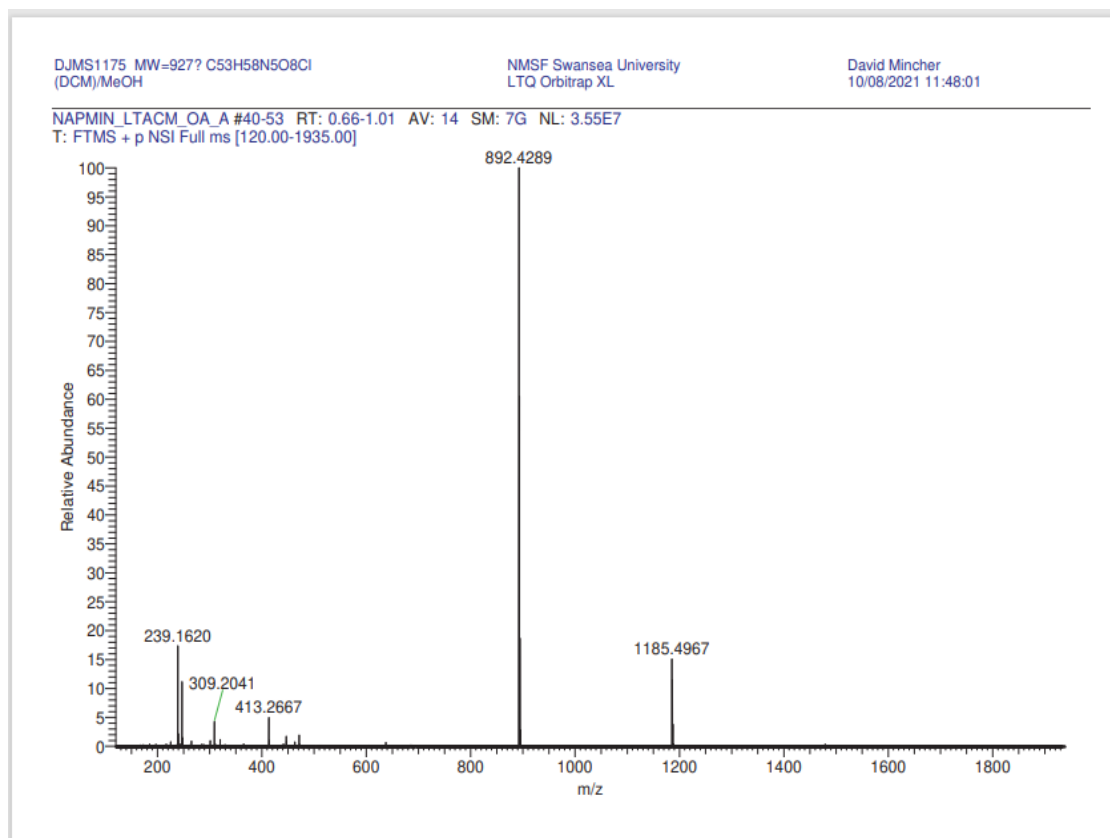


Figure 19: The high-resolution electrospray (+) mass spectrum of JA4

The structure of JA4 was confirmed by electrospray (+) mass spectrometry (Figures 19, 20, and 21). The synthesised compound is a salt with a relative molecular mass and structural formula estimated to be 928.50932 Daltons and $C_{53}H_{58}ClN_5O_8$, respectively. The base peak in the electrospray (+) mass spectrum at m/z 892.4289 for the ion $(M-Cl)^+$, as shown in the full spectrum (Figure 19) confirmed the expected molecular mass of 892.4280, for the cation component, $C_{53}H_{58}N_5O_8^+$ ($C_{53}H_{58}ClN_5O_8$ minus Cl).

NAPMIN_LTACM_OA_A #40-53 RT: 0.66-1.01 AV: 14 SM: 7G NL: 1.75E6
T: FTMS + p NSI Full ms [120.00-1935.00]

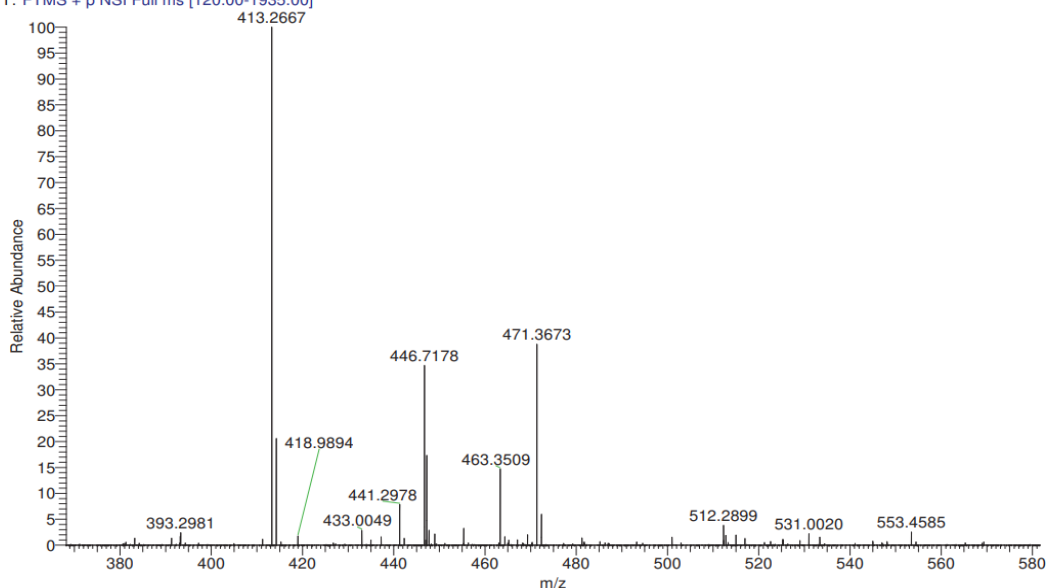


Figure 20: Expanded spectrum of the high-resolution electrospray (+) mass spectrum of JA4 the doubly charged species.

Furthermore, there is the presence of a doubly charged ion at m/z 446.7178 (Figure 20), corresponding to the species $C_{53}H_{58}N_5O_8^{2+}$ which because of the x-axis being mass/charge ratio - appears at half its real mass.

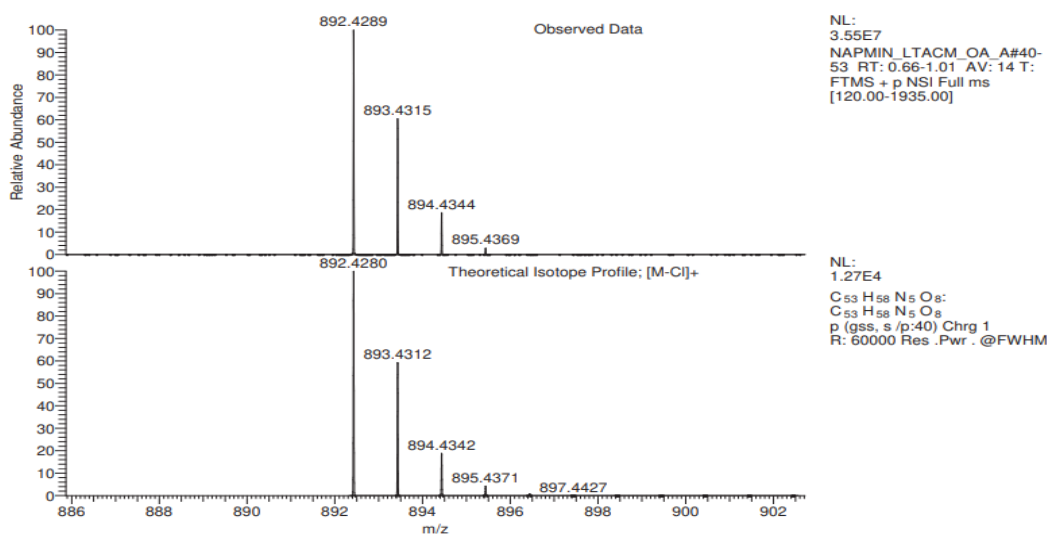


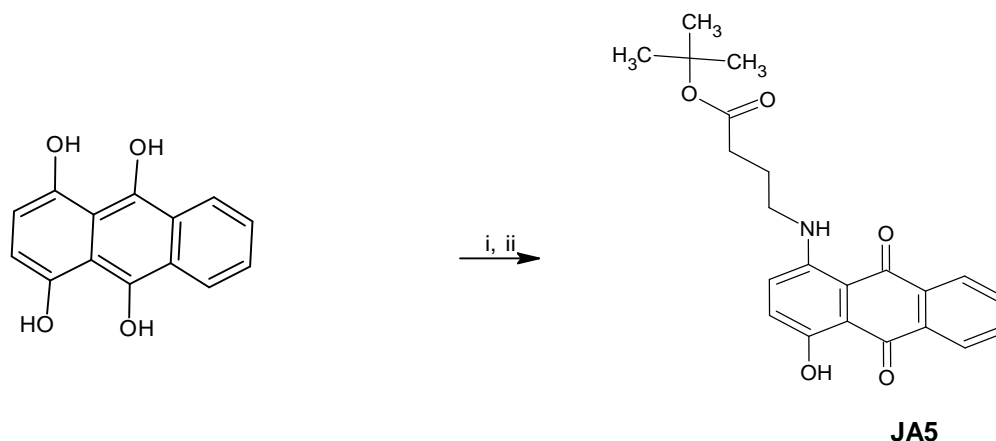
Figure 21: Mass spectroscopy results of JA4 compared to the theoretical isotope model.

A comparison between the experimentally observed data for $C_{36}H_{47}N_4O_4^+$ ($C_{36}H_{47}N_4O_4Cl$ minus Cl^-) and the theoretical isotope pattern, shows an excellent agreement between the experimentally observed data ($m/z = 892.4289$) and the expected value (892.4280) (Figure 21).

JA4 was also characterized by its 1H NMR spectrum (in $DMSO-d_6$). Characteristic signals belonging to both anthraquinone, and rhodamine chromophores were observed. For example, there was a twelve-proton triplet at 1.19 ppm for the four rhodamine methyl groups. Two very de-shielded one proton singlets were seen at 10.30 and 13.59 ppm for the anthraquinone amino and hydroxyl groups, respectively.

2.1.5 Synthesis of tert-butyl 3-[(4-hydroxy-9,10-dioxo-9,10-dihydroanthracen-1-yl) amino] propanoate (JA5)

Scheme 5: Synthesis of tert-butyl 3-[(4-hydroxy-9,10-dioxo-9,10-dihydroanthracen-1-yl) amino] propanoate (JA5)



Reagents and conditions: (i) *tert*-butyl 4-aminobutanoate, K_2CO_3 , $95^\circ C$, RT

(ii) aeration/oxidation

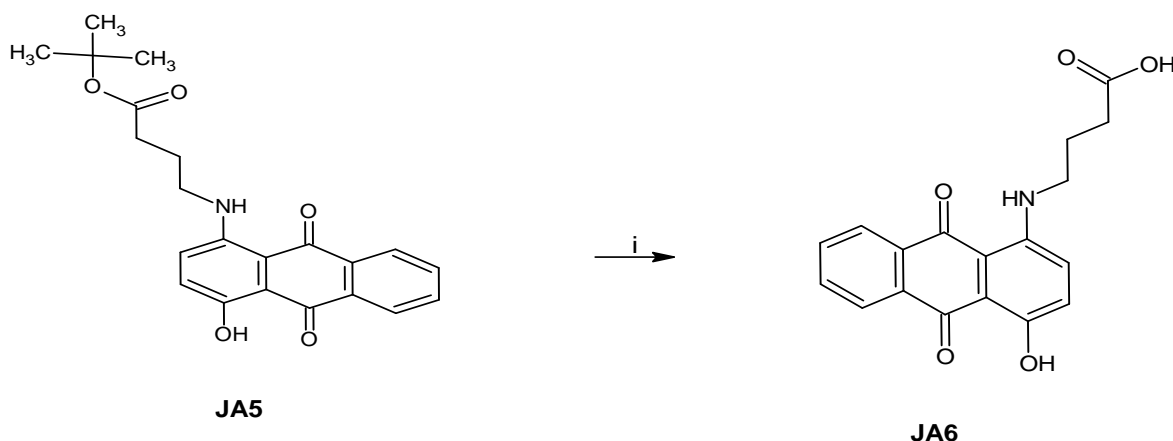
The synthesis of quencher 2 (JA5), the aminoanthraquinone component and bearer of the carboxylic acid group of the target probe 2 (JA7) also proceeded via a *tert*-Butyl protected intermediate, JA5. The hydroxyanthraquinone moiety of leucoquinizarin was linked to the amino ester, *tert*-butyl 4-aminobutanoate to obtain the aminoanthraquinone derivative JA5.

Anthracene-1,4,9,10-tetrol (leucoquinizarin) (1.0 eq), *tert*-butyl 4-aminobutanoate (3.5 eq) and anhydrous potassium carbonate (5.0 eq) were heated in DMF over a steam bath at 95°C for 1 h to obtain a brownish purple solution containing the 4,9,10-hydroxy substituted form of the product. A TLC check of the mini extract (organic layer) indicated that a major purple product has been formed. The whole solution was partitioned between dichloromethane and water to obtain the organic layer, which was washed in a large excess of water (100%) and air dried at room temperature. A silica gel column (4 cm X 10 cm) was prepared using chloroform. High running impurities of the starting material were eluted using 100% chloroform while the product of interest JA5 was eluted using chloroform: methanol; 19: 1. The resulting solution of the product was then dried under reduced pressure to obtain the title compound, JA5 as a purple solid.

2.1.6 Synthesis of 4-[(4-hydroxy-9,10-dioxo-9,10-dihydroanthracen-1-yl)amino]butanoic acid, JA6 (Quencher 2)

The *tert*-Butyl group of JA5 was removed to generate the free carboxylic acid group of the anthraquinone-beta-alanine conjugate, JA6 which will be used in the subsequent esterification reaction during the synthesis of probe 2. The anthraquinone-beta-alanine conjugate will provide the carboxylic acid component of the ester bond that will be cleaved by lipase enzyme as well as part of the hydrophobic linker for easy access to the enzyme active site. Removal of *tert*-Butyl group was achieved by the addition of TFA as shown in Scheme 6.

Scheme 6: Reaction of trifluoroacetic acid (TFA) with tert-butyl 3-[(4-hydroxy-9,10-dioxo-9,10-dihydroanthracen-1-yl) amino] propanoate (JA5) to give JA6



Reagents and conditions: (i) TFA, RT, 3h

The tert-Butyl group of JA5 was removed to generate the free carboxylic acid group of the anthraquinone-tert-butyl aminobutanoate conjugate. The resulting anthraquinone-aminobutanoic acid, JA6 will be used in the subsequent esterification reaction during the synthesis of probe 2. The anthraquinone-aminobutanoic acid, will provide the carboxylic acid component of the ester bond that will be cleaved by lipase enzyme as well as part of the hydrophobic linker for easy access to the enzyme active site. Removal of tert-Butyl group was achieved by the addition of TFA as shown in Scheme 6. TFA was added dropwise into JA5 until completely dissolved and the solution was left standing at room temperature overnight. A TLC check was performed on the resulting solution which showed that a major purple product had formed, with no trace of the starting material remaining. The resulting solution was evaporated at 40°C, under reduced pressure. The residue was solid precipitated in diethyl ether at 4°C overnight before being vacuum dried to obtain the title compound JA6 as a purple solid.

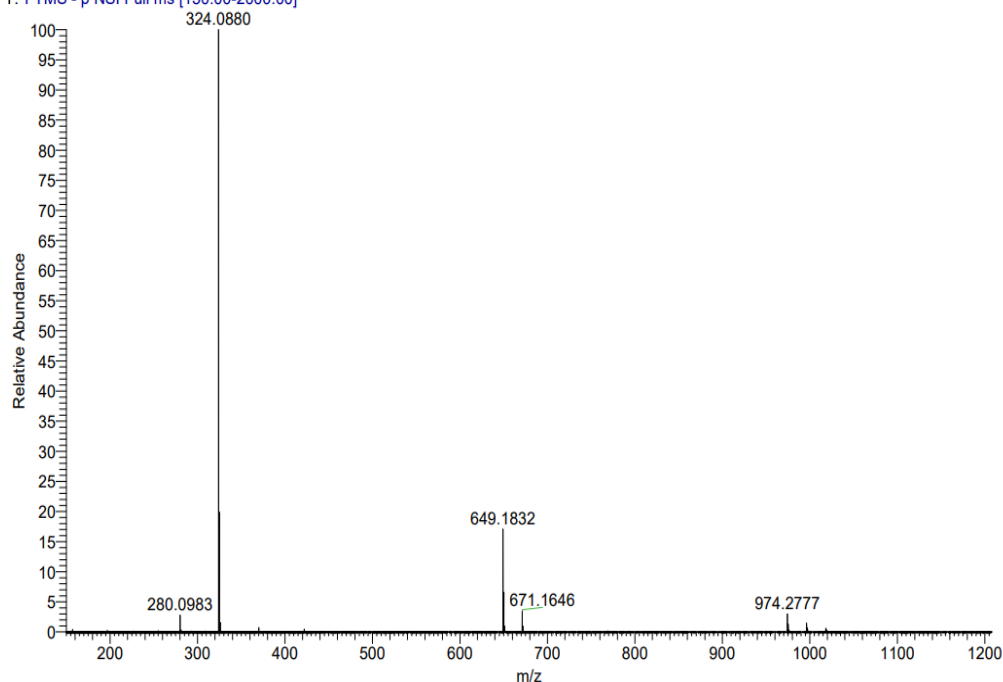
NAPMIN_LRHP_OA_A #36-52 RT: 1.97-2.41 AV: 17 SB: 16 0.27-0.68 SM: 7G NL: 9.32E7
T: FTMS - p NSI Full ms [150.00-2000.00]

Figure 22: Mass spectroscopy results of JA6 compared to the theoretical isotope model.

The structure of JA6 was confirmed by electrospray mass spectrometry in the negative mode. The main signal was at $m/z = 324.0880$ and is for the expected species $(M-H)^-$, this showed excellent agreement with the theoretical calculated at $m/z 324.0877$ (Figure 22), confirming a molecular mass (M) of 325.0956 Daltons for the whole compound. There was also a significant signal at $m/z = 649.1832$ for the dimer $(2M-H)^-$ and another lesser amounts at $m/z = 671.1646$ and $m/z = 974.2777$ corresponding to $(2M+Na-H)^-$ species and the trimer $(3M-H)^-$ respectively.

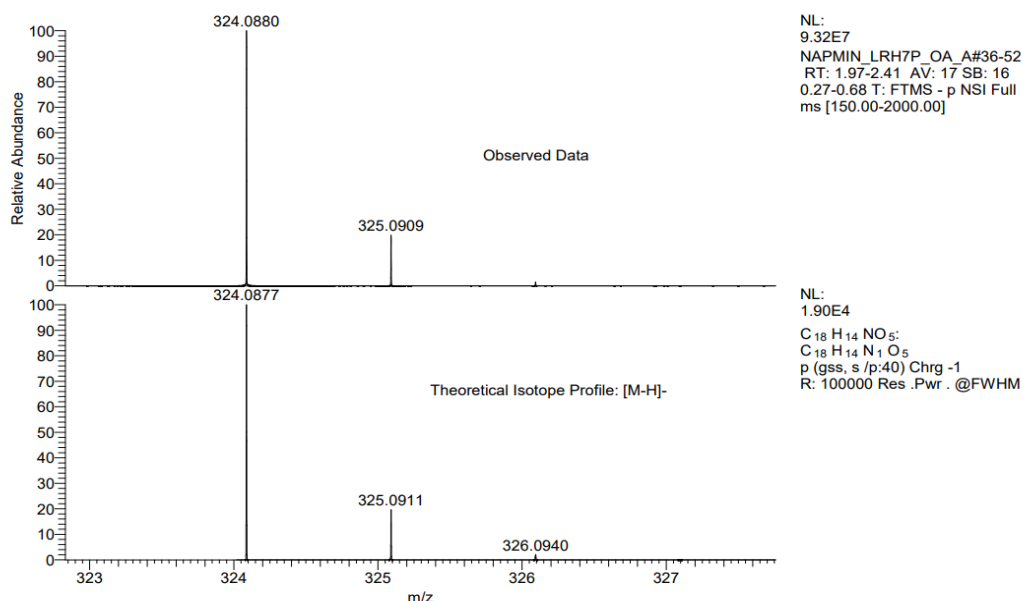


Figure 23: Results from the high-resolution electrospray (-) mass spectroscopy of JA6

A comparison of the experimentally observed data for Molecular Formula: C₁₈H₁₄NO₅⁻ ([M-H]⁻) and the theoretical isotope pattern, also shows an excellent agreement between the experimentally observed data ($m/z = 324.0880$) and the expected value (324.0877) (Figure 23).

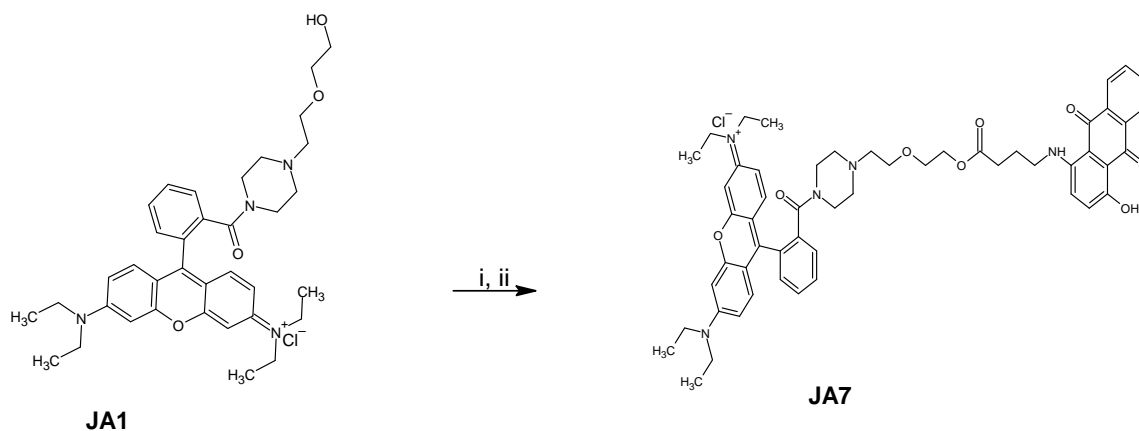
2.1.7 Synthesis of rhodamine-B derived aminoanthraquinone, JA7 (probe 2)

2.1.7.1 Synthetic strategy

This novel lipase-activatable FRET probe 2, JA7 (scheme 7) was also synthesised by the convergent method. The alcohol fragment, JA1 (fluorophore) was synthesised from rhodamine B as earlier described in section 2.1.1 (Scheme 1), before being joined to the carboxylic acid fragment, JA6 (quencher 2) synthesised from leucoquinizarin via a tert-Butyl protected intermediate, JA5.

The target rho-B derived fluorogenic probe of lipase, JA7 (Scheme 7) was synthesised by coupling the rhodamine-B derivative JA1 to the aminoanthraquinone JA6 using the coupling agent *N,N*-dicyclohexylcarbodiimine (DCC).

Scheme 7- Reactions of rhodamine_B derivative, JA1 (fluorophore 1) and 4-[(4-hydroxy-9,10-dioxo-9,10-dihydroanthracen-1-yl)amino] butanoic acid, JA6 (quencher 2) to yield JA7



Reagents and conditions: (i) JA6, DCC, DMAP, DCM, RT, 10 min (ii) DCM, RT, 1h.

4-[(4-Hydroxy-9,10-dioxo-9,10-dihydroanthracen-1-yl)amino] butanoic acid, JA6, (1.1 eq), *N,N*-dicyclohexylcarbodiimide, DCC (1.5 eq) and DMAP were dissolved in a small amount of DCM and the solution was left standing at room temperature for 10 minutes to activate the carbonyl carbon of JA6 (Scheme 7), allowing the coupling agent to generate the more active *O*-acylurea ester in-situ. The resulting solution was transferred into a solution of JA1 (1 eq) in a small amount of DCM and left standing at room temperature for 1 hour with close monitoring by TLC which showed that a major purple, non-fluorescent (UV 254 nm) product had formed but, in small amount with a large excess of the starting material JA1 (the fluorophore component) remaining. An additional amount (0.2 eq) of JA6 (the anthraquinone component) was used to top up the reaction, which was then left standing at room temperature overnight. A TLC check of the reaction showed that more of the target purple product was formed with little or no starting material remaining.

The carbodiimide *N,N*-dicyclohexylcarbodiimide (DCC) was also used as the coupling agent in this reaction which progressed in 5-steps as earlier outlined in section 2.1.4, Figure 18.

The whole solution was partitioned between dichloromethane and water to obtain the organic layer, which was washed in a large excess of water (100%) and air dried at room temperature to give a purplish pink solid of JA7. A silica gel column was prepared using chloroform. The mobile phase was changed as follows: chloroform: methanol;

96: 4 + 0.4 (4drops) acetic acid → chloroform: methanol; 97: 3 + 0.3 (3 drops) acetic acid. The product of interest, JA7 was eluted using chloroform: methanol; 97: 3 + 0.3 acetic acid. The resulting solution of the product was dried under reduced pressure to obtain the title compound, JA7 as a purplish pink solid, after solid precipitation in diethyl ether at 4°C. The product was vacuum dried to give a purplish pink amorphous solid of JA7.

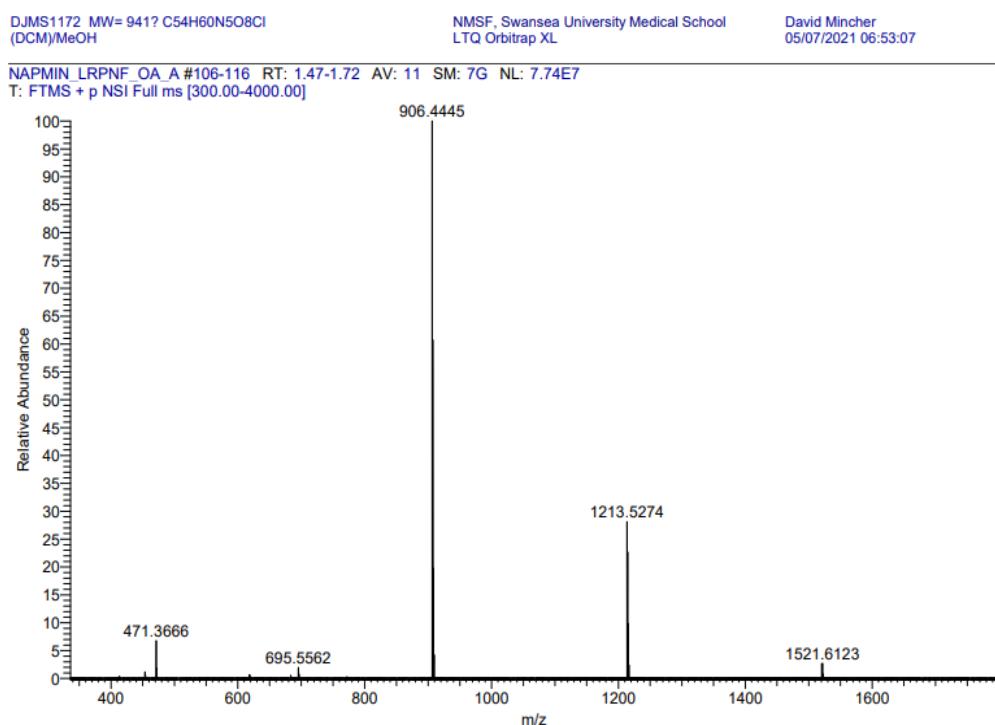


Figure 24: Results from the high-resolution electrospray (+) mass spectroscopy of JA7.

The structure of JA7 was confirmed by electrospray (+) mass spectrometry (Figures 24 and 25). The synthesised compound is a salt with a relative molecular mass and structural formula estimated to be 942.5359 Daltons and C₅₄H₆₀ClN₅O₈, respectively. The base peak in the electrospray (+) mass spectrum at m/z 906.4445 for the ion (M-Cl)⁺, as shown in the full spectrum (Figure 22) confirmed the expected molecular mass of 906.4436, for the cation component, C₅₄H₆₀N₅O₈⁺ (C₅₄H₆₀ClN₅O₈ minus Cl⁻).

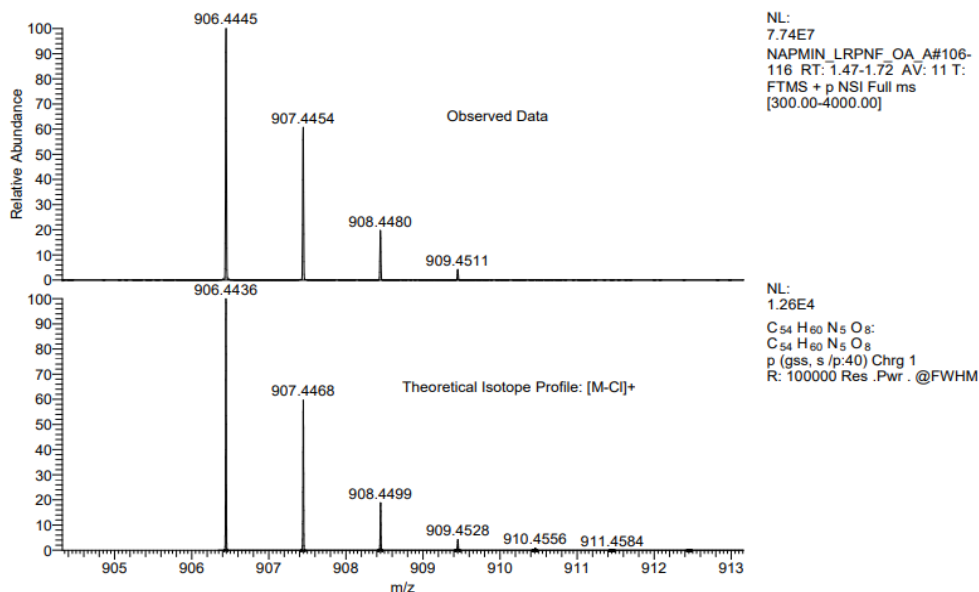


Figure 25: Mass spectroscopy results of JA7 compared to the theoretical isotope model.

A comparison between the experimentally observed data for $C_{54}H_{60}N_5O_8^+$ ($C_{54}H_{60}ClN_5O_8$ minus Cl^-) and the theoretical isotope pattern, shows an excellent agreement between the experimentally observed data ($m/z = 906.4445$) and the expected value (906.4436) (Figure 25).

2.2 UV-Vis Absorption Assay for JA1

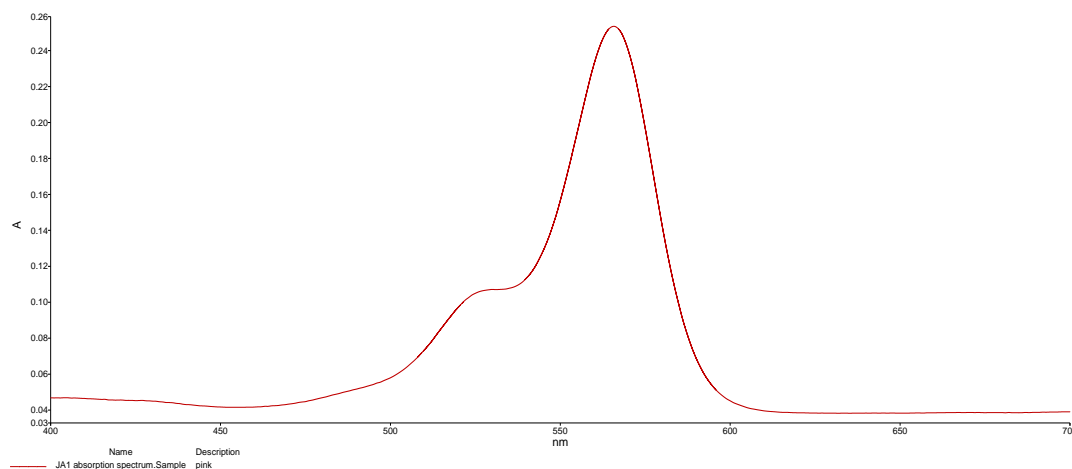


Figure 26: Absorbance spectrum of JA1. $\lambda_{maxabs} = 566$ nm (X axis = nm)

UV-Vis absorption assay was applied to JA1 to establish the wavelength of its maximum absorption (λ_{maxabs}), which will be used as its excitation wavelength when obtaining its emission spectrum. The test solution of JA1 was prepared from a 1mg/mL stock in DMSO by diluting in PBS to a final concentration of 2 μ M in a 3mL quartz cuvette. The scan wavelength was set within the visible spectrum (400 – 700nm). The data obtained (Figure 26), showed the λ_{maxabs} for JA1 to be approximately 566nm. This λ_{maxabs} of 566 nm indicates that JA1 is an efficient fluorophore for use in biological assays involving blood samples where it is desirable to avoid background fluorescence from naturally occurring endogenous fluorophores, like hemoglobin, water, and lipids which usually absorb at wavelengths close to 600 nm (Kabayashi, 2011; Linder et al., 2011).

2.3 FRET studies

FRET occurs when there is a spectral overlap between the emission spectrum of the fluorophore (donor) and the absorption spectrum of the quencher (acceptor), and both the quencher and the fluorophore are in acceptable distance (1 nm – 10 nm) for FRET to occur (Chen et al, 2013).

2.3. 1 Demonstration of spectral overlap between the donor chromophore, JA1 and the acceptor chromophores, JA3 and JA6.

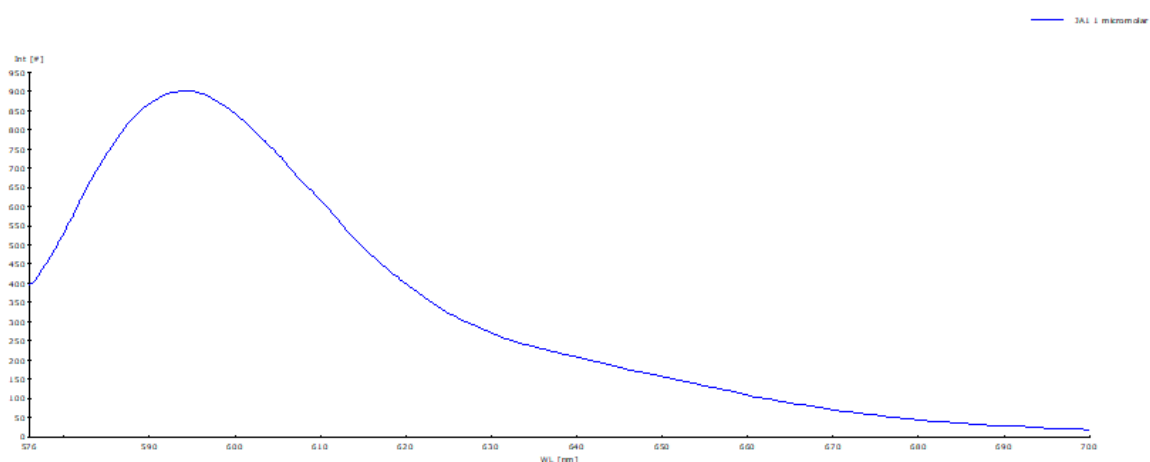


Figure 27: Fluorescence spectrum of JA1 (Y axis = RFI, X axis = nm)

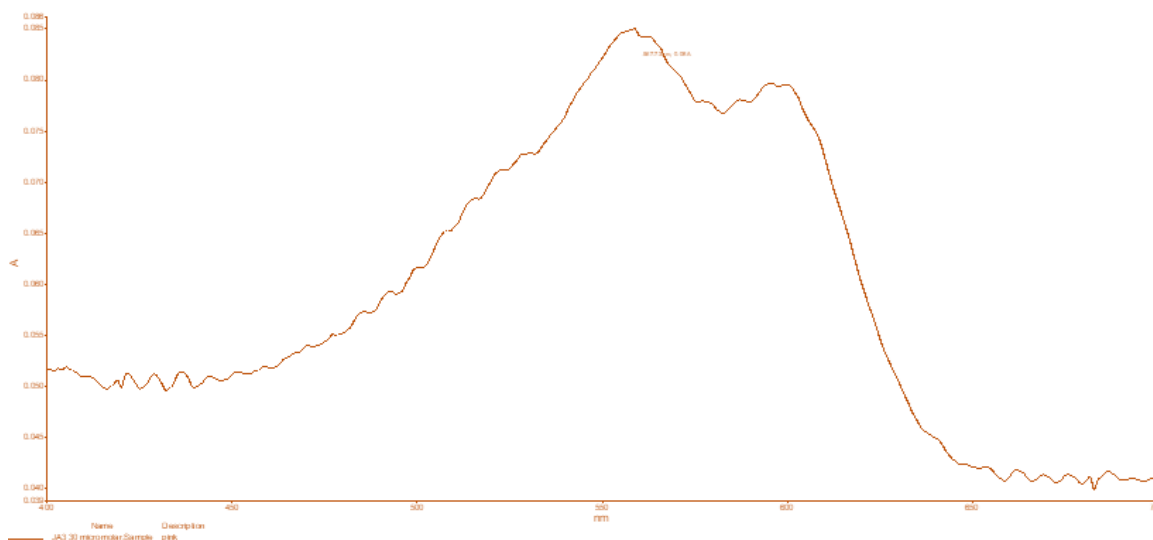


Figure 28: Absorption spectrum of JA3 (X axis = nm)

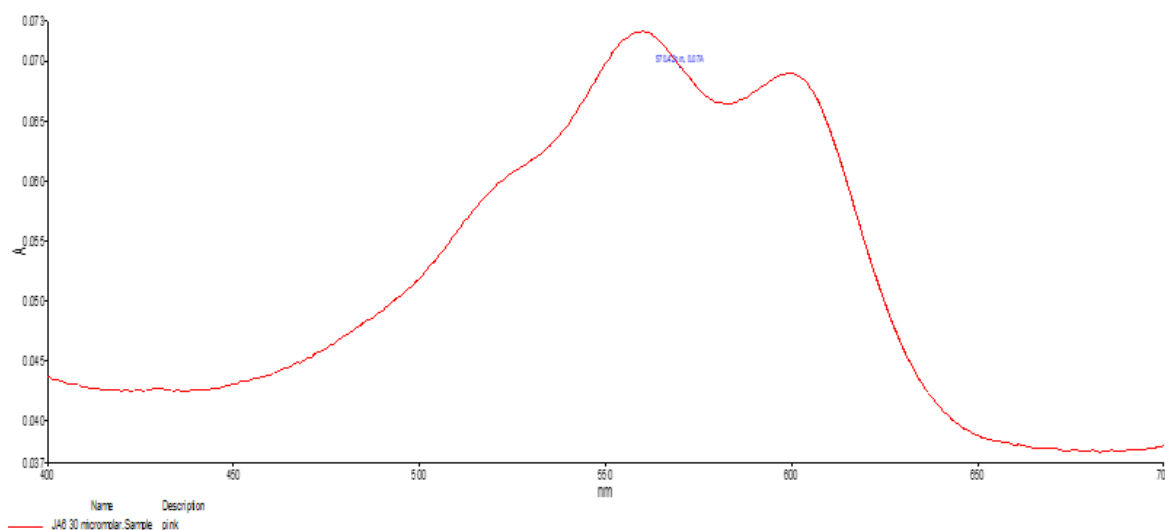


Figure 29: Absorption spectrum of JA6 (X axis = nm)

This FRET study was employed to establish that there is an overlap between the emission spectrum of the fluorophore, JA1 and the absorption spectra of the quenchers, JA3 and JA6. The fluorescence spectrum of JA1 was obtained using the PerkinElmer fluorescence spectrometer LS 55; scan speed 1200 nm/min, λ_{ex} 566, its earlier established λ_{maxex} , λ_{em} 400 – 700 nm, excitation slit, and emission slit widths

both set at 5.0. The test solution was made by diluting a 1mg/mL stock in DMSO to a final concentration of 1 μ M in PBS using a 3mL quartz cuvette. The data obtained (Figure 27) showed that the $\lambda_{\text{max}_{\text{em}}}$ for JA1 was 594 nm.

The UV-Vis absorption spectra of the quenchers (fluorescence acceptors) JA3 (Figure 28) and JA6 (Figure 29) were obtained using the PerkinElmer UV/Vis spectrometer Lambda 25 instrument. The test solutions were prepared by diluting their 1mg/mL stock solutions in DMSO to a final concentration of 30 μ M in PBS in a 3mL quartz cuvette. The scan wavelength was set within the visible spectrum (400 – 700nm). The data obtained (Figures 28 and 29) showed that both quenchers absorbed maximally between 520 and 620 nm with their $\lambda_{\text{max}_{\text{abs}}}$ as 567 nm and 570 nm respectively. This means that both quenchers can absorb within the excitation wavelength (566 nm) (Figure 26) as well as the maximum emission wavelength (594 nm) (Figure 27) of JA1 and are therefore able to capture most of the fluorescence that could be emitted by the fluorophore, JA1.

An overlay of the emission spectrum of JA1 and the absorption spectra of JA3 (Figure 30) and JA6 (Figure 31) all showed good overlap between the emission and absorption spectra. The spectral overlap between JA1 and JA3 occurred between 576 nm and 620 nm while that of the JA1 and JA6 pair occurred between 576 nm and 621 nm.

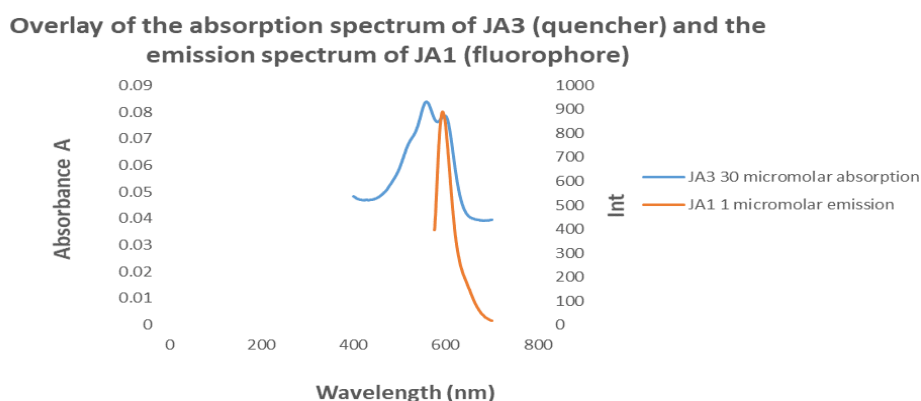


Figure 30: Absorption spectrum of JA3 vs emission spectrum of JA1, showing good overlap between the spectra.

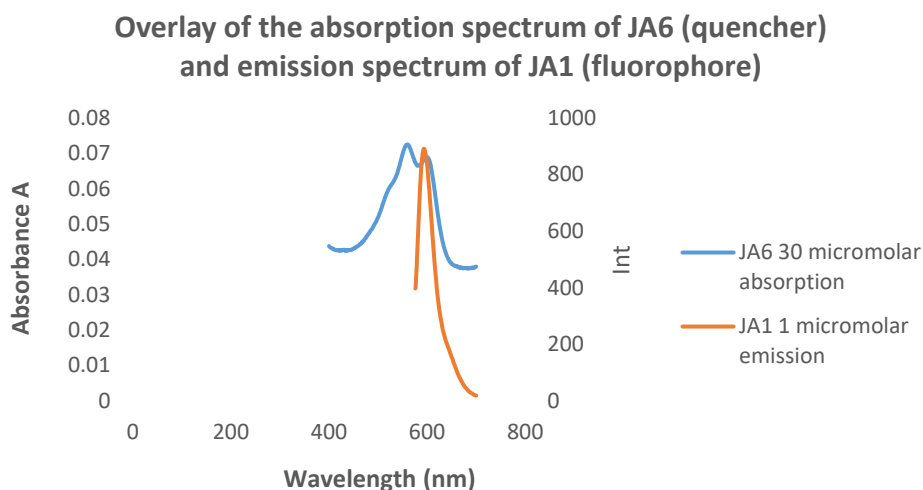


Figure 31: Absorption spectrum of JA6 vs emission spectrum of JA1, showing good overlap between the spectra.

2.3.2 Fluorescence Spectroscopy Assay

The potential of the anthraquinone dark hole quenchers 1 (JA3) and 2 (JA6) to quench the fluorescence of the fluorophore JA1 was determined by fluorescence spectroscopy. The fluorescence spectra for JA1 (the fluorophore) vs JA4 (probe 1) as well as JA1 vs JA7 (probe 2) were obtained using the PerkinElmer fluorescence spectrometer LS 55; scan speed 1200 nm/min, λ_{ex} 566 (the earlier established λ_{maxex} for JA1, λ_{em} 576 – 700 nm), excitation slit, and emission slit widths both set at 5.0. The data obtained from the fluorescence quenching studies (Figure 32) showed that at equal concentrations (1 micromolar), the relative fluorescence intensities of JA1 and JA4 at λ_{594} , the λ_{max} for the fluorophore were 910 and 14 respectively. This means that the fluorescence of the fluorophore, JA1 has been quenched 65 folds in the fluorogenic probe JA4. The data from the quenching studies for JA1 and JA7 (Figure 33) also showed that at equal concentrations (1 micromolar), the fluorescence intensities at λ_{594} were 890 and 12 respectively for JA1 and JA7. This means that the fluorescence of JA1 has been quenched 74 folds in the fluorogenic probe JA7. These results indicate that the quenchers JA3 (in JA4) and JA6 (in JA7) were able to absorb the frequencies from the fluorophore JA1 with JA6 having an extra methyl group (when compared with JA3) being a better quencher for JA1. This may be a result of the difference in distance between the quencher and fluorophore in the two probes (Jares and Jovin, 2003; Chen et al, 2013; Kozma and Kele, 2019).

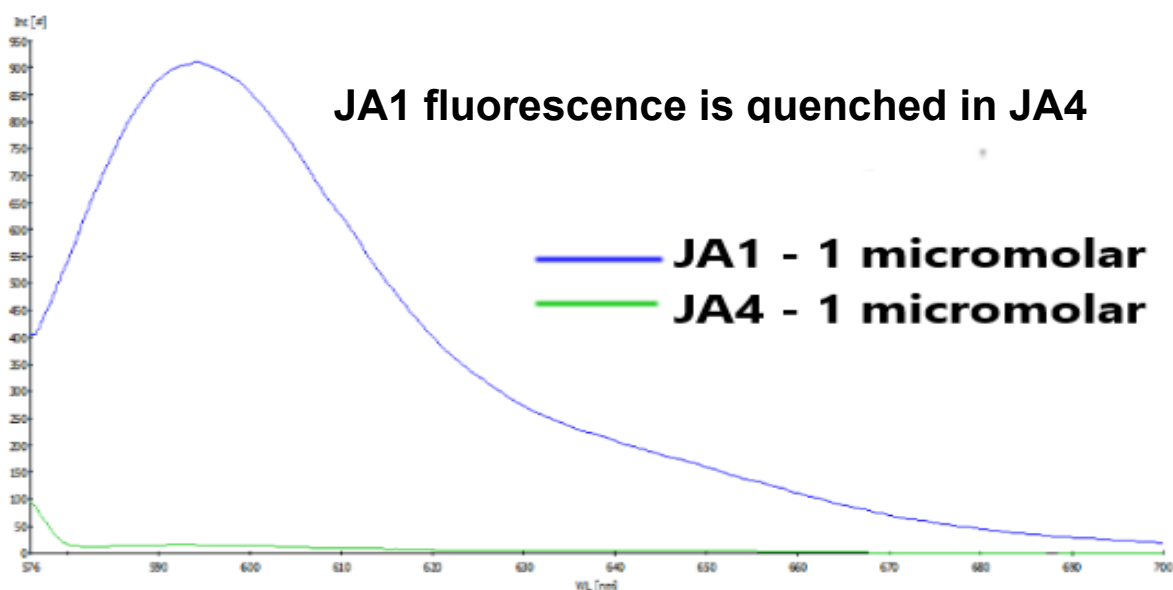


Figure 32: Fluorescence spectra for JA1(blue) and JA4 (green), showing the quenching of the fluorophore JA1 in the probe JA4 (Y axis = RFI, X axis = nm).

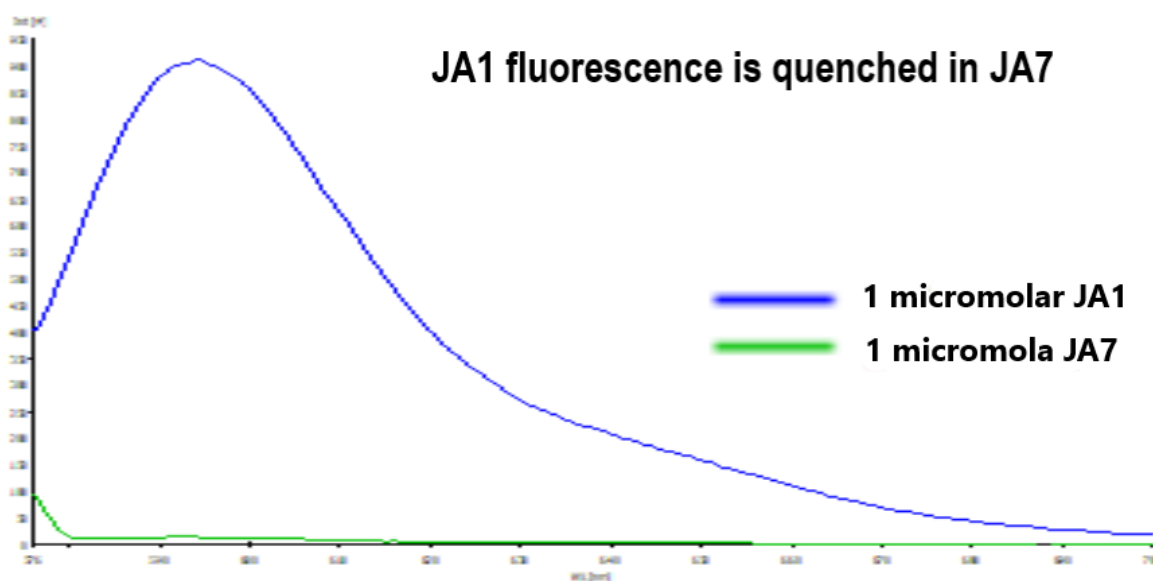


Figure 33: Fluorescence spectra for JA1(blue) and JA7 (green), showing the quenching of the fluorophore JA1 in the probe JA7 (Y axis = RFI, X axis = nm).

2.4 Determination of relative Quantum yield of probe 1

The quantum yield of the novel fluorophore, JA1 was determined by the relative method, using the parent chromophore rhodamine-B as the reference standard. The fluorophore (JA1) and the reference (rhodamine B) were prepared as stock solutions

(1mg/mL) in absolute ethanol. From this, test solutions of JA1 (1 μ M - 10 μ M in increments of 1 μ M) and rhodamine B (10 μ M - 20 μ M in increments of 2 μ M) were made using a 3mL quartz cuvette. The absorbance spectrum of each solution was recorded on a PerkinElmer UV/Vis spectrometer Lambda 25 instrument and the scan wavelength was set at 400 – 700 nm. From the data obtained (Figures 34 and 35), a plot of the absorbances at 535 nm, the λ_{ex} of the reference (Rho-B), was made against the corresponding concentrations for both the reference and the fluorophore (data not shown).

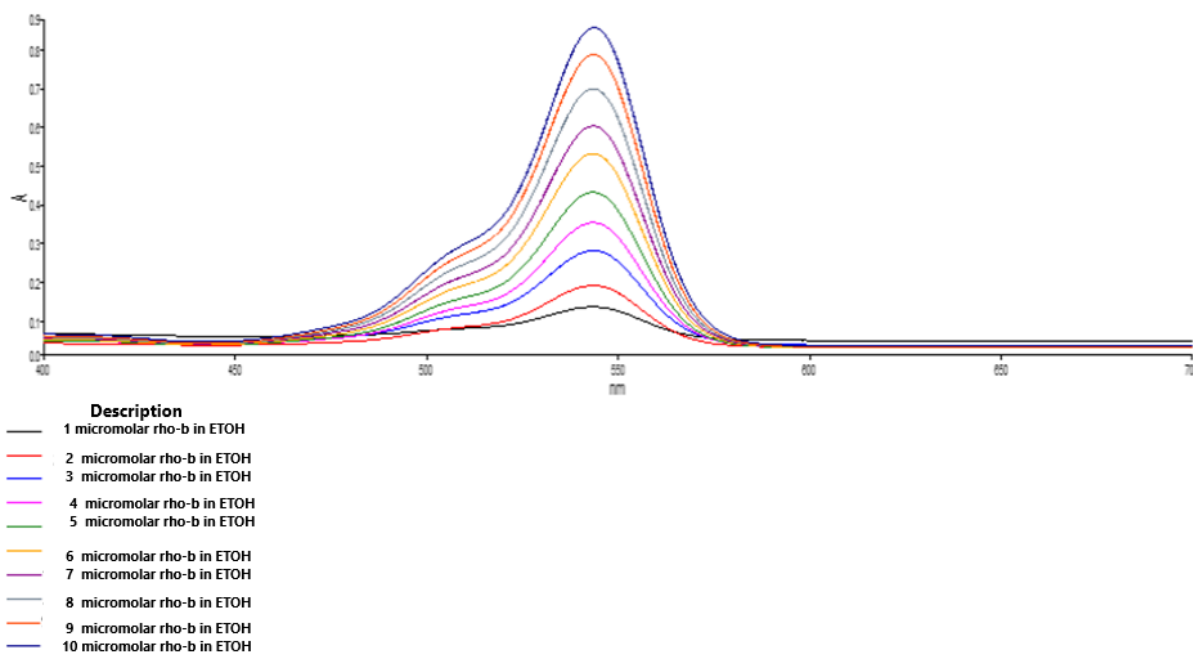


Figure 34: Emission spectrum of rho-B in ETOH (Y axis = RFI, X axis = nm)

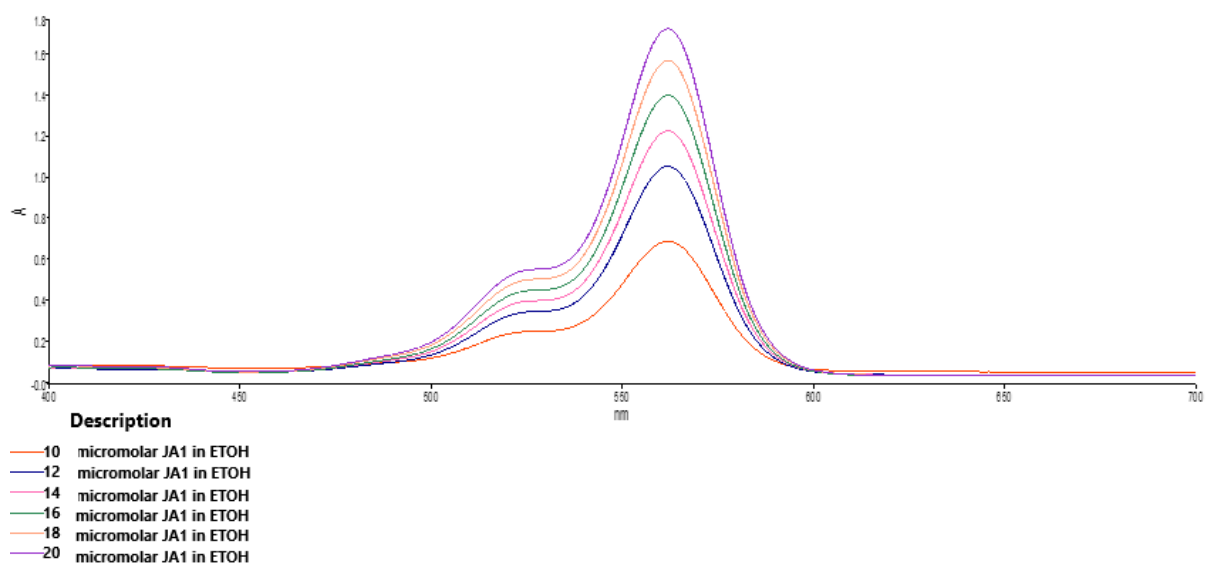


Figure 35: Emission spectrum of JA1 in ETOH (Y axis = RFI, X axis = nm)

Four absorbance values between 0.1 and 1 were selected from both plots (data not shown) and the corresponding concentrations calculated from the equation of the graphs, $y = mx + c$; where m is slope, c is intercept on absorbance axis and y and x are values on the absorbance and concentration axis, respectively. A 300 μ M stock solutions of the reference and the fluorophore in absolute ethanol were then prepared, from which test solutions of the calculated concentrations were made up in absolute ethanol using a 3 mL quartz cuvette. The absorbance spectrum of each solution was determined using PerkinElmer UV/Vis spectrometer Lambda 25 instrument; scan speed 480 nm/min, slit width 1 nm and the scan wavelength was set at 400 – 700 nm. According to Wood et al. (2018), a basic assumption of the relative method for quantum yield determination is that a pair of reference and test fluorophores having similar absorbances at the same wavelength will absorb the same number of photons. This gives the basis for comparing (in the relative quantum yield approach), their quantum yield, which is their ability to release the absorbed photons. The concentrations of the reference (Rho-B) and the test (JA1) fluorophores were adjusted and the absorbance at 535 nm for each concentration determined until 4 pairs of similar absorbances were obtained at the following concentrations (rho-B = 0.20188 μ M, 0.40377 μ M, 0.60565 μ M, 0.80754 μ M; JA1 = 4.750 μ M, 8.7458 μ M, 12.5311 μ M, 16.8314 μ M).

Table 1: Values of the absorbances @ 535 nm and the corresponding fluorescence intensities (peak area) from the 10X dilution in absolute ethanol for Rhodamine B

Rhodamine B (standard)

Concentration (μM)	Absorbance, A	Intensity, # (peak area)
0.20188	0.13717	6905.345
0.40377	0.23087	12494.312
0.60565	0.33072	17925.89
0.80754	0.44435	23380.015

Table 2: Values of the absorbances @ 535 nm and the corresponding fluorescence intensities (peak area) from the 10X dilution in absolute ethanol for JA1

JA1 (fluorophore)

Concentration (μM)	Absorbance, A	Intensity, # (peak area)
4.75	0.13942	3820.988
8.7458	0.21908	6391.714
12.5311	0.32773	9600.607
16.8314	0.43756	12216.191

These test solutions were then diluted 10X in absolute ethanol using a 3 mL quartz cuvette and the fluorescence emission spectra obtained from PerkinElmer fluorescence spectrometer LS 55; scan speed 1200 nm/min, λ_{ex} 535, λ_{em} 543 – 700 nm, excitation slit, and emission slit widths were set at 10.0 and 3.5, respectively. The peak area was calculated from the fluorescence intensity values and the itemized values in tables 1 and 2 were obtained. The integrated fluorescence intensity (peak areas) (tables 1 and 2) was plotted against the absorbances for both the reference and test fluorophores (Figures 36 and 37 respectively).

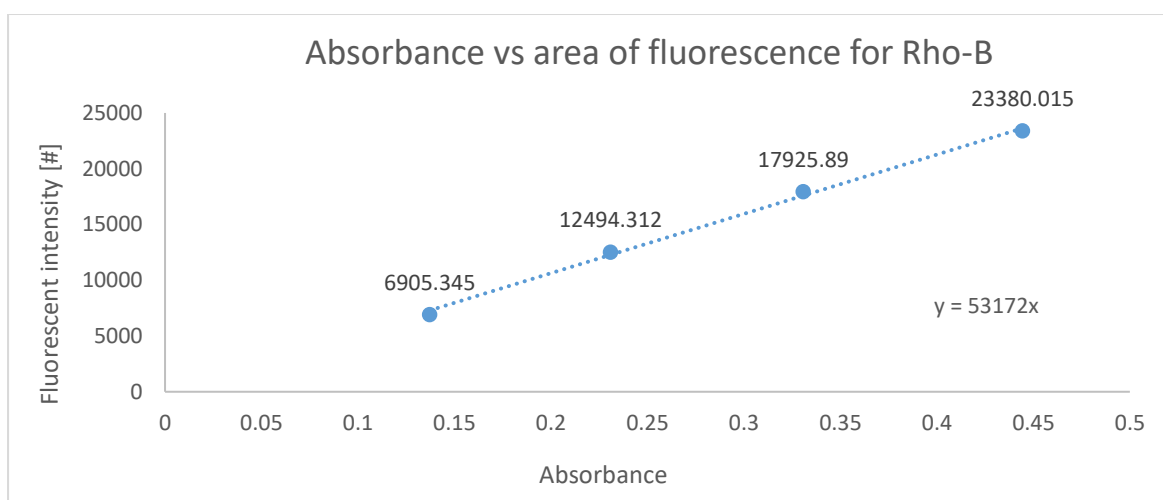


Figure 36: Plot of integrated fluorescence intensity of rho-B against absorbance

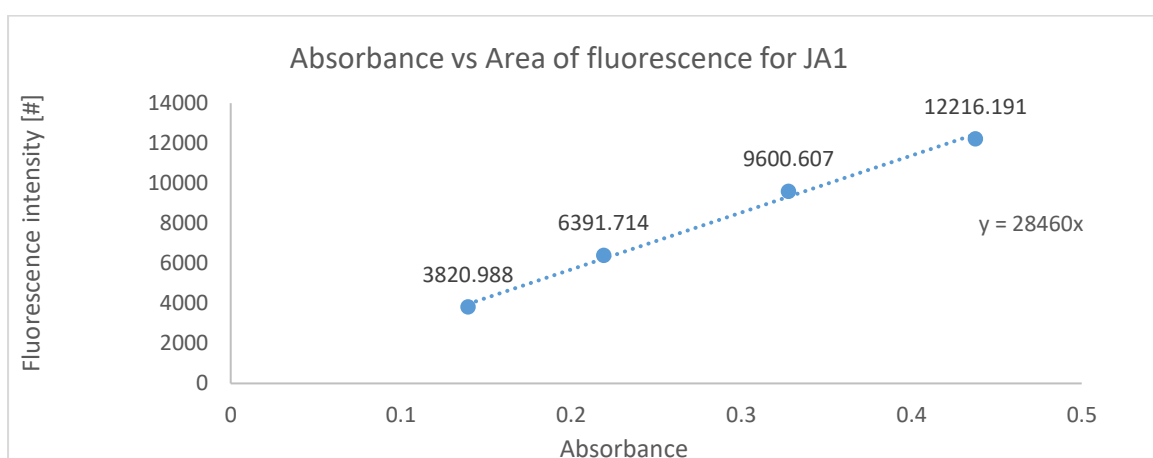


Figure 37: Plot of integrated fluorescence intensity of rho-B against absorbance

The slopes of the plots were obtained from the equation of the lines. The quantum yield was calculated using the relation: $\phi = \phi_R [m/m_R] [n^2/n^2_R]$ (Wurth et al., 2013; Mathur et al., 2019). Where m is the slope of the line obtained from the plot of the integrated fluorescence versus the absorbance; n is the refractive index of the solvent and the subscript R refers to the reference fluorophore of known quantum yield (rhodamine B, $\phi = 0.73 \pm 0.02$) (Mathur et al., 2019). The same solvent (absolute ethanol) has been used for both the reference and test fluorophores therefore, the term $[n^2/n^2_R] = 1$. The data obtained showed that the quantum yield of the novel fluorophore, JA1 was 0.37. This value was significantly lower than that of the parent chromophore (rhodamine B, $\phi = 0.73 \pm 0.02$). However, this could be attributed to the

significant difference in the excitation wavelength of the reference (Rho-B, $\lambda_{\text{ex}} = 535$ nm) and that of the test (JA1, $\lambda_{\text{ex}} = 566$ nm) fluorophores. According to Brouwer (2011) and Wurth et al. (2013), one of the major challenges of the relative method for determining quantum yield is the scarcity of well-validated reference fluorophores having a large Stoke's shift which limits the choice of the excitation wavelength that would favour the test and reference samples. The λ_{ex} for rho-B (535 nm) used in this experiment was found to be far from the λ_{ex} for JA1 ($\lambda_{\text{ex}} = 566$ nm) and this may have affected the total number of molecules of JA1 that were excited at this wavelength.

2.5 Fluorescence studies: pH Dependence of fluorescence of rhodamine B derived fluorophore JA1

Rhodamine-B has been successfully employed as a fluorophore in smart probe design (Marthur *et al.*, 2019). However, it has been shown to undergo pH dependent conformational changes that limit its application in biological assays (Kozma and Kele, 2019; Mathur *et al.*, 2019). One of the major targets in rhodamine-based probe design is to achieve a stable fluorescence response across wide pH ranges with the newly developed molecule. The stability of the novel rhodamine-based fluorophore JA1, the parent chromophore rhodamine B and that of Rho-Ala-OH an open ring rhodamine B derived molecule were compared. Buffer solutions with pH values 5 to 8 were prepared by the method of McILVaine (1921). The test solutions were prepared by making up a 1 mg/mL stock solutions of the samples with the McILVaine assay buffer to a final concentration of 10 μ M in a 3 mL quartz cuvette, across pH 5 – 8. Fluorescence emission spectra were obtained using PerkinElmer fluorescence spectrometer LS 55; scan speed 1200 nm/min, λ_{ex} 535, λ_{em} 543 – 700 nm, excitation slit, and emission slit widths were set at 10.0 and 3.5, respectively.

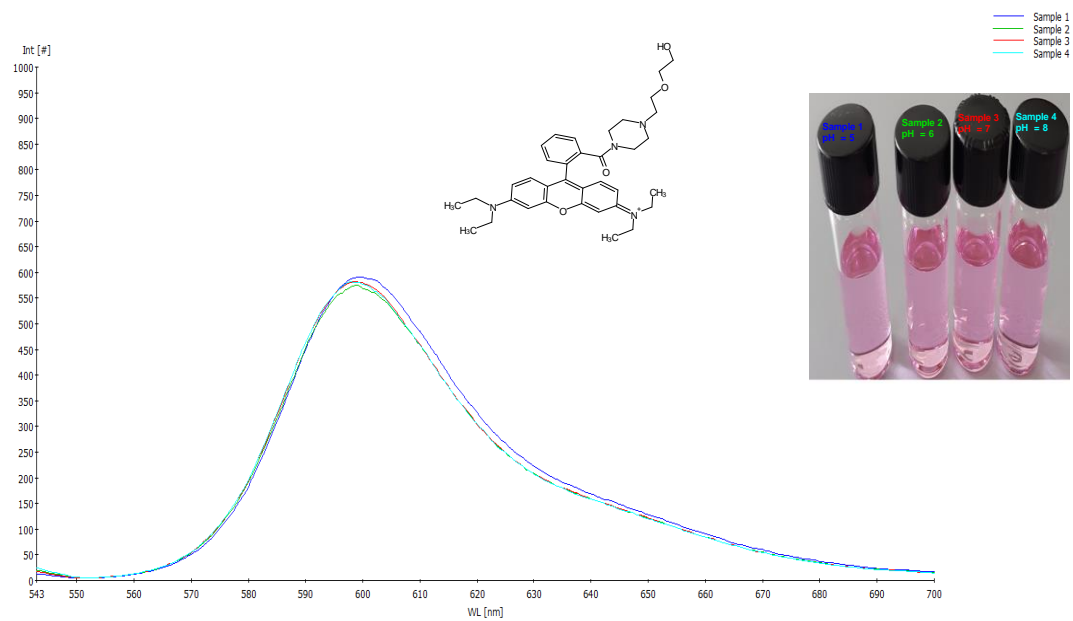


Figure 38: Fluorescence spectrum of JA1 at pH 5 – 8; showing stability of the intensity over a pH range (Y axis = RFI, X axis = nm)

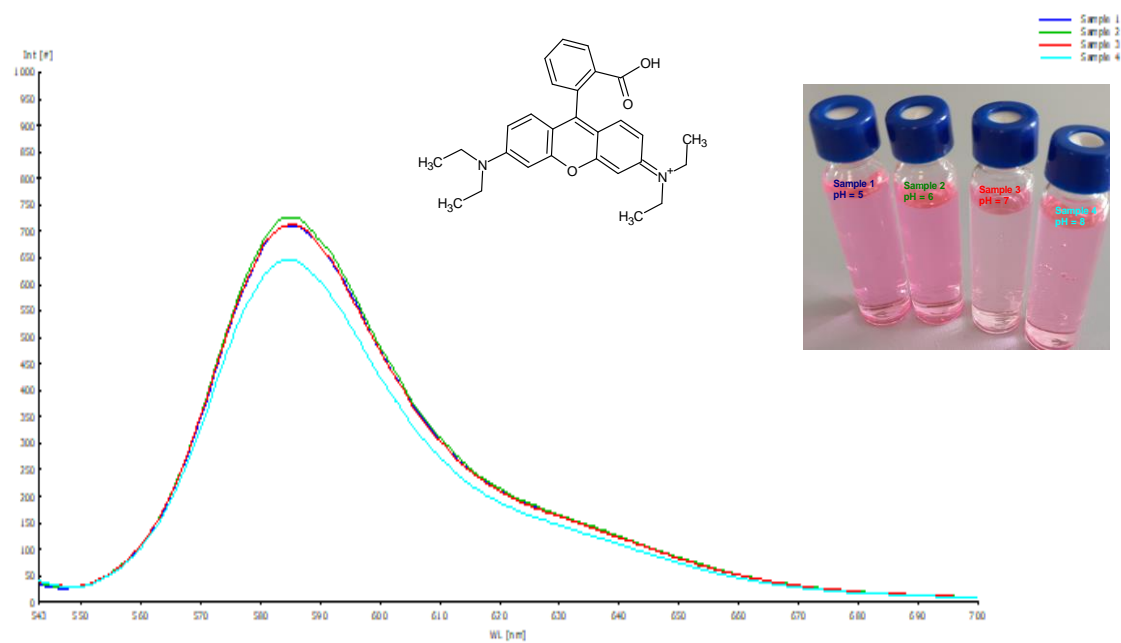


Figure 39: Fluorescence spectrum of Rho-B at pH 5 – 8; showing a gradation in intensity over the pH range (Y axis = RFI, X axis = nm)

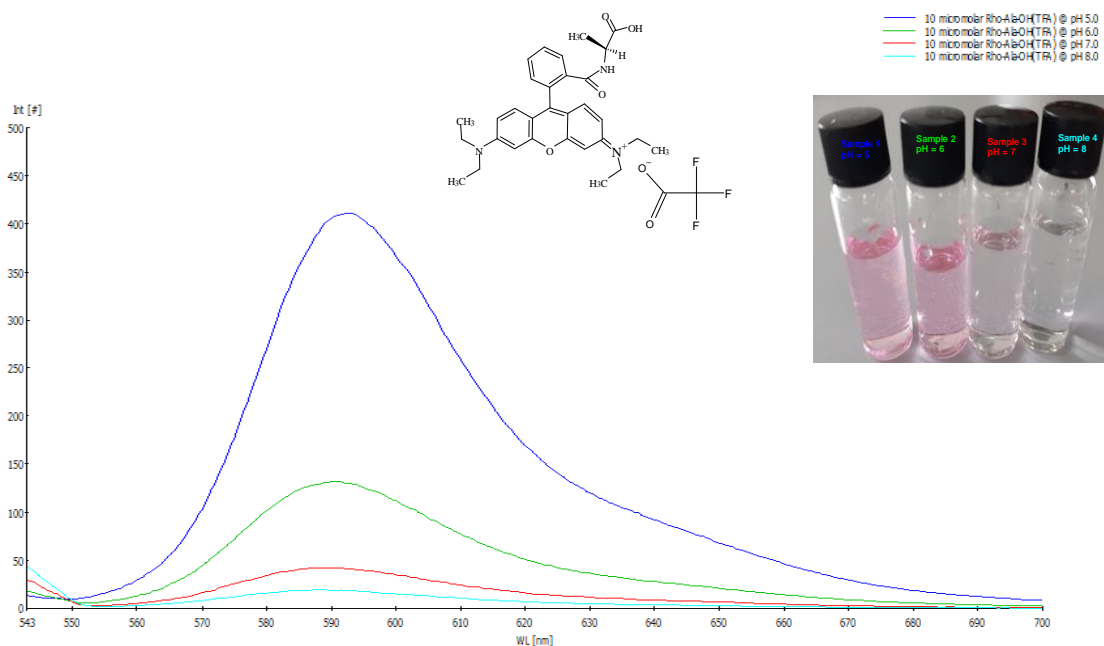


Figure 40: Fluorescence spectra of Rho-Ala-OH at pH 5 – 8; showing a very wide variation in intensity over the pH range (Y axis = RFI, X axis = nm)

The data for JA1 (Figure 38) showed that the fluorescence was more stable in the acidic and basic pH ranges when compared to the parent chromophore rho-B (Figure 39). The data for the rho-B derived compound Rho-Ala-OH, having an open ring form (Figure 40), showed much more variation in fluorescence spectra across the acidic and basic pH ranges with the fluorescence intensity being lowest in basic pH (pH = 8).

In earlier research in this laboratory, modifications at the 2' position were found to favour improved photostability in both the basic and acidic pH ranges, high relative fluorescence quantum yield, longer emission wavelength, and ease of synthesis (Mathur et al., 2019).

2.6 Activation of probes JA4 and JA7 by porcine pancreatic lipase (PPL) in vitro

To evaluate the potential of the novel fluorogenic FRET based probes JA4 and JA7 to act as substrates of lipase, an invitro fluorometric assay was developed. The probes JA4 and JA7 were prepared as stock solutions (1mg/mL) in DMSO. A portion of this stock solution of the probes (3 μ L) was each transferred to a 3 mL cuvette. The stock

solution (1mg/mL) of the enzyme porcine pancreatic lipase (PPL) was also prepared in PBS, from which 180 μ L was transferred to each of the 3mL cuvettes. The test solutions were diluted to final concentrations of 1 μ M of the probes (JA4 and JA7) and 0.06 mg/mL of the enzyme (PPL) in the 3mL cuvettes before being incubated at 37°C for 1 hour. Fluorescence emission spectra were obtained every 5 minutes starting from time zero using PerkinElmer fluorescence spectrometer LS 55; scan speed 1200 nm/min, λ_{ex} 566 nm, λ_{em} 576 – 700 nm, excitation slit, and emission slit widths were set at 5.0 and 5.0 respectively. A time dependent increase in the fluorescent intensity from the released hydrolysis product (JA1) was observed for both JA4 and JA7 (Figures 41 and 42) up to the 40th minute.

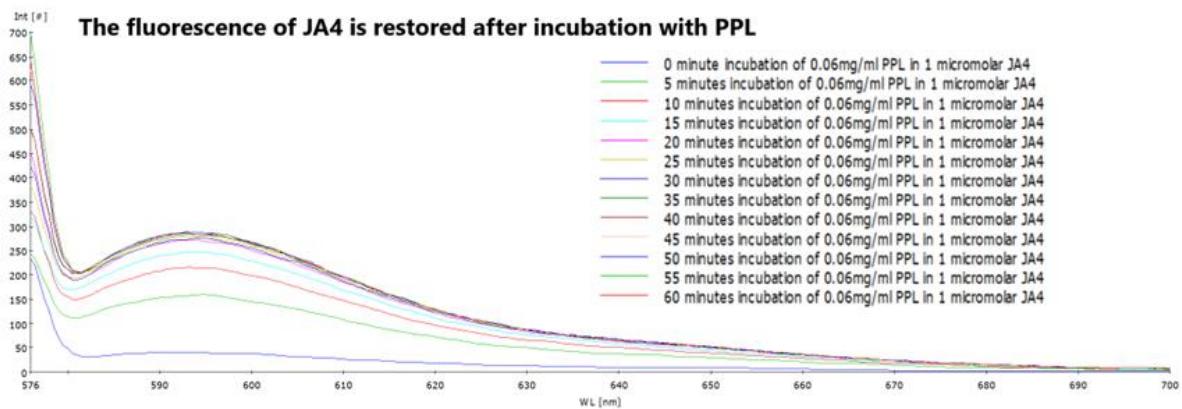


Figure 41: Fluorescence spectrum for JA1 released after JA4 (probe) incubation with PPL (Y axis = RFI, X axis = nm)

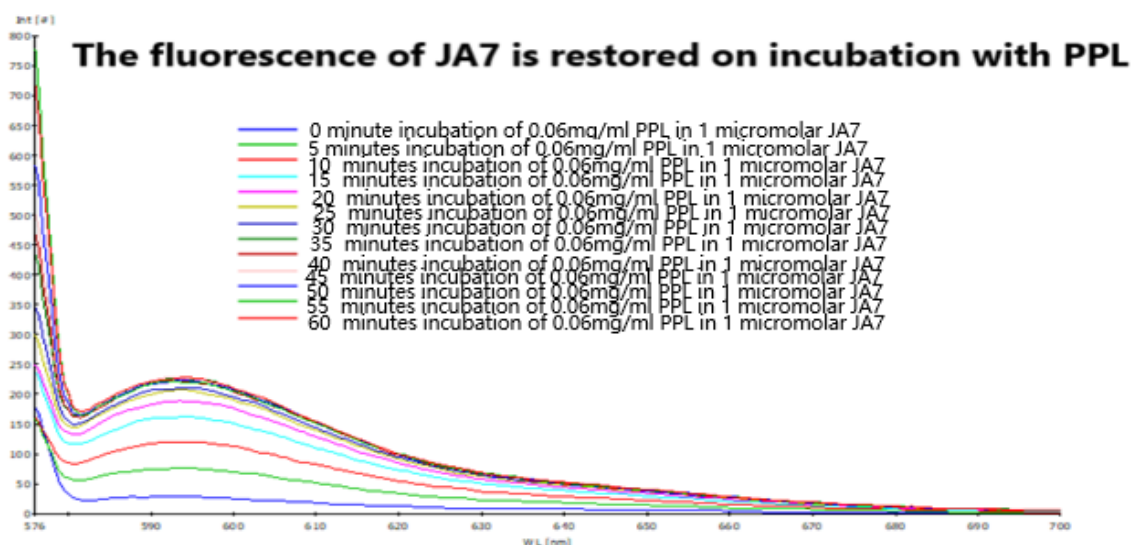


Figure 42: Fluorescence spectrum for JA1 released after JA7 (probe) incubation with PPL (Y axis = RFI, X axis = nm)

The result obtained served as a proof of concept that the probes, JA4 and JA7, can be successfully cleaved by the general lipase (PPL) to liberate the fluorophore component of the fluorogenic probes and thereby restore their fluorescence.

A plot of the average fluorescence intensity released on incubation of the probe with PPL against time was made for both JA4 and JA7 and a classical Michaelis curve was obtained for both probes (Figures 43 and 44).

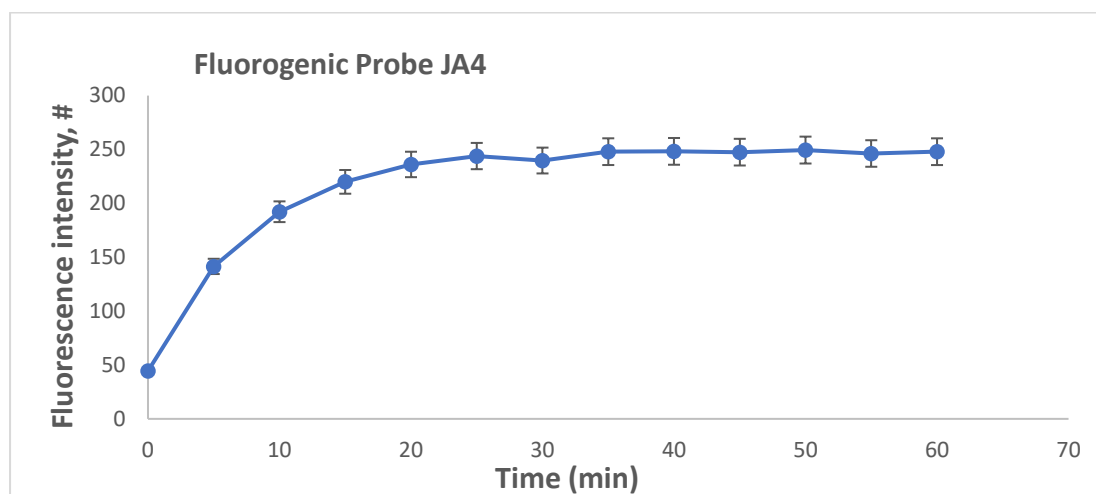


Figure 43: Plot of mean fluorescence intensity released on incubation of JA4 with PPL for 1h # (measured in a 3 mL cuvette)

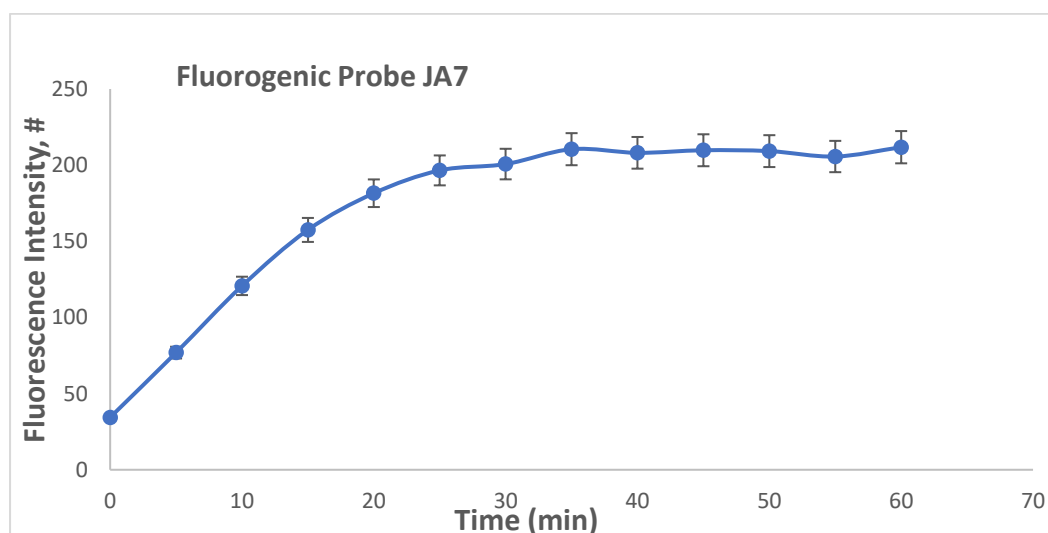


Figure 44: Plot of mean fluorescence intensity released on incubation of JA7 with PPL for 1h # (measured in a 3 mL cuvette)

This process was then scaled up for both probes JA4 and JA7 using the BMG Fluostar Omega microplate reader to attempt a translation to high through put assay method at excitation and emission wavelengths of λ_{ex} 544 nm, λ_{em} 590 nm and 1 μ M substrate concentration. However, this could not be achieved due to inconsistencies in the data obtained, which may be attributed to the lack of a matching excitation and emission wavelengths for the fluorophore (JA1; λ_{ex} 566 nm, λ_{em} 594) on the equipment (as the nearest excitation and emission wavelengths to that of the fluorophore, JA1 which the filters on the equipment could allow were respectively λ_{ex} 544 nm and λ_{em} 590 nm which may not be suitable for JA1 (JA1; λ_{ex} 566 nm, λ_{em} 594). The process was scaled down to 200 μ L total assay volume using a micro cuvette, while keeping the concentrations of the enzyme and the substrates at 0.06 mg/mL and 1 μ M respectively. This was to determine the total assay volume in micro litres, which will be most appropriate for this enzyme/substrates pair. However, no appreciable amount of fluorescence was observed at this total assay volume. The assay volume was then increased to 300 μ L total assay volume while maintaining the original concentrations of the enzyme and substrates; a time dependent increase in the fluorescent intensity was again observed for JA4 (Figure 45) up to the 40th minute. A plot of the intensity against time for this assay volume also followed a classical Michaelis Menten curve (Figure 46).

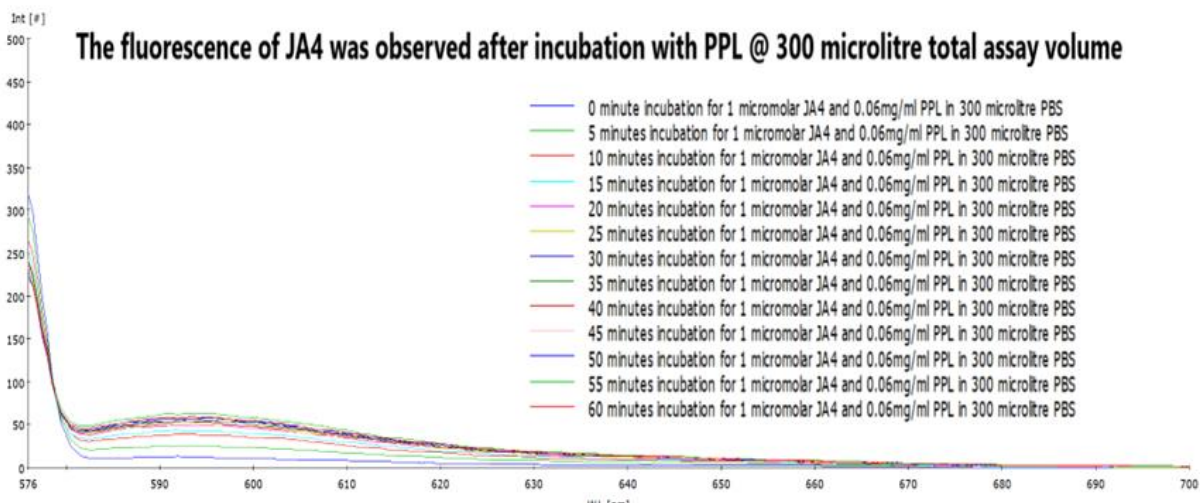


Figure 45: Fluorescence spectrum for JA1 released after JA7 (probe) incubation with PPL @ 300 μ l total assay volume (Y axis = RFI, X axis = nm)

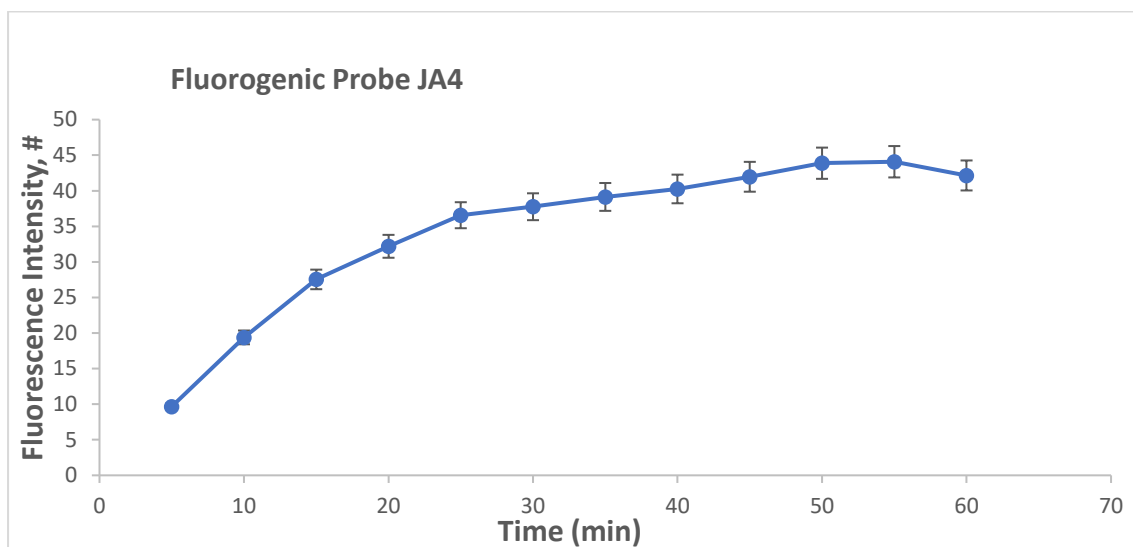


Figure 46: Plot of mean fluorescence intensity released on incubation of JA4 with PPL for 1h (measured in a 300 μ L cuvette)

Furthermore, serial dilutions of the enzyme, PPL (18 – 0.28 μ g) were prepared in a 300 μ L total assay volume, containing 1 μ M JA7 each; to determine the least concentration of the enzyme that would be required for the catalysis of the probes. It was observed that 4.5 μ g of the enzyme was sufficient for catalysis and release of the fluorescence of the fluorophore, JA1 from the probe, JA7.

2.7 TLC analysis of PPL incubation products

To determine the products of the PPL catalysis of the probes, JA4 and JA7, the hydrolysis products of their incubation with PPL from 2.6 above were subjected to TLC analysis using DCM: MeOH, 9:1. The result showed the presence of pink spot which trailed behind the reference spot (JA1). This may be due to a difference in the ionisation states of the incubation product when compared to the reference JA1.

The test samples were then subjected to TLC analysis using But: Act: H₂O, 4:5:1. The result showed the presence of a pink spot of JA1 which moved similar distance with the reference (JA1) and was fluorescent under the UV (350 nm). This confirmed the release of the fluorophore JA1 and thus the restoration of fluorescence by the hydrolytic action of PPL on the probes.

2.8 Distribution coefficient assay

The distribution coefficient ($\log D$) of small molecule drugs and probes is an important design parameter which would give a quantification of their lipophilicity and an indication of their ability to be absorbed through the cell membrane and/or accumulate within the cell (Rempel et al., 2017). It is critical that both the substrate probes and the reporter fluorophore are suitably lipophilic to facilitate cellular uptake (probes) and to be sufficiently localised at the site of enzyme catalysis (reporter fluorophore) to enable fluorescence measurements during live-cell imaging (Mathur et al., 2020; Rempel et al., 2017). The $\log D$ of the reporter fluorophore, JA1 and the probes, JA4 and JA7 were determined by the shake-flask method. The compounds JA1, JA4 and JA7 were suspended in PBS buffer (0.01 M phosphate buffer, 0.0027 M KCl and 0.137 M NaCl, pH 7.4), pre-saturated for 24h with 1-octanol (700 μL) and 1-octanol, pre-saturated for 24h with PBS buffer (700 μL) and vortexed thoroughly until dissolved. The mixtures were shaken for 24h at RT to partition the compounds between the two phases. The layers were separated by centrifugation for 3 min using a mini centrifuge before the absorbances were read from PerkinElmer fluorescence spectrometer LS 55; scan speed 1200 nm/min, λ_{ex} 566 nm, λ_{em} 576 – 700 nm, excitation slit, and emission slit widths were set at 5.0 and 5.0, respectively.

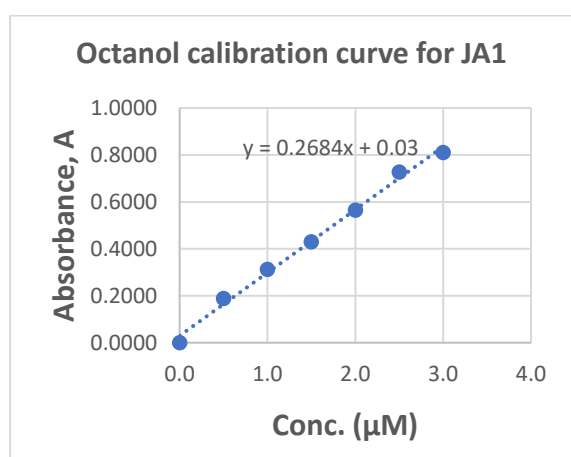


Figure 47: Plot of absorbance vs conc for JA1 (fluorophore) in octanol.

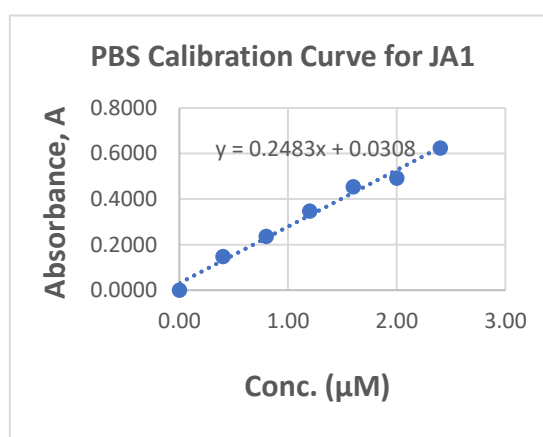


Figure 48: Plot of absorbance vs conc. for JA1 (fluorophore) in PBS

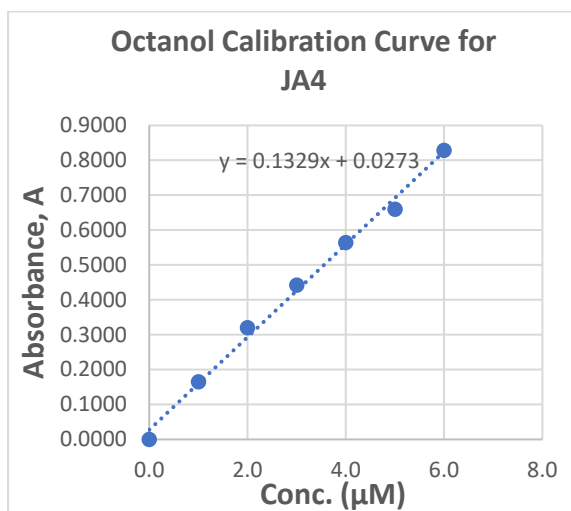


Figure 49: Plot of absorbance vs conc for JA4 (probe) in octanol.

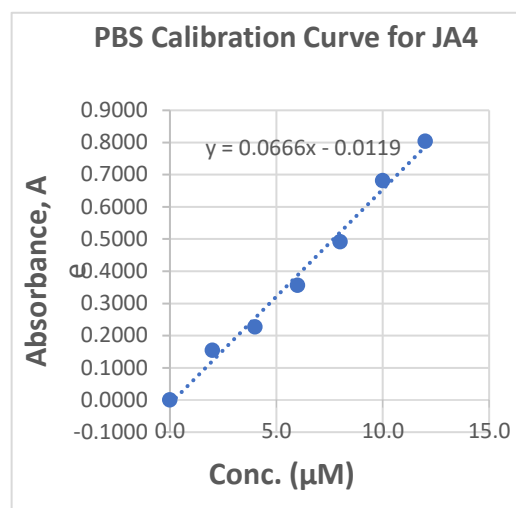


Figure 50: Plot of absorbance vs conc. for JA4 (probe) in PBS

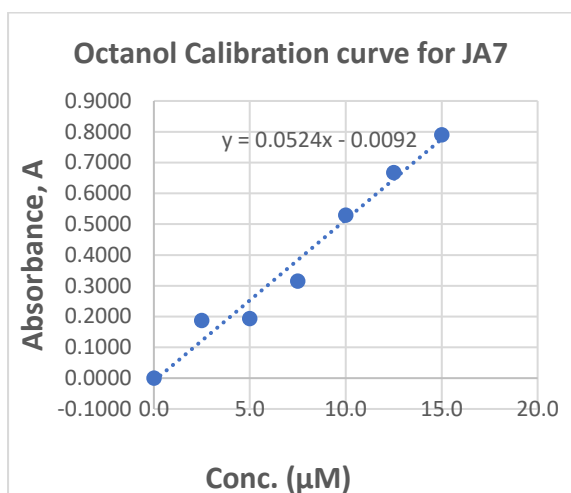


Figure 51: Plot of absorbance vs conc for JA7 (probe) in octanol.

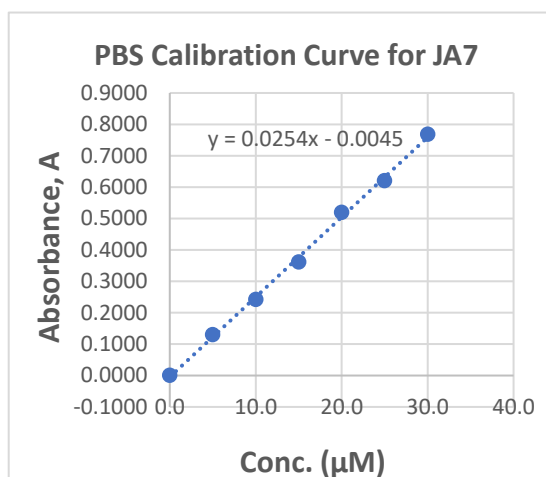


Figure 52: Plot of absorbance vs conc. for JA7 (probe) in PBS

The calibration curves of the absorbances (range = 0 – 0.7) against the concentration for the compounds, JA1, JA4 and JA7, in octanol (Figures 47, 49 and 51, respectively) and in PBS (Figures 48, 50 and 52, respectively) were obtained from the respective 1 mg/mL solutions in 100% DMSO. The concentrations of the compounds JA1, JA4 and JA7 were determined from the respective calibration curves of their absorbances verses concentration (Table 3).

Table 3: Determination of the log D of JA1, JA4 and JA7

Run No.	Solvent	absorbance in cuvette	y = mx + c	conc. in cuvette (μM)	dilution factor	original conc (μM)	Log D	Log D (mean ±)
JA1 -1	octanol	0.4256	y = 0.2684x + 0.03	1.4739	200	294.7800	0.1616	
JA1 -1	PBS	0.1317	y = 0.2483x + 0.0308	0.4064	500	203.2000		
JA1 -2	octanol	0.5932	y = 0.2684x + 0.03	2.0984	200	419.6800	0.1857	0.2243
JA1 -2	PBS	0.1667	y = 0.2483x + 0.0308	0.5473	500	273.6500		
JA1 -3	octanol	0.3154	y = 0.2684x + 0.03	1.0633	200	212.6600	0.3255	
JA1 -3	PBS	0.0807	y = 0.2483x + 0.0308	0.2010	500	100.5000		
JA4 -1	octanol	0.0621	y = 0.1329x + 0.0273	0.2617	300	78.5034	1.3547	
JA4 -1	PBS	0.0427	y = 0.0666x - 0.0119	0.4625	7.5	3.4686		
JA4 -2	octanol	0.0823	y = 0.1329x + 0.0273	0.4139	300	124.1828	1.4341	1.4044
JA4 -2	PBS	0.0525	y = 0.0666x - 0.0119	0.6094	7.5	4.5704		
JA4 -3	octanol	0.0719	y = 0.1329x + 0.0273	0.3359	300	100.7743	1.4245	
JA4 -3	PBS	0.0456	y = 0.0666x - 0.0119	0.5055	7.5	3.7916		
JA7 -1	octanol	0.0723	y = 0.0524x - 0.0092	1.2034	150	180.5153	1.2572	
JA7 -1	PBS	0.0383	y = 0.0254x - 0.0045	1.3313	7.5	9.9847		
JA7 -2	octanol	0.0702	y = 0.0524x - 0.0092	1.1633	150	174.4924	1.1706	1.2519
JA7 -2	PBS	0.0444	y = 0.0254x - 0.0045	1.5709	7.5	11.7821		
JA7 -3	octanol	0.0907	y = 0.0524x - 0.0092	1.5548	150	233.2156	1.3280	
JA7 -3	PBS	0.0416	y = 0.0254x - 0.0045	1.4611	7.5	10.9583		

The distribution coefficients were then estimated using the relationship:

$$\text{Log D}_{\text{oct/water}} = \log \left\{ \frac{[\text{compound in organic phase}]}{[\text{compound in aqueous phase}]} \right\}$$

The respective log Ds of the compounds JA1, JA4 and JA7 were found to be positive values of +0.2243, +1.4044 and +1.2519, which provides an indication that they have the potential to be efficiently absorbed through the cell membrane (Bhal, 2007). In an earlier study, Mathur et al. (2019), showed that a rhodamine-B derivative linked to the tertiary amine of proline in a novel aminoanthraquinone quenched substrate probe of legumain (Rho-Pro-Ala-Asn~Propyl-Pip-Propyl-AQ), having a log D of +1.78, was found to have been efficiently absorbed through the cell membrane and was activated by legumain to regenerate the rho-B as the reporter fluorophore tripeptide (Rho-Pro-Ala-Asn-OH), as evidenced by the accumulation of fluorescence in the lysosomes. However, the log D for JA4 (see structure at section 2.4 scheme 4), having the shorter methyl group was found to be higher than that of JA7 (see structure at section 2.7 scheme 7) with the longer methyl group attachment. This was not in agreement with the expectation that JA7 having more hydrophobic (methyl) group would have a higher log D, due may be to the effect of the nearby polar oxygen groups which may be reduced by increasing the length of the hydrophobic attachment (methyl group).

2.9 HPLC STUDIES

2.9.1 Development of an HPLC method for separation of probe JA4 and its in vitro metabolites

Given that PPL had previously been shown to induce effective production of rhodamine fluorescence emission upon incubation with probe JA4 by fluorescence spectroscopy experiments (**Section 2.6**) there remained the important question to determine the identity of the cleavage products of the reaction and confirm that these were the intended fragments produced by hydrolysis at the key ester bond. A reverse-phase HPLC method was developed to enable separation of the intact probe JA4 and its intended cleavage products JA1 and JA3 (experimental details in chapter 3, section 3.13).

Absorbance values (in AU) were recorded at the analytical wavelength of 560 nm. Chromatographic separations were achieved using an organic solvent elution with a gradient of 40-55 % over 12 minutes (Table 4). A total run time of 12 minutes was shown to be sufficient and can be regarded as an efficient chromatographic analysis.

Table 4 HPLC Gradient elution method for analysis of JA1, JA3 and JA4[#]

Time (minutes)	Mobile Phase A (%)	Mobile Phase B (%)
0	40	60
5	55	45
2	55	45
1	40	60
4	40	60

[#] Mobile phase A acetonitrile (0.1 % TFA) and mobile phase B HPLC grade water (0.08 % TFA); pH 1.79.

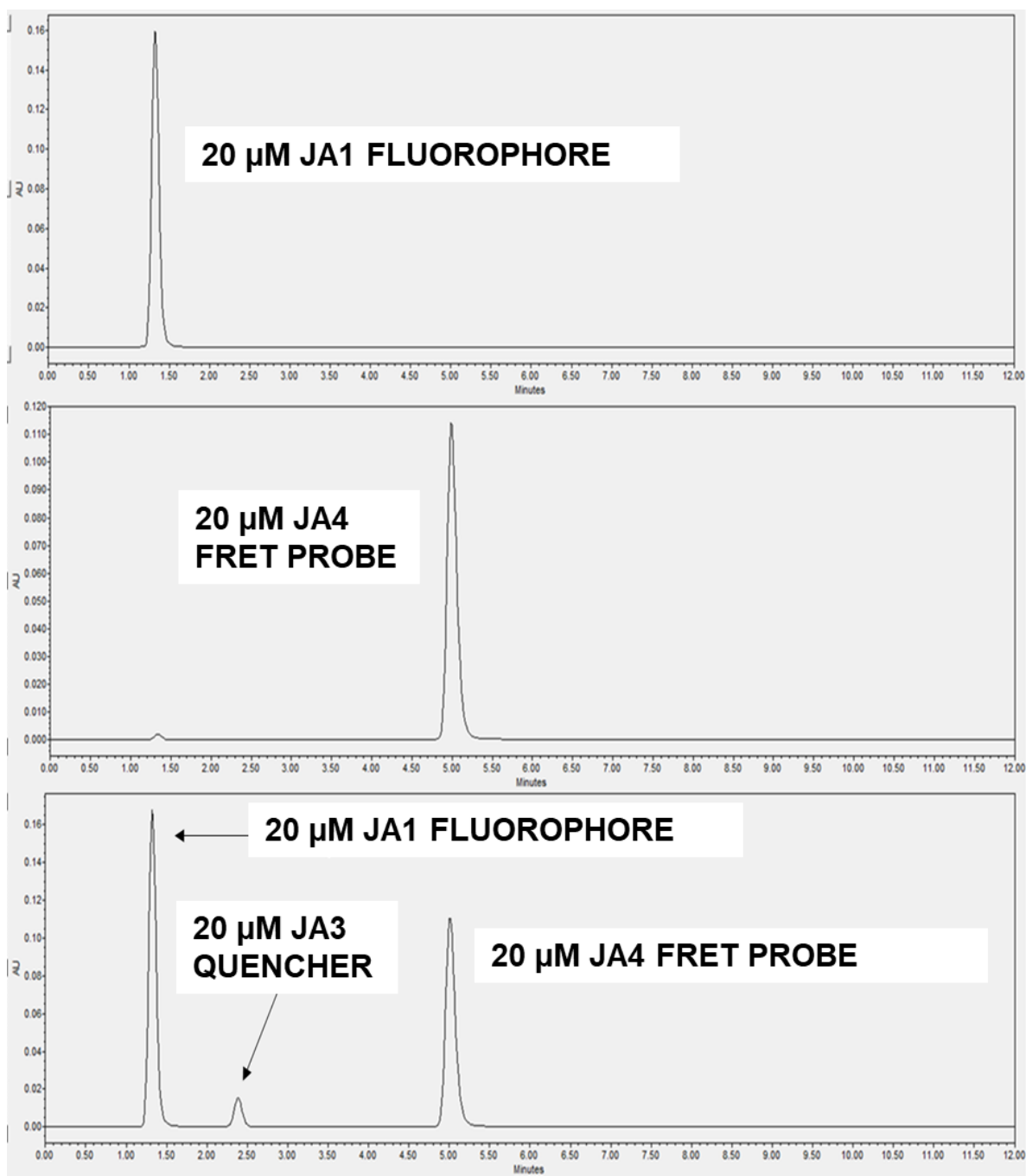


Figure 53: HPLC chromatograms of Standard compounds. JA1 (upper trace); JA4 (middle trace) and a 3-component mixture of JA1, JA3 and JA4 (each at 20 μM). The y-axis shows absorbance (AU) at the analytical wavelength λ 560 nm. The x-axis shows retention time t_R in minutes.

The rhodamine-containing fluorophore JA1 was detected at a retention time of 1.32 min; the short retention time is consistent with the more polar structure of the positively charged rhodamine fluorophore (plus a hydroxy group in its side chain) and is thus eluted more quickly from a reverse-phase HPLC column. Whereas the designed FRET

probe JA4 had the longest retention time (4.99 min), consistent with its highly hydrophobic structure [a hydrophobic anthraquinone chromophore and additional hydrophobic parts of the spacer surrounding the central ester bond (cleavage 'hotspot)]. The anthraquinone-based quencher compound JA3 had a retention time between JA1 and JA4; a t_R of 2.36 min indicates the strong influence of the polarity of the free carboxylic acid group in JA3, despite its being the relatively hydrophobic anthraquinone skeleton.

The analytical wavelength of 560 nm was chosen because all components absorbed at this wavelength; however, the rhodamine-containing compounds had the greater absorbance. Moreover, in incubations of the probe JA4 with lipase(s), the rhodamine-based fluorophore JA1 would be the reporter molecule resulting from any lipase-mediated activation of the new molecular probe, and it was therefore important to select a wavelength at which this compound had significant absorbance.

It should be noted that even though the test concentration of all three components in the mixture of standards was 20 μM , the size (area under the curve) of the JA3 signal is smaller due to the lower absorbance (smaller extinction coefficient) of the quencher at the analytical wavelength of 560 nm. Nevertheless, it proved possible to detect and quantify the amount of JA3 in subsequent *in vitro* metabolism studies using this common wavelength.

These relative order of retention times were predicted based on considering the hydrophobic physicochemical properties of each compound and were also consistent with their chromatographic behaviour (their R_f values) on normal-phase TLC.

2.9.2 HPLC determination of JA4 PPL-mediated cleavage into JA1 and JA3

Given that PPL had previously been shown to induce effective production of rhodamine fluorescence emission upon incubation with probe JA4 by fluorescence spectroscopy experiments (**Section 2.6**) there remained the important question to determine the identity of the cleavage products of the reaction and confirm that these were the intended fragments produced by hydrolysis at the key ester bond.

Incubations of the putative lipase probe JA4 were conducted using the developed gradient method at an initial probe concentration of 5 μM , and the reaction mixture

was sampled at time intervals of 30 min, 1 h, 1.5h and 4h. The HPLC chromatograms are shown in **Figure 54 to 57**.

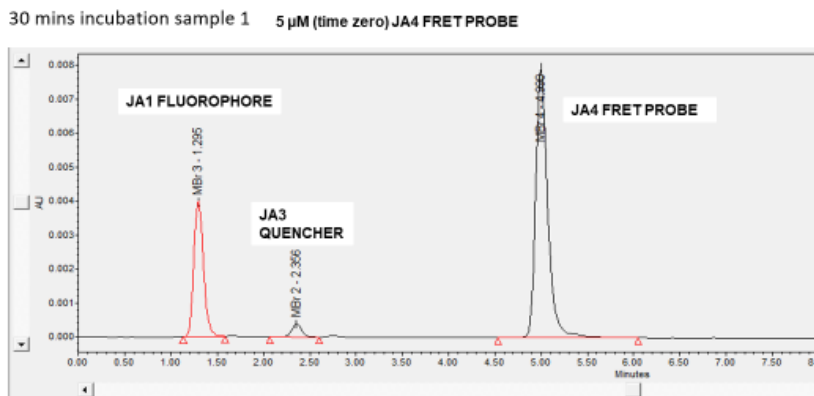


Figure 54: HPLC chromatogram of JA4 with PPL after 30 min.

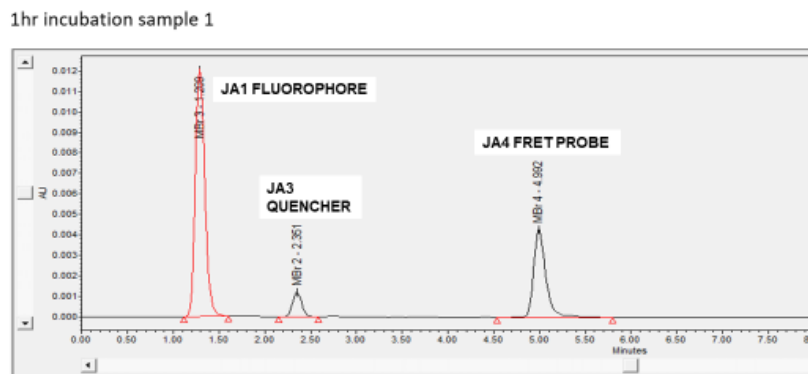


Figure 55: HPLC chromatogram of JA4 with PPL after 1 h.

1.5hr incubations sample 1

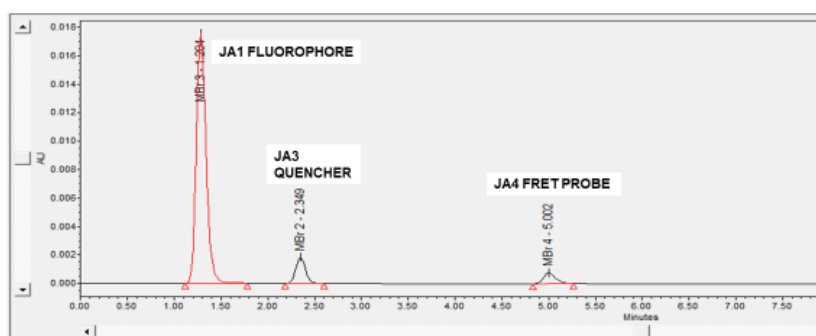


Figure 56: HPLC chromatogram of JA4 with PPL after 1.5 h.

4hrs incubation sample 1

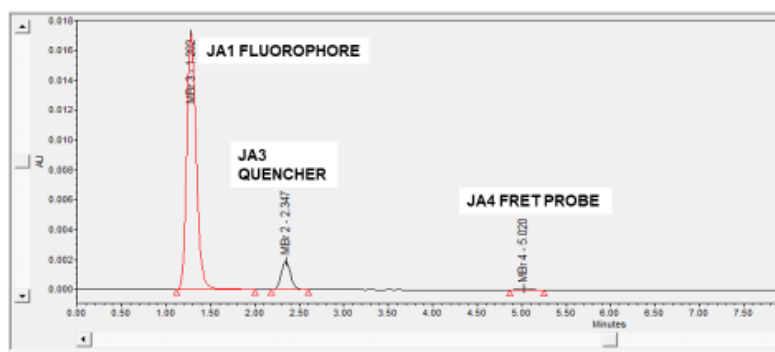


Figure 57: HPLC chromatogram of JA4 with PPL after 4 h.

The HPLC data confirmed that the probe JA4 was efficiently converted to the expected *in vitro* metabolites JA1 (reporter fluorophore) and JA3 (quencher) by comparison of the retention times of the observed signals with the experimentally determined retention times of the standards prepared for JA1, JA3 and JA4 (Figure 53 above) The concentration of probe JA4 was reduced to 5 μ M, following trial experiments over a range of concentrations, in order to achieve a rate of PPL-catalysed hydrolysis that could be followed easily, and reproducibly, by the sampling process. In conjunction with the prior fluorescence measurements of JA4 activation, it can be concluded reliably that the probe acts as an efficient substrate for PPL and that a proof of principle has been established by complementary spectroscopic and chromatographic techniques.

Conclusion

Aminoanthraquinone has been used in this study as a quencher for rhodamine-based FRET probes. The efficient overlap of the wavelengths of the fluorophore JA1 and the anthraquinone derived quenchers in the novel probes JA4 and JA7 was demonstrated by FRET test using UV spectrometry. The insertion of an ester bond within these probes enabled their activation and subsequent restoration of the rho-b derived JA1's fluorescence by the general lipase, porcine pancreatic lipase (PPL) as confirmed by the UV fluorescence analysis of the probes' incubation with PPL. This served as a proof of concept that the novel probes could be adapted for lipase determination in in-vitro bio analysis. HPLC and UV/Visible detection of the in vitro PPL-mediated cleavage products for the probe JA4 confirmed the presence of the constituent fluorophore JA1 and quencher JA3. Although the observed quantum yield for the fluorophore, JA1 was less than expected evidence from the UV detection of the compound (JA1) confirmed the efficient release of rho-b fluorescence in JA1, thereby making it a suitable novel candidate for FRET based probes. Furthermore, the positive log D values for JA1, JA4 and JA7 shows robust evidence for their ability to pass through the cell membrane and/or accumulate within the cell to enable efficient detection of enzyme activity.

The specificity of the lipase, MAGL for the novel probes could not be determined within the scope of this work. In future works, the activation of the probes by MAGL could be evaluated and its selectivity/specificity for the probes could be determined by kinetic methods.

Chapter 3: Experimental

3.0 Experimental (synthesis) procedure

3.1 General

All solvents and reagents were obtained from commercial sources and no further purification was performed unless stated. TLC was performed on Merk 60 F254 silica gel plates. Before performing a TLC where DMF was the solvent, a mini solvent extraction was carried out using dichloromethane and water (1:5). Column chromatography was performed using solid phase silica gel with columns of varied sizes. High resolution mass spectrometry was carried out at National Mass Spectrometry Facility EPSRC National Facility, Swansea, Wales using an LTQ Orbitrap XL with electrospray ionisation (ESI) of a methanolic solution.

3.2 Column sizes used for column chromatography

- i) 21 cm X 3.5 cm
- ii) 18 cm X 3.5 cm
- iii) 11.5 cm X 4.5 cm
- iv) 6.6 cm X 4.5 cm
- v) 6 cm X 4.5 cm

3.3 Solvents used for column chromatography

- a) 100% chloroform
- b) 98:2 chloroform: methanol
- c) 97:3 chloroform: methanol
- d) 96:4 chloroform: methanol
- e) 95:5 chloroform: methanol
- f) 19:1 chloroform: methanol
- g) 9:1 chloroform: methanol

- h) 19:1 chloroform: ethyl acetate
- i) 100% dichloromethane
- j) 19:1 dichloromethane: methanol
- k) 19:1 dichloromethane: ethyl acetate
- l) 24:1 chloroform: methanol + 0.1 (1drop) acetic acid
- m) 19:1 chloroform: methanol + 0.1 (1drop) acetic acid
- n) 97:3 chloroform: methanol + 0.3 (3drops) acetic acid

3.4 Solvents for TLC

- 1) 19:1 chloroform: methanol
- 2) 9:1 chloroform: methanol
- 3) 4:1 chloroform: methanol
- 4) 100% dichloromethane
- 5) 19:1 dichloromethane: ethyl acetate
- 6) 9:1 dichloromethane: methanol
- 7) 4:1 dichloromethane: methanol
- 8) 4:1 chloroform: methanol + 0.1 (1drop) acetic acid
- 9) 4:5:1 But: Act: H₂O
- 10) 9:1 DCM: MeOH

3.5 solvents for HPLC

acetonitrile (0.1 % TFA)

HPLC grade water (0.08 % TFA) pH 1.79

3.6 HPLC column size and condition

Phenomenex Synergi Polar RP80A (30 mm X 4.6 mm, particle size 4 μ m) HPLC reverse-phase column at 1 mL/minute flow rate, 10 μ L per injection volume, temperature 30 $^{\circ}$ C, 500 psi threshold.

3.7 Synthetic procedures

3.7.1 Synthesis of rhodamine B derived fluorophore (JA1)

Rhodamine B HCl (1.0g, 208 mmol) and 1- [bis (dimethylamino) methylene]-1H-1,2,3-triazolo [4,5-b] pyridinium 3-oxide hexafluorophosphate, HATU (1.2g, 313 mmol) were suspended in DMF (15 mL) and N-Ethyl-N-(propan-2-yl) propan-2-amine, DIPEA (1305 μ L, 752 mmol) was added and the solution was left standing at RT for 15 min. 1-(2-hydroxyethyl) piperazine (375 μ L, 228 mmol) was added and the solution stirred at RT for 2 hrs. A small amount (a pinch) of the solution was partitioned between DCM (2 mL) and water (10mL) and the organic layer was collected.

T.l.c. of the crude extract (chloroform: methanol, 9:1): Rf 0.26 (pink) rhodamine B, 0.13 (pink) product.

The remaining solution was air dried over night at room temperature. The residue was redissolved in dichloromethane and the whole solution was partitioned between dichloromethane (30 mL) and water (210 mL) to obtain the organic layer, which was washed twice in a large excess of water (100%) and air dried at RT. The resulting residue was redissolved in dichloromethane and subjected to a silica gel chromatography column (11.5 cm X 4.5 cm). Eluting solvents were used in order of increasing polarity a, b, c, d, and e, respectively, to give compound (JA1) as a pink, solid after evaporation under pressure at 35 – 40 $^{\circ}$ C. The residue from the purification product above was re-dissolved in dichloromethane and re-subjected to silica gel chromatography column (6.0 cm X 4.5 cm) using c, d, e, in increasing order of the solvent polarity, respectively. The resulting solution was evaporated under pressure at 35 – 40 $^{\circ}$ C to give compound (JA1) as a pink, solid after solid precipitation in diethyl ether at 4 $^{\circ}$ C. Approximate Yield (0.6557g) (53%)

T.l.c of the purified product (chloroform: Methanol, 4:1) Rf 0.50 (pink) standard, 0.64 (pink) product.

ESI(+) m/z: 599.3582(100%)(M - Cl)⁺.

¹H NMR (DMSO-*d*₆, 300 MHz): δ (ppm) 1.23 (t, 12H, 4×CH₃), 2.21 (t, 2H, CH₂), 2.37 (t, 2H, CH₂), 3.25 (t, 2H, CH₂), 3.37 (m, 8H, 4×CH₂), 3.44 (t, 2H, CH₂), 3.65 (m, 8H, 4×CH₂), 6.95 (s, 2H, H-4 and H-5), 7.13 (m, 4H, H-1, -2, -7, -8, Rho), 7.53 (m, 1H H-6 ϕ) 7.64 (m, 1H, H-4 ϕ), 7.74 (m, 2H, H-3 ϕ , H-5 ϕ).

¹³C NMR (DMSO-*d*₆, 75.5 MHz): δ (ppm) 12.93 (+ve, 4×CH₃-Rho), 41.59 (-ve, CH₂), 45.85 (-ve, CH₂), 47.37 (-ve, CH₂), 53.08 (-ve, CH₂), 53.42 (-ve, CH₂), 57.48 (-ve, CH₂), 60.65 (-ve, CH₂), 68.65 (-ve, CH₂), 72.63 (-ve, CH₂), 96.35 (+ve, CH_{AR}), 113.48 (abs, C_{AR}), 114.72 (+ve, CH_{AR}), 127.88 (+ve CH_{AR}), 130.04 (+ve CH_{AR}), 130.27 (+ve, CH_{AR}), 130.76 (+ve, CH_{AR}), 131.00 (abs, C_{AR}), 132.37 (+ve, CH_{AR}), 135.99 (abs, C_{AR}), 155.56 (abs, C_{AR}), 156.09 (abs, C_{AR}), 157.52 (abs, C_{AR}), 166.63 (abs, C_{AR}).

3.7.2 Synthesis of 3-(9, 10-Dihydro-anthracen-9-ylamino)-propionic acid tert-butyl ester (JA2)

Leucoquinizarin (1.01 g, 4.13 mmol), β-Alanine tert butyl ester hydrochloride (2.63g, 14.46 mmol) and anhydrous potassium carbonate (2.86g, 20.66 mmol) were suspended in DMF (50 mL) and the solution was heated over water bath at 95°C for 1 h. The resulting solution (brown) containing the 4,9,10-hydroxy substituted form of the product was aerated at RT until completely oxidized to give a purple solution. The whole solution was partitioned between dichloromethane (60 mL) and water (200 mL) to obtain the organic layer, which was washed in a large excess of water (100%), and air dried at RT.

T.L.C of crude extract (dichloromethane, 100%) Rf 0.46 (yellow) leucoquinizarin (starting material) 0.21 (orange) unknown, 0.13 (purple) product (JA2) 0.03 (brown) unknown.

The crude extract was re-dissolved in dichloromethane and subjected to a silica gel chromatography column (10 cm X 4.0 cm) using eluents i, and k, in order of increasing

polarity. All fractions containing the product of interest (JA2) were pulled together, T.L.C checked and air-dried overnight at RT.

T.L.C. purification product (dichloromethane: ethyl acetate, 19:1) Rf 0.53 (blue) compound suspected to be di-substituted form of JA2, 0.78 (purple) product, JA2.

The residue from the air-dried purification product above was re-dissolved in dichloromethane and re-subjected to silica gel chromatography column (6.6 cm X 4.5 cm) using i, k, in increasing order of the solvent polarity to give compound JA2 as a purple solid after evaporation in vacuo.

T.L.C. purified product (dichloromethane: ethyl acetate, 19:1) Rf 0.78 (purple) product.

3.7.3 Deprotection of 3-(9, 10-Dihydro-anthracen-9-ylamino)-propionic acid tert-butyl ester (JA2) to form 3-[(4-hydroxy-9,10-dioxo-9,10-dihydroanthracen-1-yl) amino] propanoic acid (JA3)

TFA was added dropwise into JA2 until completely dissolved. The solution was left standing at RT for 3 hours, T.L.C. checked and evaporated at 40°C. The resultant residue (purple) was solid precipitated overnight in diethyl ether at 4°C and vacuum dried to obtain the compound JA3 as a purple solid. Yield (0.2539g) (19%)

T.L.C. reaction progress (dichloromethane: methanol, 9:1) Rf 0.86 (purple) starting material (JA2), 0.32 (purple) product.

ESI(-) m/z: 310.0718(33%) (M-H)-, m/z: 266.0826 (100%) (M – COOH), m/z: 621.1522(100%) (2M-H)- and (2M+Na-2H)-

¹H NMR (DMSO-*d*₆, 300 MHz): d (ppm) 2.37 (t, 2H, CH₂-COOH), 3.51 (q, 2H, CH₂-NH-Aq), 7.19 (d, 1H, H-2), 7.38 (d, 1H, H-3), 7.75 (m, 2H, H-6 and H-7), 8.07 (m, 2H, H-5 and H-8), 10.14 (t, 1H, Aq-NH), 12.31 (s, 1H, COOH), 13.46 (s, 1H, Aq-OH).

¹³C NMR (DMSO-*d*₆, 75.5 MHz): d (ppm) 34.50 (-ve, CH₂), 38.54 (-ve, CH₂), 107.96 (abs, C), 113.38 (abs, C), 125.78 (+ve, CH_{AR}), 126.44 (+ve CH_{AR}), 126.80 (+ve CH_{AR}), 129.26 (+ve CH_{AR}), 132.35 (abs, C), 133.45 (+ve, CH_{AR}), 135.14 (+ve, CH_{AR}), 135.18 (abs, C), 147.45 (abs, C), 155.57 (abs, C), 173.26 (abs, C), 181.34 (abs, C), 187.26 (abs, C).

3.7.4 Synthesis of rho-B derived aminoanthraquinone (JA4, probe 1)

3-[(4-Hydroxy-9,10-dioxo-9,10-dihydroanthracen-1-yl) amino] propanoic acid, JA3 (0.1420g, 0.37mmol), N,N-dicyclohexylcarbodiimide (0.1390g, 0.5mmol) and DMAP (0.0042g) were weighed into a beaker and DCM (4ml) was added. The solution was left standing at RT for 10 min. The resulting solution was transferred to a solution of JA1 (0.2036g, 0.33mmol) in DCM (4ml), left standing at RT for 1 h and T.L.C checked, which revealed the presence of a large excess of the starting material JA1 and a small amount of the target product JA4.

T.L.C. of reaction progress 1 (chloroform: methanol, 4:1) R_f 0.73 (purplish pink) reference, 0.58 (pink) compound suspected to be JA1, 0.73 (purplish pink) product (JA4).

The reaction mixture was left standing at RT for another 4 hours and then T.L.C checked, which showed an increased amount of the target product with the presence of a reasonable amount of the starting material JA1.

T.L.C. of reaction progress 2 (chloroform: methanol, 4:1) R_f 0.782 (purplish pink) reference, 0.586 (pink) compound suspected to be JA1, 0.739 (purplish pink) product (JA4).

An additional amount of the reactant in limiting quantity 3-[(4-Hydroxy-9,10-dioxo-9,10-dihydroanthracen-1-yl) amino] propanoic acid, JA3 (0.0222g, 0.0713mmol, 0.2eq), N,N-dicyclohexylcarbodiimide, DCC (0.0275g, 0.1334 mmol, 0.27eq) and DMAP (a pinch) was added to the reaction mixture which was left standing at room temperature overnight. A T.L.C check of the reaction progress showed the presence of large amount of the target product with no detectable presence of the (excess) starting material JA1.

T.L.C. of reaction progress 3 (chloroform: methanol, 4:1) R_f 0.60 (purplish pink) reference, 0.62 (purplish pink) product (JA4), 0.60 (purplish pink) mixture.

The whole solution was solubilised in 100% DCM and filtered through the sintered funnel using a vacuum evaporator before being washed twice in water (100%). The organic layer was collected and left standing at room temperature over the weekend.

The residue was subjected to silica gel chromatography column (18 cm X 3.5 cm), using 100% chloroform. Eluting solvents were used in order of increasing polarity d, l, m, f, g, respectively, to give compound (JA4) as a purple-pink, solid after evaporation under pressure at 35 – 40 °C. The resultant product was solid precipitated at 4°C for two days, vacuum evaporated and kept in a vacuum desiccator until a constant mass of the purple-pink amorphous solid of JA4 was obtained. Yield (0.2695g) (89%).

T.L.C. of reaction purified product (chloroform: methanol, 4:1) Rf 0.67 (purplish pink) reference, 0.67 (purplish pink) product (JA4), 0.67 (purplish pink) mixture.

ESI(+) m/z: 892.4289100% (M-Cl)⁺, m/z 446.7178(37%) C₅₃H₅₈N₅O₈²⁺.

¹H NMR (DMSO-*d*₆, 300 MHz): δ (ppm) 1.19 (t, 12H, 4× CH₃), 2.30 (m, 2H, CH₂), 2.71 (m, 2H, CH₂), 3.34-3.41 (m, unresolved 10H, 5×CH₂), 3.52-3.69 (m, unresolved 12H, 6×CH₂), 4.15 (m, 2H, CH₂), 6.90 (s, 2H, H-4-Rho and H-5-Rho), 7.04 (m, 4H, H-1-Rho, H-2-Rho, H-7-Rho, H-8-Rho), 7.33 (m, 2H), 7.52 (m, 2H), 7.73 (m, 2H), 7.85 (m, 2H), 8.21 (m, 2H), 10.30 (t, 1H, Aq-NH), 13.59 (s, 1H, Aq-OH).

3.7.5 Synthesis of 4- (9, 10-Dihydro-anthracene-9-ylamino)-butyric acid tert-butyl ester (JA5)

Leucoquinizarin (0.9602g, 3.99mmol, 1.0 eq), tert-butylamino butanoate (2.7347g, 13.97mmol, 3.5 eq) and anhydrous potassium carbonate (2.7574g, 19.95mmol, 5.0 eq) were suspended in DMF (50 mL) and the solution was heated over water bath at 95°C for 1 h. The resulting solution (brown) containing the 4,9,10-hydroxy substituted form of the product was aerated at RT until completely oxidized to give a purple solution. A mini extraction of the reaction mixture was performed using a minute amount of the reaction mixture in DCM (2 mL) and water (10mL) and the organic layer was collected.

T.L.C of reaction progress (dichloromethane: ethyl acetate; 19:1) Rf 0.67 (purple) product; 0.042 (brown) unknown.

The whole solution was partitioned between dichloromethane (60 mL) and water (200 mL) to obtain the organic layer, which was washed twice in a large excess of water (100%) and air dried at RT.

The crude extract was re-dissolved in dichloromethane and subjected to a silica gel chromatography column (10 cm X 4.0 cm) using eluents f, g, in order of increasing polarity. All fractions containing the product of interest (JA5) were pulled together, T.L.C checked and air-dried over the weekend at RT to give the title compound JA5 as a purple solid.

T.L.C. purification products (dichloromethane: ethyl acetate, 19:1) Rf 0.42 (blue) compound suspected to be di-substituted form of JA5; 0.64 (purple) product, JA5.

The residue from the air-dried purification product above was found to be very dry and therefore weighed. Approximate yield 0.6819g.

T.L.C. purified product (dichloromethane: ethyl acetate, 19:1) Rf 0.62 (purple) product.

3.7.6 Deprotection of 4- (9, 10-Dihydro-anthracene-9-ylamino)-butyric acid tert-butyl ester (JA5) to form 4-[(4-hydroxy-9,10-dioxo-9,10-dihydroanthracen-1-yl) amino] butanoic acid (JA6)

Small amount of TFA was added to JA5 in a rbf until completely dissolved. The solution was left standing at RT overnight, before being T.L.C. checked and evaporated in vacuo at 40°C.

T.L.C. reaction progress (dichloromethane: methanol, 9:1) Rf 0.95 (purple) starting material (JA5), 0.32 (purple) product.

The resultant residue (purple) was solid precipitated overnight in diethyl ether at 4°C and vacuum dried to obtain the compound JA6 as a purple solid. Yield (0.5337g) (40%).

ESI(-) m/z: m/z = 324.0880(100%) (M-H)⁻, m/z = 649.1832(17%) (2M-H)⁻ m/z = 974.2777(3%) (2M+Na-H)⁻, (3M-H)⁻.

3.7.7 Synthesis of rhodamine-B derived aminoanthraquinone, JA7 (probe 2)

4-[(4-hydroxy-9,10-dioxo-9,10-dihydroanthracen-1-yl) amino] butanoic acid, JA6 (0.1226g, 0.37mmol, 1.1eq), N,N-dicyclohexylcarbodiimide (0.1098g, 0.5mmol) and DMAP (0.095g) were weighed into a beaker and DCM (4ml) was added. The solution was left standing at RT for 15 min. The resulting solution was transferred to a solution of JA1 (0.2033g, 0.33mmol, 1 eq) in DCM (4ml), and left standing at RT for 1 h and T.L.C checked, which revealed the presence of a large excess of the starting material JA1 and a small amount of the target product JA7.

T.L.C. of reaction progress (chloroform: methanol, 4:1) Rf 0.46 (pink) JA1, 0.65 (purplish pink) product (JA7).

An additional amount of the reactant in limiting quantity 4-[(4-hydroxy-9,10-dioxo-9,10-dihydroanthracen-1-yl)amino]butanoic acid, JA6 (0.0215g, 0.0661 mmol, 0.2eq), N,N-dicyclohexylcarbodiimide, DCC (0.1230g, 0.5971 mmol, 0.27eq) and DMAP (0.0150g) were solubilised in DCM (2 mL) and then added to the reaction mixture which was left standing at room temperature overnight. A T.L.C check of the reaction progress showed the presence of large amount of the target product with no detectable presence of the (excess) starting material JA1.

T.L.C. of reaction progress (chloroform: methanol, 4:1) Rf 0.5 (pink) JA1, 0.64 (purplish pink) product (JA7).

The resultant oily, purplish pink paste (reaction mixture) was solubilised in DCM and filtered in vacuo using a sintered funnel. The filtrate was washed twice in in a large excess of water (100%), the organic layer was collected and left standing over the weekend to air dry. The residue was subjected to silica gel chromatography column (21 cm X 3.5 cm), using 100% chloroform. Eluting solvents were used in order of increasing polarity a, d, l, m, l, n, respectively, to give compound (JA7) as a purple-pink, solid after evaporation under pressure at 35 – 40 °C. The resultant product was solid precipitated at 4°C over the weekend, and evaporated in vacuo, using a vacuum evaporator, and then placed in a vacuum desiccator until a constant mass of the purple-pink, amorphous solid of JA7 was obtained. Yield (0.2904g) (96%).

T.L.C. purification product (chloroform: methanol, 4:1) R_f 0.56 (purplish pink) product JA7.

ESI(+) m/z 906.4445(100%) (M-Cl)⁺.

Consensus Log P_{o/w} (SwissADME) was found to be 3.97.

3.8 UV-Vis Absorption Assay for JA1

The UV-Vis absorption assay for JA1 was recorded on a PerkinElmer UV/Vis spectrometer Lambda 25, the scan wavelength was set within the visible range (400 – 700 nm), and the slit width was set at 1 nm. A mg/ml stock solution of JA1 was prepared in DMSO. The test solution of JA1 was made from the 1mg/mL stock by diluting in PBS to a final concentration of 2μM in a 3mL quartz cuvette.

λ_{maxabs} for JA1 was found to be 566 nm.

3.9 FRET studies

3.9.1 Demonstration of spectral overlap between the emission spectrum of the donor chromophore, JA1 and the absorption spectra of the acceptor chromophores, JA3 and JA6.

The fluorescence spectrum of JA1 was obtained using the PerkinElmer fluorescence spectrometer LS 55; scan speed 1200 nm/min, λ_{ex} 566, its earlier established λ_{maxem}, λ_{em} 400 – 700 nm, excitation slit, and emission slit widths were both set at 5.0. A 1mg/ml stock solution of JA1 was prepared in DMSO. From which the test solution was made by diluting to a final concentration of 1 μM in PBS using a 3mL quartz cuvette. The λ_{maxem} for JA1 was found to be 594 nm.

The UV-Vis absorption spectra of the quenchers (fluorescence acceptors) JA3 and JA6 were obtained on a PerkinElmer UV/Vis spectrometer Lambda 25 instrument. The stock solutions (1mg/ml) were made in DMSO. The test solutions were prepared by diluting their 1mg/mL stock solutions to a final concentration of 30μM in PBS in a 3mL quartz cuvette. The scan wavelength was set within the visible spectrum (400 – 700nm). λ_{maxabs} were found to be JA3 (567 nm), and JA6 (570 nm).

An overlay of the emission spectrum of JA1 and the absorption spectra of JA3 and JA6 showed the spectral overlap between JA1 and JA3 to occur between 576 nm and 620 nm while that of the JA1 and JA6 pair occurred between 576 nm and 621 nm.

3.9.2 Fluorescence Spectroscopy Assay

The fluorescence spectra for JA1 (the fluorophore) and JA4 (probe 1) were obtained in a single experiment, using the PerkinElmer fluorescence spectrometer LS 55; scan speed 1200 nm/min, λ_{exc} 566, the earlier established λ_{maxex} for JA1, λ_{em} 576 – 700 nm, excitation slit, and emission slit widths both set at 5.0. The fluorescence spectra for JA1 and JA7 (probe 2) were also obtained in another single experiment using the same conditions. A 1 mg/ml solution of JA1, JA4 and JA7 were prepared in DMSO. The test solutions were then made up by diluting the stocks to 1 μM in PBS using a 3 mL quartz cuvette. The relative fluorescence intensities were taken at a single wavelength (λ_{594}) and was found to be 910 and 14 respectively for JA1 and JA4, and that for JA1 and JA7 were found to be 890 and 12, respectively.

3.10 Determination of relative Quantum yield of JA1

The fluorophore (JA1) and the reference (rhodamine B) were prepared as stock solutions (1mg/mL) in absolute ethanol. From this, test solutions of JA1 (1 μM - 10 μM in increments of 1 μM) and rhodamine B (10 μM - 20 μM in increments of 2 μM) were made using a 3mL quartz cuvette. The absorbance spectrum of each solution was recorded on a PerkinElmer UV/Vis spectrometer Lambda 25 instrument; scan wavelength (400 – 700 nm) and slit width (1 nm). A plot of the absorbances at 535 nm was made against the corresponding concentrations for both the reference and the fluorophore.

Four absorbance values between 0.1 and 1 were selected from both plots and the corresponding concentrations calculated from the equation of the graphs, $y = mx + c$; where m is slope, c is intercept on absorbance axis and y and x are values on the absorbance and concentration axis, respectively. A 300 μM stock solutions of the reference and the fluorophore in absolute ethanol were then prepared, from which test solutions of the calculated concentrations were made up in absolute ethanol using a

3 mL quartz cuvette. The absorbance spectrum of each solution was determined using PerkinElmer UV/Vis spectrometer Lambda 25 instrument; scan speed 480 nm/min, slit width 1 nm and the scan wavelength was set at 400 – 700 nm. The concentrations of the reference (Rho-B) and the test (JA1) fluorophores were adjusted and the absorbance at each concentration determined until 4 pairs of similar absorbances (Rho-B = 0.13717, 0.23087, 0.33072, 0.44435; JA1 = 0.13942, 0.21908, 0.32773, 0.43756) were obtained at the following concentrations (rho-B = 0.20188 μ M, 0.40377 μ M, 0.60565 μ M, 0.80754 μ M; JA1 = 4.750 μ M, 8.7458 μ M, 12.5311 μ M, 16.8314 μ M). The test solutions were then diluted 10X in absolute ethanol using a 3 mL quartz cuvette and the fluorescence emission spectra obtained from PerkinElmer fluorescence spectrometer LS 55; scan speed 1200 nm/min, λ_{ex} 535, λ_{em} 543 – 700 nm, excitation slit, and emission slit widths were set at 10.0 and 3.5, respectively. The integrated fluorescence intensity (peak areas) was plotted against the absorbances for both the reference and test fluorophores. The slopes of the plots were obtained from the equation of the lines. The quantum yield was calculated using the relation: $\phi = \phi_R [m/m_R] [n^2/n_R^2]$ (Wurth et al., 2013; Mathur et al., 2019), where m is the slope of the line obtained from the plot of the integrated fluorescence versus the absorbance; n is the refractive index of the solvent and the subscript R refers to the reference fluorophore of known quantum yield (rhodamine B, $\phi = 0.73 \pm 0.02$) (Mathur et al., 2019). The same solvent (absolute ethanol) has been used for both the reference and test fluorophores therefore, the term $[n^2/n_R^2] = 1$. The quantum yield of JA1 was found to be 0.37.

3.11 Fluorescence studies: pH Dependence of fluorescence of rhodamine b derived fluorophore JA1

Buffer solutions with pH values 5 - 8 were prepared by mixing various amounts of Na_2HPO_4 (0.2 M) and citric acid (0.1 M) according to the method of McILVaine (1921). A 1 mg/ml stock solutions of rhodamine b HCl, Rho-Ala-OH, and JA1, were prepared in absolute ethanol. The test solutions were prepared by making up the 1 mg/mL stock solutions of the samples with the McILVaine assay buffer to a final concentration of 10 μ M in a 3 mL quartz cuvette at the required pH. Fluorescence emission spectra were obtained using PerkinElmer fluorescence spectrometer LS 55; scan speed 1200

nm/min, λ_{ex} 535, λ_{em} 543 – 700 nm, excitation slit, and emission slit widths were set at 10.0 and 3.5, respectively. The fluorescence of JA1 was found to be stable over the pH (5-8) range while those of rhodamine b HCl, Rho-Ala-OH varied, with Rho-Ala-OH showing the most variation.

3.12 Activation of probes JA4 and JA7 by porcine pancreatic lipase (PPL) in vitro

The probes JA4 and JA7 were prepared as stock solutions (1mg/mL) in DMSO. A portion of this stock solution of the probes (3 μ L) was each transferred to a 3 mL cuvette. The stock solution (1mg/mL) of the enzyme porcine pancreatic lipase (PPL) was prepared in PBS, from which 180 μ L was also transferred to each of the 3mL cuvettes. The test solutions were diluted to final concentrations of 1 μ M of the probes (JA4 and JA7) and 0.06 mg/mL of the enzyme (PPL) in the 3mL cuvette before being incubated at 37°C for 1 hour. Fluorescence emission spectrum was obtained every 5 minutes starting from time zero using PerkinElmer fluorescence spectrometer LS 55; scan speed 1200 nm/min, λ_{ex} 566 nm, λ_{em} 576 – 700 nm, excitation slit, and emission slit widths were set at 5.0 and 5.0, respectively. The experiment was performed in triplicates. The result obtained indicated that the probes, JA4 and JA7, can be successfully cleaved by porcine pancreatic lipase to give rise to a time dependent increase in fluorescent intensity.

3.13 TLC analysis of PPL incubation products

The products of the JA4 and JA7 incubation with PPL from 4.0 above were subjected to TLC analysis using DCM: MeOH, 9:1. The result showed the presence of pink spot which trailed behind the reference spot (JA1).

T.L.C. PPL incubation for JA4 (DCM: MeOH, 9:1) Rf 0.17 (pink) JA1 and Rf 0.06 (pink) incubation product.

T.L.C. PPL incubation for JA7 (DCM: MeOH, 9:1) Rf 0.28 (pink) JA1 and Rf 0.09 (pink) incubation product.

The test samples were then subjected to TLC analysis using But: Act: H₂O, 4:5:1. The result showed the presence of a pink spot of JA1 which moved similar distance with the reference (JA1) and was fluorescent under the UV (350 nm)

T.L.C. PPL incubation for JA4 (But: Act: H₂O, 4:5:1) Rf 0.09 (pink) JA1 and incubation product.

T.L.C. PPL incubation for JA7 (But: Act: H₂O, 4:5:1) Rf 0.13 (pink) JA1 and incubation product.

3.14 Distribution coefficient assay

The distribution coefficient of the fluorophore, JA1 and the probes, JA4 and JA7 were determined by the shake-flask method. The compounds JA1, JA4 and JA7 were suspended in PBS buffer (0.01 M phosphate buffer, 0.0027 M KCl and 0.137 M NaCl, pH 7.4), pre-saturated for 24h with 1-octanol (700 μ L) and 1-octanol, pre-saturated for 24h with PBS buffer (700 μ L) and vortexed thoroughly until dissolved. The mixtures were shaken for 24h at RT to partition the compounds between the two phases. The layers were separated by centrifugation for 3 min using a mini centrifuge before the absorbances were read from PerkinElmer fluorescence spectrometer LS 55; scan speed 1200 nm/min, λ_{ex} 566 nm, λ_{em} 576 – 700 nm, excitation slit, and emission slit widths were set at 5.0 and 5.0, respectively. The calibration curves of the absorbances (range = 0 – 0.7) against the concentration for the compounds, JA1, JA4 and JA7 were also prepared from the respective 1 mg/mL solutions in 100% DMSO. The concentrations of the compounds JA1, JA4 and JA7 were determined from the respective calibration curves of their absorbances verses concentration. The experiments were performed in triplicates and the distribution coefficients were estimated using the relationship:

$$\text{Log } D_{\text{oct/water}} = \log \left\{ \frac{[\text{compound in organic phase}]}{[\text{compound in aqueous phase}]} \right\}$$

The log D of the compounds JA1, JA4 and JA7 were found to be 0.2243, 1.4044 and 1.2519, respectively.

3.15 HPLC STUDIES

3.15.1 HPLC method development

Solutions of 20 μM JA1 (rhodamine-based fluorophore), JA3 (anthraquinone-based quencher), and JA4 (target FRET probe) were prepared using 30 % acetonitrile as diluent and a blank. In addition, a mixed sample of all 3 JA compounds at the same concentrations were prepared for analysis.

Mobile phases A and B consisted respectively of acetonitrile (0.1 % TFA) and HPLC grade water (0.08 % TFA) pH 1.79. The HPLC reverse-phase column was a Phenomenex Synergi Polar RP80A (30 mm X 4.6 mm, particle size 4 μm). Settings for the method were: a 1 mL/minute flow rate, 10 μL per injection volume, temperature 30 $^{\circ}\text{C}$, 500 psi threshold.

Absorbance values (in AU) were recorded at the analytical wavelength of 560 nm. Chromatographic separations were achieved using an organic solvent elution with a gradient of 40-55 % over 12 minutes (Table 5).

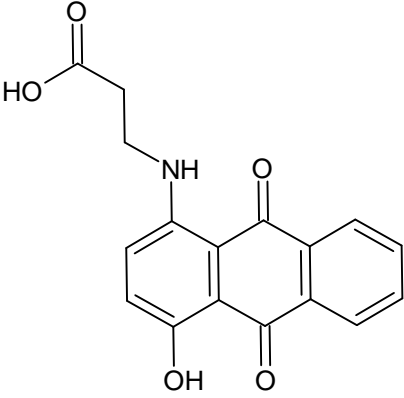
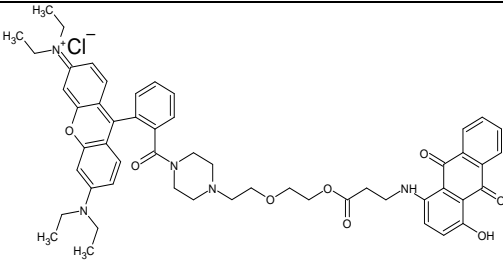
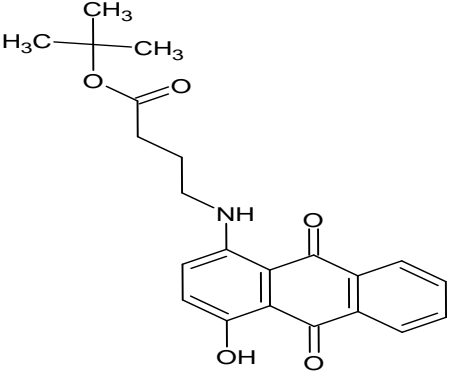
Table 5 HPLC Gradient elution method for analysis of JA1, JA3 and JA4

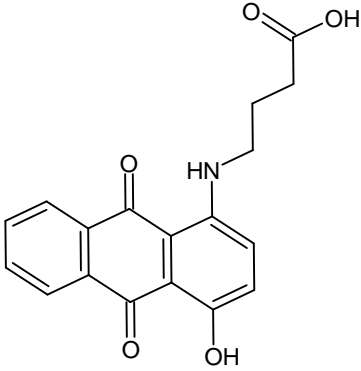
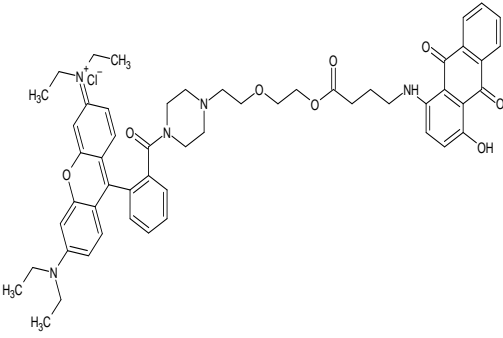
Time (minutes)	Mobile Phase A (%)	Mobile Phase B (%)
0	40	60
5	55	45
2	55	45
1	40	60
4	40	60

3.15.2 HPLC Analysis of JA4 (FRET probe) incubation with PPL (pancreatic porcine lipase)

Four separate JA4 (10 μM) samples were prepared (as above section 3.13) where 1 MB4 sample would serve as a no incubation control. A single mix of JA1 (10 μM), JA3 (10 μM) and JA4 (10 μM) served as standards and were prepared with PBS as diluent,

and a PBS blank. Three remaining 10 μM solutions of JA4 were used as incubation test samples. JA4 samples were incubated with solutions of PPL (0.06 mg/mL) at 37 $^{\circ}\text{C}$ for 2.5 hours. After incubation, 100 μL of each of the incubated and non-incubated samples, standards and PBS blank were diluted 2-fold with 100 μL of acetonitrile to achieve 5 μM JA4 equivalence solutions, and 50 % acetonitrile, followed by mixing and centrifugation for 5 minutes at RT. Aliquots of the supernatants (175 μL) were taken for HPLC analysis using the gradient (Table 5).

		
JA4		Molecular Formula: $C_{53}H_{58}ClN_5O_8$ Formula Weight: 928.50932
JA5		Molecular Formula: $C_{22}H_{23}NO_5$ Formula Weight: 381.42172
JA6		Molecular Formula: $C_{18}H_{15}NO_5$ Formula Weight: 325.3154

		
JA7		Molecular Formula: C₅₄H₆₀ClN₅O₈ Formula Weight: 942.5359

REFERENCES

- Adamczyk, M., & Grote, J. (2003). Synthesis of probes with broad pH range fluorescence. *Bioorganic and Medicinal Chemistry Letters*, 13(14), 2327–2330. [https://doi.org/10.1016/S0960-894X\(03\)00411-6](https://doi.org/10.1016/S0960-894X(03)00411-6)
- Baba, Y., Funakoshi, T., Mori, M., Emoto, K., Masugi, Y., Ekmekcioglu, S., Amagai, M., & Tanese, K. (2017). Expression of monoacylglycerol lipase as a marker of tumor invasion and progression in malignant melanoma. *Journal of the European Academy of Dermatology and Venereology*, 31(12), 2038–2045. <https://doi.org/10.1111/jdv.14455>
- Beija, M., Afonso, C. A. M., & Martinho, J. M. G. (2009). Synthesis and applications of rhodamine derivatives as fluorescent probes. *Chemical Society Reviews*, 38(8), 2410–2433. <https://doi.org/10.1039/b901612k>
- Bertrand, T., Augé, F., Houtmann, J., Rak, A., Vallée, F., Mikol, V., Berne, P. F., Michot, N., Cheuret, D., Hoornaert, C., & Mathieu, M. (2010). Structural Basis for Human Monoglyceride Lipase Inhibition. *Journal of Molecular Biology*, 396(3), 663–673. <https://doi.org/10.1016/j.jmb.2009.11.060>
- Birtalan, E., Rudat, B., Kölmel, D. K., Fritz, D., Vollrath, S. B. L., Schepers, U., & Bräse, S. (2011a). Investigating rhodamine B-labeled peptoids: scopes and limitations of its applications. *Biopolymers*, 96(5), 694–701. <https://doi.org/10.1002/bip.21617>
- Birtalan, E., Rudat, B., Kölmel, D. K., Fritz, D., Vollrath, S. B. L., Schepers, U., & Bräse, S. (2011b). Investigating rhodamine B-labeled peptoids: scopes and limitations of its applications. *Biopolymers*, 96(5), 694–701. <https://doi.org/10.1002/bip.21617>
- Blankman, J. L., Simon, G. M., & Cravatt, B. F. (2007). A Comprehensive Profile of Brain Enzymes that Hydrolyze the Endocannabinoid 2-Arachidonoylglycerol. *Chemistry and Biology*, 14(12), 1347–1356. <https://doi.org/10.1016/j.chembiol.2007.11.006>
- Bossi, M., Belov, V., Polyakova, S., & Hell, S. W. (2006). Reversible red fluorescent molecular switches. *Angewandte Chemie - International Edition*, 45(44), 7462–7465. <https://doi.org/10.1002/anie.200602591>

Bowman, A. L., & Makriyannis, A. (2009). Refined homology model of monoacylglycerol lipase: Toward a selective inhibitor. *Journal of Computer-Aided Molecular Design*, 23(11), 799–806. <https://doi.org/10.1007/s10822-009-9289-9>

Carpino, L. A., Imazumi, H., Foxman, B. M., Vela, M. J., Henklein, P., El-Faham, A., Klose, J., & Bienert, M. (2000). Comparison of the effects of 5- and 6-HOAt on model peptide coupling reactions relative to the cases for the 4- and 7-isomers. *Organic Letters*, 2(15), 2253–2256. <https://doi.org/10.1021/ol006013z>

Chen, H., Sun, T., Chen, H., Tian, R., Zhang, T., Chen, Z., & Ni, Z. (2014a). Structural and energetic insights into the selective interactions of monoacylglycerol lipase with its natural substrate and small-molecule inhibitors. *Medicinal Chemistry Research*, 23(5), 2391–2404. <https://doi.org/10.1007/s00044-013-0832-9>

Chen, H., Sun, T., Chen, H., Tian, R., Zhang, T., Chen, Z., & Ni, Z. (2014b). Structural and energetic insights into the selective interactions of monoacylglycerol lipase with its natural substrate and small-molecule inhibitors. *Medicinal Chemistry Research*, 23(5), 2391–2404. <https://doi.org/10.1007/s00044-013-0832-9>

Chen, H., Tian, R., Ni, Z., Zhang, Z., Chen, H., Guo, Q., & Saier, M. H. (2014). Conformational Transition Pathway in the Inhibitor Binding Process of Human Monoacylglycerol Lipase. *Protein Journal*, 33(6), 503–511. <https://doi.org/10.1007/s10930-014-9572-z>

Chyan, W., & Raines, R. T. (2018). Enzyme-Activated Fluorogenic Probes for Live-Cell and in Vivo Imaging. In *ACS Chemical Biology* (Vol. 13, Issue 7, pp. 1810–1823). American Chemical Society. <https://doi.org/10.1021/acscchembio.8b00371>

Daniel, J., Maamar, H., Deb, C., Sirakova, T. D., & Kolattukudy, P. E. (2011). Mycobacterium tuberculosis uses host triacylglycerol to accumulate lipid droplets and acquires a dormancy-like phenotype in lipid-loaded macrophages. *PLoS Pathogens*, 7(6). <https://doi.org/10.1371/journal.ppat.1002093>

Delorme, V., Diomandé, S. v., Dedieu, L., Cavalier, J. F., Carrière, F., Kremer, L., Leclaire, J., Fotiadu, F., & Canaan, S. (2012). MmPPOX Inhibits Mycobacterium tuberculosis Lipolytic Enzymes Belonging to the Hormone-Sensitive Lipase Family

and Alters Mycobacterial Growth. *PLoS ONE*, 7(9).
<https://doi.org/10.1371/journal.pone.0046493>

Deng, H., & Li, W. (2020). Monoacylglycerol lipase inhibitors: modulators for lipid metabolism in cancer malignancy, neurological and metabolic disorders. In *Acta Pharmaceutica Sinica B* (Vol. 10, Issue 4, pp. 582–602). Chinese Academy of Medical Sciences. <https://doi.org/10.1016/j.apsb.2019.10.006>

Dias, E. L., Hettenbach, K. W., & Am Ende, D. J. (2005). Minimizing isobutylene emissions from large scale tert-butoxycarbonyl deprotections. *Organic Process Research and Development*, 9(1), 39–44. <https://doi.org/10.1021/op049837v>

Esteves, A. R., & Cardoso, S. M. (2020). Differential protein expression in diverse brain areas of Parkinson's and Alzheimer's disease patients. *Scientific Reports*, 10(1). <https://doi.org/10.1038/s41598-020-70174-z>

Glen, A., Evans, C. A., Gan, C. S., Cross, S. S., Hamdy, F. C., Gibbins, J., Lippitt, J., Eaton, C. L., Noirel, J., Wright, P. C., & Rehman, I. (2010). Eight-plex iTRAQ analysis of variant metastatic human prostate cancer cells identifies candidate biomarkers of progression: An exploratory study. *Prostate*, 70(12), 1313–1332. <https://doi.org/10.1002/pros.21167>

Grimm, J. B., English, B. P., Chen, J., Slaughter, J. P., Zhang, Z., Revyakin, A., Patel, R., Macklin, J. J., Normanno, D., Singer, R. H., Lionnet, T., & Lavis, L. D. (2015). A general method to improve fluorophores for live-cell and single-molecule microscopy. *Nature Methods*, 12(3), 244–250. <https://doi.org/10.1038/nmeth.3256>

Grininger, C., Leypold, M., Aschauer, P., Pavkov-Keller, T., Riegler-Berket, L., Breinbauer, R., & Oberer, M. (2021). Structural changes in the cap of rv0183/mtbmgl modulate the shape of the binding pocket. *Biomolecules*, 11(9). <https://doi.org/10.3390/biom11091299>

Gupta, G. P., Nguyen, D. X., Chiang, A. C., Bos, P. D., Kim, J. Y., Nadal, C., Gomis, R. R., Manova-Todorova, K., & Massagué, J. (2007). Mediators of vascular remodelling co-opted for sequential steps in lung metastasis. *Nature*, 446(7137), 765–770. <https://doi.org/10.1038/nature05760>

Henry Boom, W., Schaible, U. E., & Achkar, J. M. (2021). The knowns and unknowns of latent *Mycobacterium tuberculosis* infection. In *Journal of Clinical Investigation* (Vol. 131, Issue 3). American Society for Clinical Investigation. <https://doi.org/10.1172/JCI136222>

Hernández-Torres, G., Cipriano, M., Hedén, E., Björklund, E., Canales, A., Zian, D., Feliú, A., Mecha, M., Guaza, C., Fowler, C. J., Ortega-Gutiérrez, S., & López-Rodríguez, M. L. (2014). A reversible and selective inhibitor of monoacylglycerol lipase ameliorates multiple sclerosis. *Angewandte Chemie - International Edition*, 53(50), 13765–13770. <https://doi.org/10.1002/anie.201407807>

Heymsfield, S. B., & Wadden, T. A. (2017). Mechanisms, Pathophysiology, and Management of Obesity. *New England Journal of Medicine*, 376(3), 254–266. <https://doi.org/10.1056/nejmra1514009>

Holtfrerich, A., Makharadze, T., & Lehr, M. (2010). High-performance liquid chromatography assay with fluorescence detection for the evaluation of inhibitors against human recombinant monoacylglycerol lipase. *Analytical Biochemistry*, 399(2), 218–224. <https://doi.org/10.1016/j.ab.2009.12.015>

Hu, B., Lin, J. Z., Yang, X. B., & Sang, X. T. (2020). Aberrant lipid metabolism in hepatocellular carcinoma cells as well as immune microenvironment: A review. In *Cell Proliferation* (Vol. 53, Issue 3). Blackwell Publishing Ltd. <https://doi.org/10.1111/cpr.12772>

Jernigan, F. E., & Lawrence, D. S. (2013). A broad spectrum dark quencher: Construction of multiple colour protease and photolytic sensors. *Chemical Communications*, 49(60), 6728–6730. <https://doi.org/10.1039/c3cc42628a>

Jha, V., Biagi, M., Spinelli, V., di Stefano, M. D., Macchia, M., Minutolo, F., Granchi, C., Poli, G., & Tuccinardi, T. (2021a). Discovery of monoacylglycerol lipase (MAGL) inhibitors based on a pharmacophore-guided virtual screening study. *Molecules*, 26(1). <https://doi.org/10.3390/molecules26010078>

Jha, V., Biagi, M., Spinelli, V., di Stefano, M. D., Macchia, M., Minutolo, F., Granchi, C., Poli, G., & Tuccinardi, T. (2021b). Discovery of monoacylglycerol lipase (MAGL)

inhibitors based on a pharmacophore-guided virtual screening study. *Molecules*, 26(1). <https://doi.org/10.3390/molecules26010078>

Joullié, M. M., & Lassen, K. M. (2010). Evolution of amide bond formation. *Arkivoc*, 2010(8), 189–250. <https://doi.org/10.3998/ark.5550190.0011.816>

Jun, J. v., Petersson, E. J., & Chenoweth, D. M. (2018a). Rational Design and Facile Synthesis of a Highly Tunable Quinoline-Based Fluorescent Small-Molecule Scaffold for Live Cell Imaging. *Journal of the American Chemical Society*, 140(30), 9486–9493. <https://doi.org/10.1021/jacs.8b03738>

Jun, J. v., Petersson, E. J., & Chenoweth, D. M. (2018b). Rational Design and Facile Synthesis of a Highly Tunable Quinoline-Based Fluorescent Small-Molecule Scaffold for Live Cell Imaging. *Journal of the American Chemical Society*, 140(30), 9486–9493. <https://doi.org/10.1021/jacs.8b03738>

Kaplan, R. N., Riba, R. D., Zacharoulis, S., Bramley, A. H., Vincent, L., Costa, C., MacDonald, D. D., Jin, D. K., Shido, K., Kerns, S. A., Zhu, Z., Hicklin, D., Wu, Y., Port, J. L., Altorki, N., Port, E. R., Ruggero, D., Shmelkov, S. v., Jensen, K. K., ... Lyden, D. (2005). VEGFR1-positive haematopoietic bone marrow progenitors initiate the pre-metastatic niche. *Nature*, 438(7069), 820–827. <https://doi.org/10.1038/nature04186>

Karlsson, M., Contreras, J. A., Hellman, U., Tornqvist, H., & Holm, C. (1997). cDNA cloning, tissue distribution, and identification of the catalytic triad of monoglyceride lipase. Evolutionary relationship to esterases, lysophospholipases, and haloperoxidases. *Journal of Biological Chemistry*, 272(43), 27218–27223. <https://doi.org/10.1074/jbc.272.43.27218>

King, A. R., Lodola, A., Carmi, C., Fu, J., Mor, M., & Piomelli, D. (2009a). A critical cysteine residue in monoacylglycerol lipase is targeted by a new class of isothiazolinone-based enzyme inhibitors. *British Journal of Pharmacology*, 157(6), 974–983. <https://doi.org/10.1111/j.1476-5381.2009.00276.x>

King, A. R., Lodola, A., Carmi, C., Fu, J., Mor, M., & Piomelli, D. (2009b). A critical cysteine residue in monoacylglycerol lipase is targeted by a new class of isothiazolinone-based enzyme inhibitors. *British Journal of Pharmacology*, 157(6), 974–983. <https://doi.org/10.1111/j.1476-5381.2009.00276.x>

Kinnaird, A., Zhao, S., Wellen, K. E., & Michelakis, E. D. (2016). Metabolic control of epigenetics in cancer. In *Nature Reviews Cancer* (Vol. 16, Issue 11, pp. 694–707). Nature Publishing Group. <https://doi.org/10.1038/nrc.2016.82>

Kobayashi, H., Ogawa, M., Alford, R., Choyke, P. L., & Urano, Y. (2010). New strategies for fluorescent probe design in medical diagnostic imaging. *Chemical Reviews*, 110(5), 2620–2640. <https://doi.org/10.1021/cr900263j>

Kozma, E., & Kele, P. (2019a). Fluorogenic probes for super-resolution microscopy. *Organic and Biomolecular Chemistry*, 17(2), 215–233. <https://doi.org/10.1039/c8ob02711k>

Kozma, E., & Kele, P. (2019b). Fluorogenic probes for super-resolution microscopy. *Organic and Biomolecular Chemistry*, 17(2), 215–233. <https://doi.org/10.1039/c8ob02711k>

Labar, G., Bauvois, C., Borel, F., Ferrer, J. L., Wouters, J., & Lambert, D. M. (2010a). Crystal structure of the human monoacylglycerol lipase, a key actor in endocannabinoid signaling. *ChemBioChem*, 11(2), 218–227. <https://doi.org/10.1002/cbic.200900621>

Labar, G., Bauvois, C., Borel, F., Ferrer, J. L., Wouters, J., & Lambert, D. M. (2010b). Crystal structure of the human monoacylglycerol lipase, a key actor in endocannabinoid signaling. *ChemBioChem*, 11(2), 218–227. <https://doi.org/10.1002/cbic.200900621>

Lauria, S., Casati, S., & Ciuffreda, P. (2015). Synthesis and characterization of a new fluorogenic substrate for monoacylglycerol lipase and application to inhibition studies. *Analytical and Bioanalytical Chemistry*, 407(26). <https://doi.org/10.1007/s00216-015-8991-9>

Lee, S., Xie, J., & Chen, X. (2010). Peptide-based probes for targeted molecular imaging. In *Biochemistry* (Vol. 49, Issue 7, pp. 1364–1376). <https://doi.org/10.1021/bi901135x>

Linder, K. E., Metcalfe, E., Nanjappan, P., Arunachalam, T., Ramos, K., Skedzielewski, T. M., Marinelli, E. R., Tweedle, M. F., Nunn, A. D., & Swenson, R. E. (2011a). Synthesis, in vitro evaluation, and in vivo metabolism of fluor/quencher

compounds containing IRDye 800CW and black hole quencher-3 (BHQ-3). *Bioconjugate Chemistry*, 22(7), 1287–1297. <https://doi.org/10.1021/bc100457s>

Linder, K. E., Metcalfe, E., Nanjappan, P., Arunachalam, T., Ramos, K., Skedzielewski, T. M., Marinelli, E. R., Tweedle, M. F., Nunn, A. D., & Swenson, R. E. (2011b). Synthesis, in vitro evaluation, and in vivo metabolism of fluor/quencher compounds containing IRDye 800CW and black hole quencher-3 (BHQ-3). *Bioconjugate Chemistry*, 22(7), 1287–1297. <https://doi.org/10.1021/bc100457s>

Liu, L., Lan, D., Wang, Q., Gao, C., Li, Z., Yang, B., & Wang, Y. (2013). A “bridge-like” structure responsible for the substrate selectivity of mono- and diacylglycerol lipase from *Aspergillus oryzae*. *Journal of Molecular Catalysis B: Enzymatic*, 97, 144–149. <https://doi.org/10.1016/j.molcatb.2013.08.006>

Makohon-Moore, A. P., Zhang, M., Reiter, J. G., Bozic, I., Allen, B., Kundu, D., Chatterjee, K., Wong, F., Jiao, Y., Kohutek, Z. A., Hong, J., Attiyeh, M., Javier, B., Wood, L. D., Hruban, R. H., Nowak, M. A., Papadopoulos, N., Kinzler, K. W., Vogelstein, B., & Iacobuzio-Donahue, C. A. (2017). Limited heterogeneity of known driver gene mutations among the metastases of individual patients with pancreatic cancer. *Nature Genetics*, 49(3), 358–366. <https://doi.org/10.1038/ng.3764>

Mathur, S., Turnbull, A., Akaev, I., Stevens, C., Agrawal, N., Chopra, M., & Mincher, D. (2020). Design of a New Peptide Substrate Probe of the Putative Biomarker Legumain with Potential Application in Prostate Cancer Diagnosis Ex Vivo. *International Journal of Peptide Research and Therapeutics*, 26(4), 1965–1980. <https://doi.org/10.1007/s10989-019-09994-1>

May, J. P., Brown, L. J., van Delft, I., Thelwell, N., Harley, K., & Brown, T. (2005). Synthesis and evaluation of a new non-fluorescent quencher in fluorogenic oligonucleotide probes for real-time PCR. *Organic and Biomolecular Chemistry*, 3(14), 2534–2542. <https://doi.org/10.1039/b504759e>

Meimetis, L. G., Carlson, J. C. T., Giedt, R. J., Kohler, R. H., & Weissleder, R. (2014). Ultrafluorogenic coumarin-tetrazine probes for real-time biological imaging. *Angewandte Chemie - International Edition*, 53(29), 7531–7534. <https://doi.org/10.1002/anie.201403890>

Miceli, M., Casati, S., Ottria, R., di Leo, S., Eberini, I., Palazzolo, L., Parravicini, C., & Ciuffreda, P. (2019). Set-up and validation of a high throughput screening method for human monoacylglycerol lipase (MAGL) based on a new red fluorescent probe. *Molecules*, *24*(12). <https://doi.org/10.3390/molecules24122241>

Mills, G. B., & Moolenaar, W. H. (2003). The emerging role of lysophosphatidic acid in cancer. In *Nature Reviews Cancer* (Vol. 3, Issue 8, pp. 582–591). <https://doi.org/10.1038/nrc1143>

Minkkilä, A., Myllymäki, M. J., Saario, S. M., Castillo-Melendez, J. A., Koskinen, A. M. P., Fowler, C. J., Leppänen, J., & Nevalainen, T. (2009). The synthesis and biological evaluation of para-substituted phenolic N-alkyl carbamates as endocannabinoid hydrolyzing enzyme inhibitors. *European Journal of Medicinal Chemistry*, *44*(7), 2994–3008. <https://doi.org/10.1016/j.ejmech.2009.01.007>

Morera, L., Labar, G., Ortar, G., & Lambert, D. M. (2012). Development and characterization of endocannabinoid hydrolases FAAH and MAGL inhibitors bearing a benzotriazol-1-yl carboxamide scaffold. *Bioorganic and Medicinal Chemistry*, *20*(21), 6260–6275. <https://doi.org/10.1016/j.bmc.2012.09.011>

Mulvihill, M. M., & Nomura, D. K. (2013). Therapeutic potential of monoacylglycerol lipase inhibitors. *Life Sciences*, *92*(8–9), 492–497. <https://doi.org/10.1016/j.lfs.2012.10.025>

Nasr, M. L., Shi, X., Bowman, A. L., Johnson, M., Zvonok, N., Janero, D. R., Vemuri, V. K., Wales, T. E., Engen, J. R., & Makriyannis, A. (2013). Membrane phospholipid bilayer as a determinant of monoacylglycerol lipase kinetic profile and conformational repertoire. *Protein Science*, *22*(6), 774–787. <https://doi.org/10.1002/pro.2257>

Nguyen, T., & Francis, M. B. (2003a). Practical synthetic route to functionalized rhodamine dyes. *Organic Letters*, *5*(18), 3245–3248. <https://doi.org/10.1021/ol035135z>

Nguyen, T., & Francis, M. B. (2003b). Practical synthetic route to functionalized rhodamine dyes. *Organic Letters*, *5*(18), 3245–3248. <https://doi.org/10.1021/ol035135z>

- Nomura, D. K., Long, J. Z., Niessen, S., Hoover, H. S., Ng, S. W., & Cravatt, B. F. (2010). Monoacylglycerol Lipase Regulates a Fatty Acid Network that Promotes Cancer Pathogenesis. *Cell*, *140*(1), 49–61. <https://doi.org/10.1016/j.cell.2009.11.027>
- Pascual, G., Avgustinova, A., Mejetta, S., Martín, M., Castellanos, A., Attolini, C. S. O., Berenguer, A., Prats, N., Toll, A., Hueto, J. A., Bescós, C., di Croce, L., & Benitah, S. A. (2017). Targeting metastasis-initiating cells through the fatty acid receptor CD36. *Nature*, *541*(7635), 41–45. <https://doi.org/10.1038/nature20791>
- Pascual, G., Domínguez, D., & Benitah, S. A. (2018). The contributions of cancer cell metabolism to metastasis. In *DMM Disease Models and Mechanisms* (Vol. 11, Issue 8). Company of Biologists Ltd. <https://doi.org/10.1242/dmm.032920>
- Patent, U. S. (2010). United States Patent: 7413882 United States Patent : 7413882. *October, 183*(8), 551–565.
- Peinado, H., Alečković, M., Lavotshkin, S., Matei, I., Costa-Silva, B., Moreno-Bueno, G., Hergueta-Redondo, M., Williams, C., García-Santos, G., Ghajar, C. M., Nitadori-Hoshino, A., Hoffman, C., Badal, K., Garcia, B. A., Callahan, M. K., Yuan, J., Martins, V. R., Skog, J., Kaplan, R. N., ... Lyden, D. (2012). Melanoma exosomes educate bone marrow progenitor cells toward a pro-metastatic phenotype through MET. *Nature Medicine*, *18*(6), 883–891. <https://doi.org/10.1038/nm.2753>
- Poli, G., Lapillo, M., Jha, V., Mouawad, N., Caligiuri, I., Macchia, M., Minutolo, F., Rizzolio, F., Tuccinardi, T., & Granchi, C. (2019). Computationally driven discovery of phenyl(piperazin-1-yl)methanone derivatives as reversible monoacylglycerol lipase (MAGL) inhibitors. *Journal of Enzyme Inhibition and Medicinal Chemistry*, *34*(1), 589–596. <https://doi.org/10.1080/14756366.2019.1571271>
- Rempel, B. P., Price, E. W., & Phenix, C. P. (2017). Molecular Imaging of Hydrolytic Enzymes Using PET and SPECT. In *Molecular Imaging* (Vol. 16). SAGE Publications Inc. <https://doi.org/10.1177/1536012117717852>
- Saario, S. M., Salo, O. M. H., Nevalainen, T., Poso, A., Laitinen, J. T., Järvinen, T., & Niemi, R. (2005). Characterization of the sulfhydryl-sensitive site in the enzyme responsible for hydrolysis of 2-arachidonoyl-glycerol in rat cerebellar membranes.

Chemistry and Biology, 12(6), 649–656.
<https://doi.org/10.1016/j.chembiol.2005.04.013>

Scalvini, L., Piomelli, D., & Mor, M. (2016). Monoglyceride lipase: Structure and inhibitors. *Chemistry and Physics of Lipids*, 197, 13–24.
<https://doi.org/10.1016/j.chemphyslip.2015.07.011>

Schalk-Hihi, C., Schubert, C., Alexander, R., Bayoumy, S., Clemente, J. C., Deckman, I., DesJarlais, R. L., Dzordzorme, K. C., Flores, C. M., Grasberger, B., Kranz, J. K., Lewandowski, F., Liu, L., Ma, H., Maguire, D., Macielag, M. J., McDonnell, M. E., Haarlander, T. M., Miller, R., ... Kuo, L. C. (2011). Crystal structure of a soluble form of human monoglyceride lipase in complex with an inhibitor at 1.35 Å resolution. *Protein Science*, 20(4), 670–683. <https://doi.org/10.1002/pro.596>

Schlosburg, J. E., Blankman, J. L., Long, J. Z., Nomura, D. K., Pan, B., Kinsey, S. G., Nguyen, P. T., Ramesh, D., Booker, L., Burston, J. J., Thomas, E. A., Selley, D. E., Sim-Selley, L. J., Liu, Q. S., Lichtman, A. H., & Cravatt, B. F. (2010). Chronic monoacylglycerol lipase blockade causes functional antagonism of the endocannabinoid system. *Nature Neuroscience*, 13(9), 1113–1119.
<https://doi.org/10.1038/nn.2616>

Serhan, M., Sprowls, M., Jackemeyer, D., Long, M., Perez, I. D., Maret, W., Tao, N., & Forzani, E. (2019). Total iron measurement in human serum with a smartphone. *AICHE Annual Meeting, Conference Proceedings, 2019-November*.
<https://doi.org/10.1039/x0xx00000x>

Soh, N. (2006). Recent advances in fluorescent probes for the detection of reactive oxygen species. *Analytical and Bioanalytical Chemistry*, 386(3), 532–543.
<https://doi.org/10.1007/s00216-006-0366-9>

Suzuki, Y., & Yokoyama, K. (2015). Development of functional fluorescent molecular probes for the detection of biological substances. In *Biosensors* (Vol. 5, Issue 2, pp. 337–363). MDPI AG. <https://doi.org/10.3390/bios5020337>

Tallman, K. R., Levine, S. R., & Beatty, K. E. (2016). Small-Molecule Probes Reveal Esterases with Persistent Activity in Dormant and Reactivating Mycobacterium

tuberculosis. *ACS Infectious Diseases*, 2(12), 936–944.
<https://doi.org/10.1021/acsinfecdis.6b00135>

Tuccinardi, T., Granchi, C., Rizzolio, F., Caligiuri, I., Battistello, V., Toffoli, G., Minutolo, F., Macchia, M., & Martinelli, A. (2014). Identification and characterization of a new reversible MAGL inhibitor. *Bioorganic and Medicinal Chemistry*, 22(13), 3285–3291.
<https://doi.org/10.1016/j.bmc.2014.04.057>

Tyukhtenko, S., Ma, X., Rajarshi, G., Karageorgos, I., Anderson, K. W., Hudgens, J. W., Guo, J. J., Nasr, M. L., Zvonok, N., Vemuri, K., Wagner, G., & Makriyannis, A. (2020). Conformational gating, dynamics and allostery in human monoacylglycerol lipase. *Scientific Reports*, 10(1). <https://doi.org/10.1038/s41598-020-75497-5>

Vrettos, E. I., Sayyad, N., Mavrogiannaki, E. M., Stylos, E., Kostagianni, A. D., Papas, S., Mavromoustakos, T., Theodorou, V., & Tzakos, A. G. (2017). Unveiling and tackling guanidinium peptide coupling reagent side reactions towards the development of peptide-drug conjugates. *RSC Advances*, 7(80), 50519–50526.
<https://doi.org/10.1039/c7ra06655d>

Wu, L., Ishigaki, Y., Hu, Y., Sugimoto, K., Zeng, W., Harimoto, T., Sun, Y., He, J., Suzuki, T., Jiang, X., Chen, H. Y., & Ye, D. (2020). H₂S-activatable near-infrared afterglow luminescent probes for sensitive molecular imaging in vivo. *Nature Communications*, 11(1). <https://doi.org/10.1038/s41467-020-14307-y>

Xu, Y., Hu, J., Wang, X., Xuan, L., Lai, J., Xu, L., Chen, S., Yang, L., Luo, G., Zhu, K., Wu, X., & Li, Y. (2015). Overexpression of MALT1-A20-NF- κ B in adult B-cell acute lymphoblastic leukemia. *Cancer Cell International*, 15(1).
<https://doi.org/10.1186/s12935-015-0222-0>

Zhao, J., Jin, G., Weng, G., Li, J., Zhu, J., & Zhao, J. (2017a). Recent advances in activatable fluorescence imaging probes for tumor imaging. In *Drug Discovery Today* (Vol. 22, Issue 9, pp. 1367–1374). Elsevier Ltd.
<https://doi.org/10.1016/j.drudis.2017.04.006>

Zhao, J., Jin, G., Weng, G., Li, J., Zhu, J., & Zhao, J. (2017b). Recent advances in activatable fluorescence imaging probes for tumor imaging. In *Drug Discovery Today*

(Vol. 22, Issue 9, pp. 1367–1374). Elsevier Ltd.
<https://doi.org/10.1016/j.drudis.2017.04.006>